UNIVERSITY OF BRASILIA

FACULTY OF TECHNOLOGY

DEPARTMENT OF CIVIL AND ENVIRONMENTAL ENGINEERING

ANALYSIS OF GEOSYNTHETIC ENCASED COLUMNS IN VERY SOFT SOIL

NIMA ROSTAMI ALKHORSHID

SUPERVISOR: GREGÓRIO LUIS SILVA ARAUJO, DSc
CO-SUPERVISOR: ENNIO MARQUES PALMEIRA, PhD

A THESIS SUBMITTED FOR THE DEGREE OF DOCTOR OF SCIENCE IN GEOTECHNICS

PUBLICATION: G.TD-133/17

BRASÍLIA / DF: JULY/2017

FACULTY OF TECHNOLOGY
DEPARTMENT OF CIVIL AND ENVIRONMENTAL ENGINEERING

ANALYSIS OF GEOSYNTHETIC ENCASED COLUMNS IN VERY SOFT SOIL

NIMA ROSTAMI ALKHORSHID

THESES OF PhD SUBMITTED TO THE DEPARTMENT OF CIVIL ENGINEERING OF THE UNIVERSITY OF BRASILIA AS PART OF THE NECESSARY REQUIREMENTS TO OBTAIN THE DEGREE OF DOCTOR OF SCIENCE.

APROVED BY:

_____

GREGÓRIO LUIS SILVA ARAUJO, D.Sc. (UnB)
(SUPERVISOR)

_____

ENNIO MARQUES PALMEIRA, Ph.D. (UnB)
(CO-SUPERVISOR)

_____

JUAN FELIX RODRIGUEZ REBOLLEDO D.Sc. (UnB)
(INTERNAL EXAMINER)

_____

MARCOS MASSAO FUTAI, D.Sc. (USP)
(EXTERNAL EXAMINER)

_____

CARLOS MEDEIROS SILVA, D.Sc. (EMBRE)
(EXTERNAL EXAMINER)

DATE: BRASÍLIA/DF, June 20th, 2017.

CATALOGUING DATA

ALKHORSHID, NIMA ROSTAMI
Analysis of Geosynthetic Encased Columns in Very Soft Soil. Distrito Federal, 2017.
xxvii, 147 p., 210x297 mm (ENC/FT/UnB, Doctor of Science, Geotechnics, 2017).
Doctoral thesis – University of Brasilia, Faculty of Technology, Department of Civil and Environmental Engineering.
1. Geosynthetics 2. Granular columns
3. Very soft soil 4. Embankment
I. ENC/FT/UnB II. Title (series)

BIBLIOGRAPHIC REFERENCE

ALKHORSHID, N.R (2017). Analysis of Geosynthetic Encased Columns in Very Soft Soil. Tese de Doutorado, Publicação G.TD-133/17, Departamento de Engenharia Civil e Ambiental, Universidade de Brasília, Brasília, DF,128 p.

CESSÃO DE DIREITOS

NOME DO AUTOR: Nima Rostami Alkhorshid
TÍTULO DA TESE DE DOUTORADO: Analysis of Geosynthetic Encased Columns in Very Soft Soil.
GRAU / ANO: Doutor / 2017.

Nima Rostami Alkhorshid
EQN 410/ 411 BLOCO A, Apartamento 86
Bairro: Asa Norte
CEP.: 70.865-405 – Brasília/DF - Brasil

DEDICATION

To My grandfather, Barani Rostami Alkhorshid, that passed away in 2014, who is always a man that I look up to.

To my love, Mahshid Ghasemi Boroon, that I am everlastingly indebted for all the sacrifices she did during my PhD.

Last but not least, to my parents, Esmaeil Rostami Alkhorshid and Zarin taj Bijani, who are always my role models.

Do not fear to be eccentric in opinion,
For every opinion now accepted was once eccentric.
Bertrand Russell

ACKNOWLEDGMENT

It has been a great honor to be part of the geotechnical program at the University of Brasilia. Thus I would like to express my special gratitude for the help I received from the faculty members.

To Prof. Gregório Luis Silva Araujo, my supervisor, for stamina, devotion, friendship, assistance and other qualities that contributed a lot to the development of this thesis. I am thankful for all his suggestions that came from his acquaintance with my study.

To Prof. Ennio Marques Palmeira, my co-supervisor, who has willingly supported my work and gave me precious suggestions throughout this study.

To Prof. Renato Pinto da Cunha, who has been my dear friend since day one in Brazil and I have learned so many things from him. Thanks for being a member of my qualifying exam.

To professors, Juan Felix Rodriguez Rebolledo, Carlos Medeiros Silva, Marcos Massao Futai for their participation and contributions in my defense. Undoubtedly, your suggestions were of paramount importance for the improvement of this thesis.

To the technicians of the laboratory of the department of mechanical engineering, specially to Mr. Artur for making the pieces which were used during this work.

To the technicians of the laboratory of geotechnics, Mr. Adolfo, Saimon, Thiago, Jonas, Mr. João for the help I received from them.

To CNPq and the University of Brasilia, for financial support.

To Huesker LTDA, especially Eng. André Estêvão Silva, for providing the materials that were needed for this study and also for his great help in the development of this work.

To Mr. Moacyr for his assistance on providing the pieces which were needed for starting the laboratory experiments.

ABSTRACT

Soft soils, commonly, can be encountered in coastal areas. Thus, embankment construction on these problematic soil is always a challenge for geotechnical engineers. There are several soil improvement techniques to overcome these challenges. Granular columns is one of the popular techniques for supporting embankments. When it comes to very soft soils, the application of granular columns is almost impossible, because of the low confinement provided by the surrounding soil. Geosynthetic encased granular columns is a recently developed technique that has been successfully used in various embankment projects dealing with soft soils.

This research aimed at studying the performance of encased columns with different types of the encasement and column materials. Instrumented large scale laboratory tests as well as numerical analysis using the Finite Element Method were carried out. Three types of column material (sand, gravel and construction waste) and also three types of woven geotextile (G-1, G-2 and G-3) with different tensile stiffness were tested. The tests were performed with and without encasement to evaluate the efficiency of the former in increasing the load bearing capacity of the columns. The influence of the displacement installation method on the surrounding soil was also studied. In addition, the role of columns in dissipating excess pore water pressures and imposing lateral pressures to the surrounding soil was evaluated. Finally, the back analysis of the laboratory tests and also analysis of a full-scale embankment, using the Finite Element Method, were conducted.

The laboratory tests indicated that the role of encasement in very soft soils is of paramount importance, since it considerably improved the column performance. It was also observed that the displacement installation method generated excess pore water pressures and caused consolidation of the surrounding soil. The back analyzed results showed good agreement with the tests results. Ultimately, the full scale analysis of an embankment indicated that the columns which were close to the middle of embankment presented larger settlements than those under the embankment slope, which were mainly affected by lateral deflection.

RESUMO

De uma forma geral, parte das as áreas costeiras são cobertas por solos moles. Assim, a construção do aterro sobre esses solos problemáticos é sempre um desafio para engenheiros geotécnicos. Existem várias técnicas de melhoria dos solos para superar esses desafios. Nesse contexto, as colunas granulares têm apresentado sucesso para esse tipo de construção. Para solos muito moles, a aplicação de colunas granulares é de difícil execução e rendimento, tendo em vista o baixo confinamento lateral na parte superior da coluna. As colunas granuladas encamisadas com geossintéticos são uma técnica recentemente desenvolvida que tem sido utilizada com sucesso em vários projetos de aterros sobre solos moles.

Esta pesquisa teve como objetivo estudar o desempenho de colunas encamisadas com diferentes tipos de materiais de encamisamento e de preenchimento das colunas. Para realizar isso, foram realizados testes laboratoriais em grande escala e também análises numéricas usando o Método dos Elementos Finitos. Foram utilizados três tipos de material de coluna (areia, brita e resíduos de construção) e também três tipos de geotêxtil tecido (G-1, G-2 e G-3) com diferentes valores de rigidez à tração. Os ensaios foram realizados com e sem encamisamento para avaliar a sua eficiência no aumento da capacidade de carga das colunas. A influência do método de instalação de vibro-deslocamento no solo circundante também foi estudada. Além disso, avaliou-se o papel das colunas na dissipação do excesso de poropressão e na pressão lateral imposta ao solo circundante. Finalmente, foram realizadas as análises dos testes laboratoriais e também a análise de uma simulação em escala real do aterro por meio do Método dos Elementos Finitos.

Baseando-se nos resultados obtidos, os ensaios de laboratório indicaram que o papel do encamisamento em solos muito moles é de grande importância, pois melhorou consideravelmente o desempenho da coluna. Foi observado também que o uso de colunas de brita e de resíduo de construção aumentou a capacidade de carga comparando com a das colunas de areia, que método de instalação de deslocamento gerou excesso de poropressão e causou a densificação do solo circundante. Por sua vez, os resultados das análise numéricas mostraram boa concordância com os resultados obtidos nos ensaios. A análise numérica em escala real de um aterro indicou que as colunas próximas do meio do aterro sofriam mais recalque e que as colunas que estavam sob a talude do aterro foram mais afetadas pela deflexão lateral.

TABLE OF CONTENTS

LIST OF TABLES

LIST OF FIGURES

LIST OF ABBREVIATIONS AND SYMBOLS

2D: Two dimensional

3D: Three dimensional

ABNT: Brazilian Association of Technical Standards

A_r: Area replacement ratio

B_g: Breakage index of coarse-grained materials

c´: Effective cohesion

C_4, C_5: Material/geometrical constants

$C_{c:}$ Compression index

c_g: Constant coefficient related to columns arrangement

C_s: Swelling index

d_e: Diameter of the unit cell

DSS: Direct Simple Shear

E´: Young's modulus

EA: Tensile stiffness

E_{oed}: Oedometer modulus

$E_{oed,s}$: Oedometric modulus of soft soil

f_m: Physical measures that are relate to the model

f_P: Physical measures that are related to the prototype

F_R: Circumferential force

g: Gravity acceleration

GEC: Geosynthetic Encased Columns

H: Column height

Jg: Tensile stiffness,

$K_{0,s}$: Coefficient of lateral earth pressure at rest for soft soil

$K_{a,c}$: Coefficient of active earth pressure

$K_{a,c}$: Coefficient of active earth pressure of column

K_ψ: Dilation constant

L: Encasement length,

LC: Load cell

NCL: Normal consolidation line

OCL: Over-consolidation line

OCR: Over consolidation ratio.

P_{geo}: Pressure contributed by the encasemen

P'_L: Effective stress

q_A: Applied vertical distributed load

r_c: Sand cutting radius, internal to the geotextile

r_{geo}: Initial radius of geotextile

s: Distance between adjacent columns

$S_{E:}$ Seam strength efficiency

SF: Safety factor

S_u: Undrained shear strength.

TC: Triaxial Compression

TE: Triaxial Extension

t_g: Encasement thickness

T_g: Tensile strength,

T_{seam}: Wide width seam strength

UD: User-Defined soil models

u_z: Final settlement

w_L: Liquid limit

w_P: Plastic limit

y: Yield

z: Depth

β^{el}, β^p: Settlement reduction factors

γ_s: Unit weight of soil

γ_{sat}: Saturated unit weight,

Δr_{geo}: Lateral bulging

$\Delta\sigma$: Applied stress at the top of unit cell

$\Delta\sigma_{v,s}$: Increase of vertical stress on soft ground

ε_z (z): Total vertical deformation

κ^*: Modified swelling index

λ: Scaling factor

$\lambda^{*:}$ Modified compression index

ν': Poisson's ratio

ν_s: Poisson's ratio of soft soil

ρ: Geosyntheic density

$\sigma_{v,0,c}$: Initial stress on the column before loading

$\sigma_{v,0,s}$: Initial stress on soft soil before loading

φ': Effective friction angle,

ψ: Dilatancy angle,

1. INTRODUCTION

1.1. PROBLEM STATEMENT

Coastal areas usually can be involved with the problem of soft soils. These soils are not usually suitable for supporting desired engineering structures such as buildings, embankments, dams or bridges. Over the years, it is becoming more difficult to find good construction sites for these kind of structures. Considering the need for the improvement of these soils, different types of ground stabilization techniques have been developed in the last fifty years. The type of improvement technique that will be applied on soil depends on the type of the problematic soil existing on site. Granular column reinforcement elements have advantages over other improvement techniques when there is short time for the construction and it is not economically acceptable to let the foundation soil improve its shear strength and compressibility by going through the consolidation process. Based on the stiffness of granular columns, they work like piles (semi-rigid) considering the bearing capacity and also act like vertical drains. The main aim of granular column reinforcement is to increase the bearing capacity and to accelerate the consolidation rate of the soft soil and hence decreases the duration of the settlement process.

Due to the inadequate lateral confinement provided by very soft soils to the columns, the construction and the application of conventional granular columns became difficult. This problem can be solved by the application of geosynthetic encasement that provides lateral confinement to the columns material. The use of the foundation system presented as geotextile encased columns (GEC) has been used successfully and it is well established in engineering practice (Raithel and Kempfert, 2000; Raithel et al., 2002, for instance). The GEC method is considered as a recent improvement technique. Thus, there need be a better understanding of the method and of the principal parameters which are of paramount importance to improve the column behavior. To this end, more researches should be developed.

1.2. OBJECTIVES OF STUDY

This research aims to investigate the behavior of single conventional and encased granular column in order to reach a better understanding of its performance. The following aspects are outlined below to achieve these objectives:

I. To study the influence of encasement on the behavior of granular column using large scale laboratory tests and the finite element method;
II. To investigate the effect of column installation method on the soil strength and the pore water pressure of soil;
III. To study different column material and their effect on the bearing capacity;
IV. To investigate the effect of geotextile stiffness and strength as the encasement on the behavior of column.

1.3. THESIS OUTLINE

This study is divided in five chapters: the first chapter deals with a general approach of the subject, reporting potential problems related to the type of work and its solutions, as well as the objectives and justification of the research addressed by this study. The second chapter is the literature review found on the subject, by outlining studies conducted in other researches. Chapter three discusses the materials and methodology used in this research. Chapter four shows and discusses the results of the large scale tests and numerical simulations. In this chapter are shown the results of the laboratory tests; load-settlement curves, lateral bulging of the column, lateral earth pressure due to the installation and loading of the column. Finally, the results of numerical simulations and their comparison with the tests are presented and also numerical simulations were carried out to evaluate a full scale embankment reinforced by encased and conventional columns. The fifth and final chapter presents conclusions obtained from the study and suggestions for future researches.

2. LITERATURE REVIEW

2.1. INTRODUCTION

The problem of dealing with soft soils especially in coastal areas can be of major concern for geotechnical projects. In these areas, the water table is so high that in some cases the soil presents high compressibility and low shear strength. Due to the urban development, these areas are becoming increasingly busy and the need to have safe constructions on the very soft soils is increasing every day. In these areas, low bearing capacity and differential and absolute settlement are particular concern to geotechnical engineers. Commonly for soft soil, the two limit states (ultimate limit state and serviceability limit state) should be considered, but generally, it's the serviceability limit state that governs the project. Thus, for both flexible or non-flexible construction, differential settlement is of major importance. Differential settlement may not fail the construction structurally, but can make it useless. This can cause high maintenance cost to many projects.

There are different methods to improve soft soils behavior. Particle size distribution and soil type are two important factors in choosing the improvement method (Han, 2015). Figure 2.1 shows some improvement method.

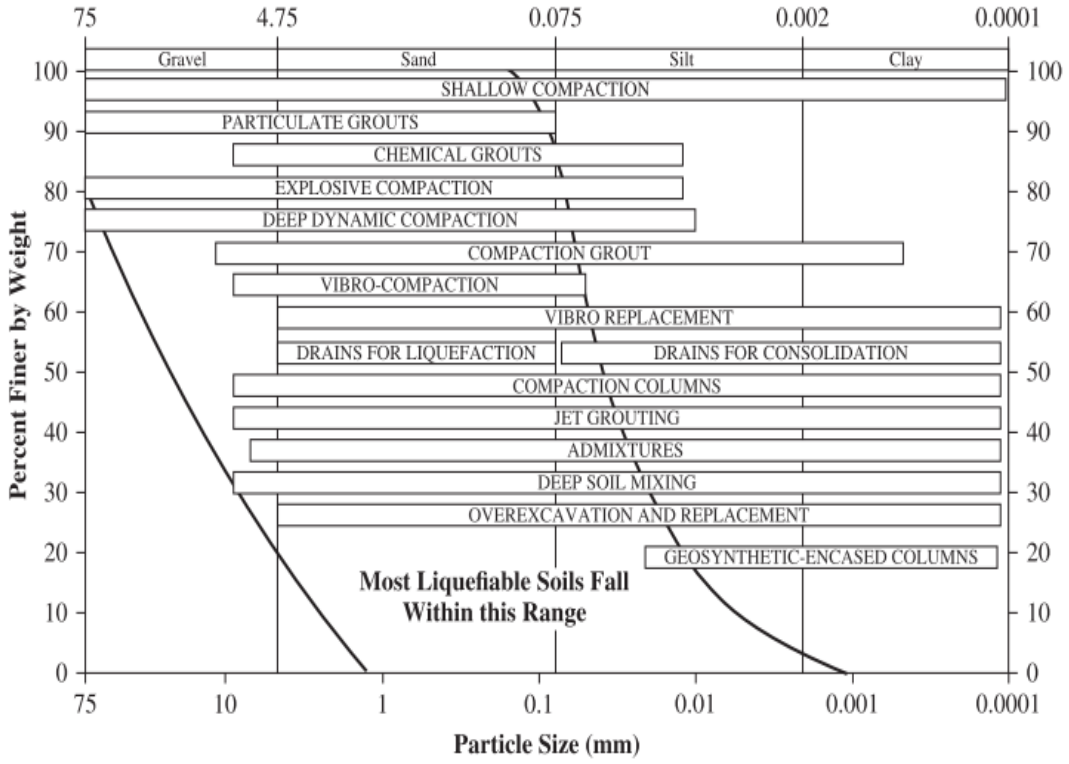

Figure 2.1. Ground improvement methods (modified from Schaefer et al., 2012; Han, 2015).

There are different methods to execute granular columns. The two main methods are a) displacement method and b) excavation method and which can be applied to a wide range of soil types (Figure 2.2). In displacement method, pipe is pushed down by vibration to the rigid layer. The casing tip has two small traps which are closed through driving, resulting in displacement of the surrounding soft soil. Then, the geosynthetic is putted and it is filled up inside. Finally, the pipe is pulled out and two small traps are opened due to the weight of the column content above it. The installation of the displacement method is most widely used for construction of GEC in very soft soils.

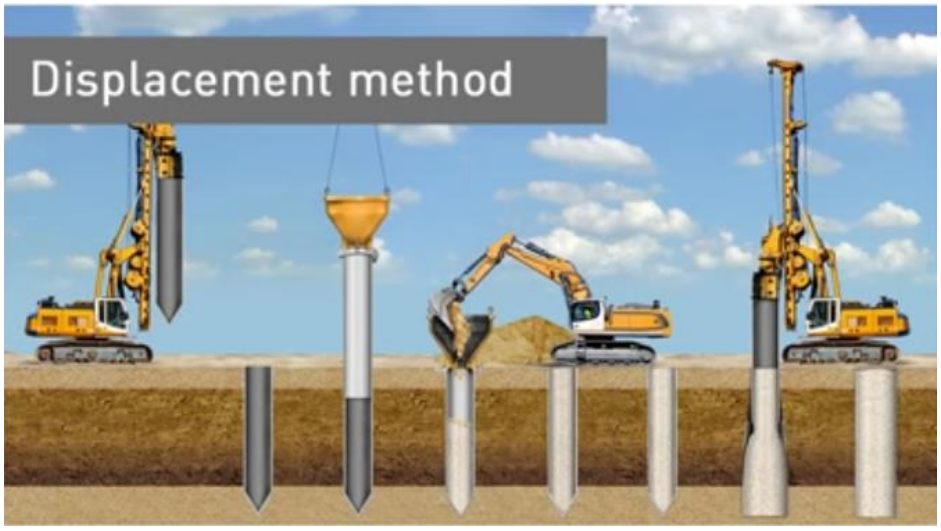

(a)

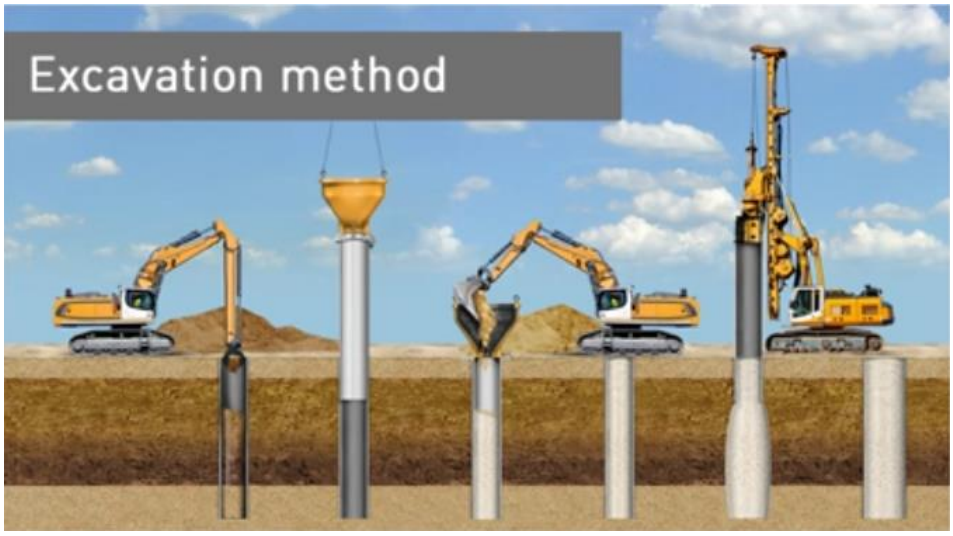

(b)

Figure 2.2. Granular column installation; (a) displacement method and (b) excavation method (Huesker company, 2012).

The replacement method uses an open-bottom pipe (casing) equal in diameter to the GEC and this pipe is pushed down until the underlying rigid layer. The soft soil within the pipe is withdrawn using helical auger. The geosynthetic is then placed inside the pipe and filled with the granular material. The material of granular columns consists of sand and gravel. After the geosynthetic encasement has been filled, the pipe is pulled out. The granular column is compacted by vibrating the pipe as long as the pipe is dragged out.

2.2. INVESTIGATION OF GRANULAR COLUMN

2.2.1. BASIC CONCEPT (UNIT CELL)

Most of designs developed by researchers (Aboshi et al., 1979; Goughnour & Bayuk, 1979; Balaam & Booker, 1981; Van Impe & De Beer, 1983; Madhav &Van Impe, 1994; Priebe, 1995; Raithel & Kempfert, 2000; Han and Ye, 2001; Pulko et al, 2011; Castro and Sagaseta, 2011) is based on the unit cell concept. Basically, the unit cell contains two parts (Balaam & Booker, 1981): (i) granular column and (ii) the surrounding soil within the region of effect of the granular column.

The relation between the column spacing and the unit cell diameter is given by:

$$d_e = s.c_g \qquad (2.1)$$

where,

d_e = Diameter of the unit cell

s = Distance between adjacent columns

c_g = Constant coefficient related to columns arrangement

In triangular arrangement, c_g = 1.05, in square arrangement, c_g = 1.13, and for hexagonal arrangement, c_g = 1.29 (Figure 2.3).

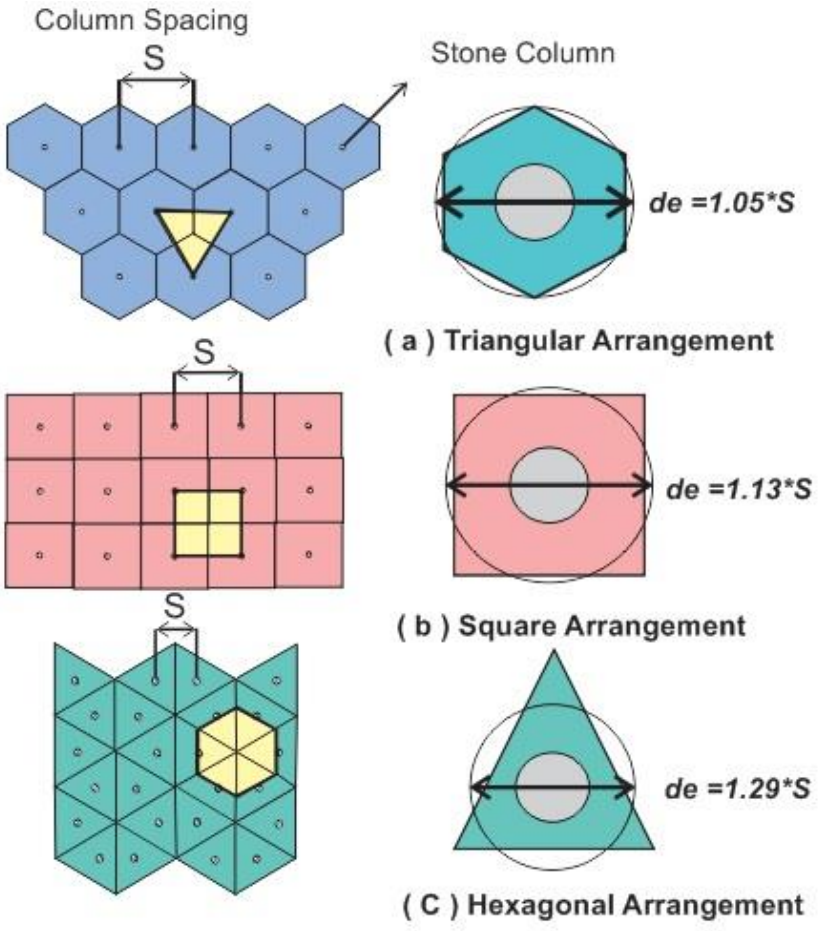

Figure 2.3. Arrangement of columns.

2.2.2. FAILURE MODES

Hughes & Withers (1974) performed tests on sand columns with the diameter (d) from 12.5 to 38 mm and a length of 150 mm. They showed the bulging failure of sand column as shown in Figure 2.4. They suggested that columns shorter than 4d would fail by punching, as long as the sum of shear stress at the column interface and end-bearing stress are lower than the stress needed to bulge the column. Another interesting finding from this laboratory study is that only the clay within a cylinder of diameter of 2.5d is significantly strained, which suggests that 2.5d may be the maximum distance between consecutive columns.

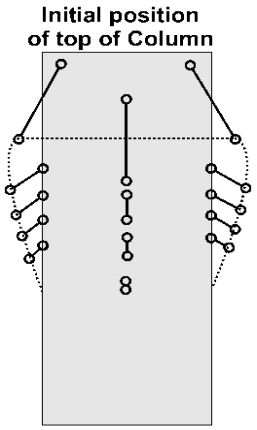

Figure 2.4. The bulging failure of sand column (Hughes & Withers, 1974).

Goughnour and Bayuk (1979) proposed the elasto-plastic examination (incremental procedure) for granular column. In this examination, three assumptions were used:

I. At the beginning, the column is linearly elastic;

II. At failure, the column is completely plastic;

They used the unit cell concept with an incremental method for investigating the issue. The application of incremental method is slow and difficult because this method needs to obtain the soil characteristics at high quality.

Barksdale & Bachus (1983) proposed three types of failure styles for granular columns (Figure 2.5), which are: (a) bulging failure, (b) shear failure, (c) punching failure.

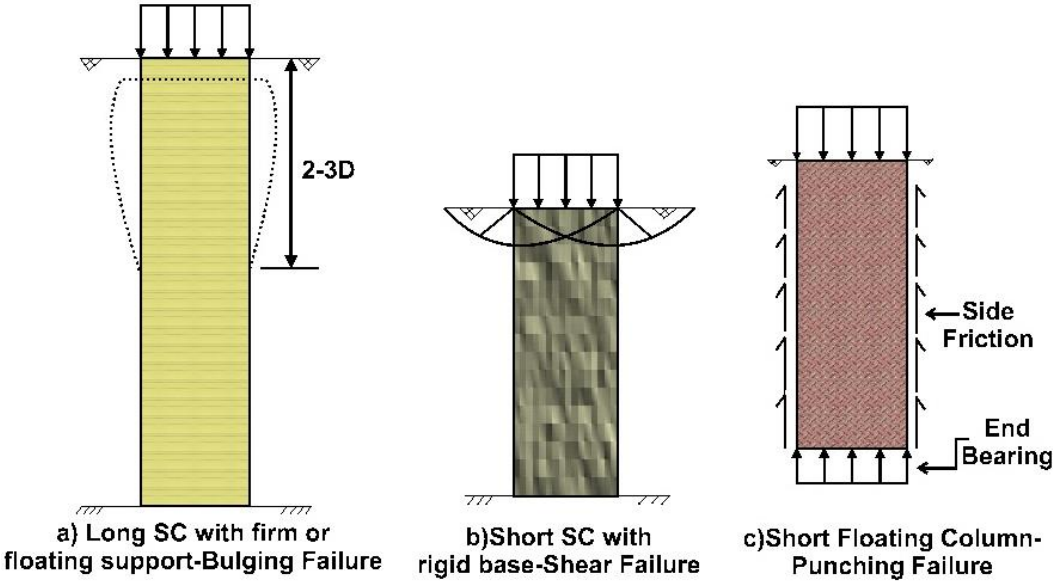

Figure 2.5. Failure styles of single granular column (Barksdale & Bachus, 1983).

They stated that, the ultimate bearing capacity of a group of columns per column is slightly greater than an isolated single column. They also concluded that underneath an extensive flexible loading structure like an embankment, the settlement of columns and the soft soil are roughly equal. The failure mode of the granular column group under embankment is illustrated in Figure 2.6.

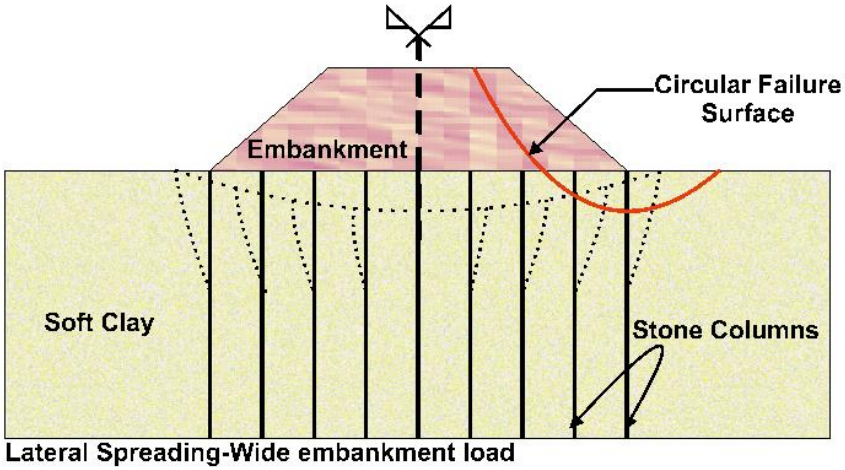

Figure 2.6. Failure styles of granular columns under embankment (Barksdale & Bachus, 1983).

2.2.3. SMEAR ZONE

The displacement method can cause a smear zone (disturbed zone) around the location of column. This zone was of interest for various studies (Walker and Indraratna, 2006; Weber et al., 2010; Wang, 2009) in order to find the its diameter and the changes that can be occurred due to displacement of soil.

In terms of size of the smear zone, Walker and Indraratna (2006) stated that the radius of smear zone (r_s) can be estimated between 2 to 3 times the radius of column (r_c).

Weber et al. (2010) supposed r_s as double r_c and Wang (2009) was assumed r_s to be between 1 to 2.5 times r_c and also k_s/k_h equal to 0.1, where k_s and k_h are permeability of smear zone and horizontal permeability of soil, respectively. Figure 2.7, illustrates the smear zone around the column after the column installation.

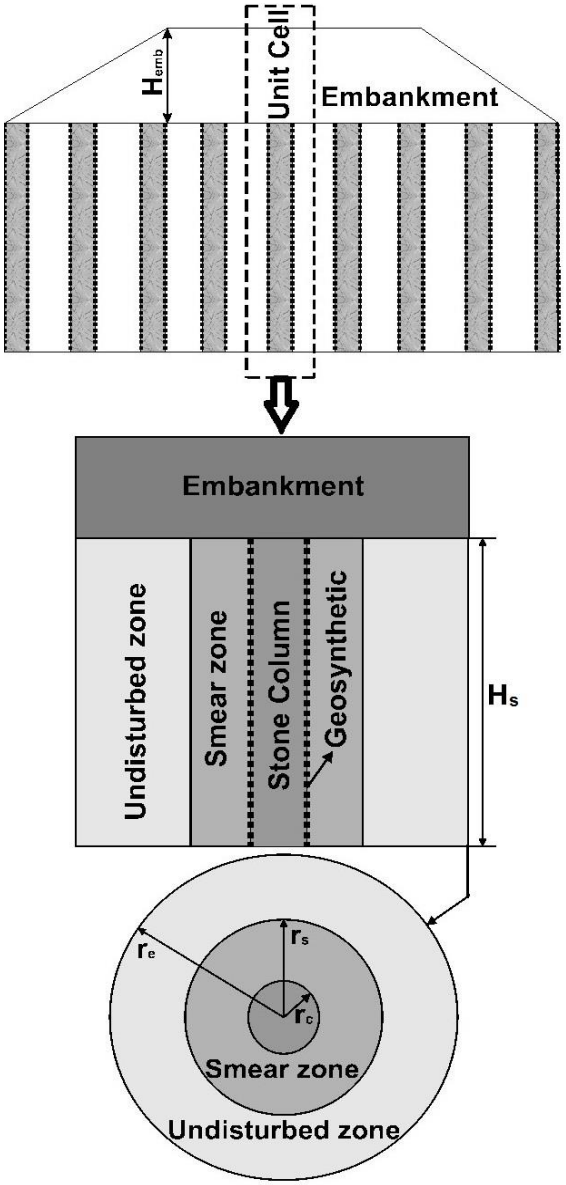

Figure 2.7. Smear zone around column.

2.3. GEOSYNTHETIC ENCASED GRANULAR COLUMNS (GEC)

In this improvement technique, since the columns material are aggregates which have no cementation between their particles, the main part of the bearing capacity of columns comes from the lateral support, in this case, provided by the geosynthetic-encasement stiffness and strength. Thus, the higher portion of the surface load is supported by the columns. Once the load is applied, the column material goes through lateral squeezing transferring the stress to the encasement. This is the main difference between GEC and conventional granular column. Figure 2.8 shows the application of encased column for freeways and railways.

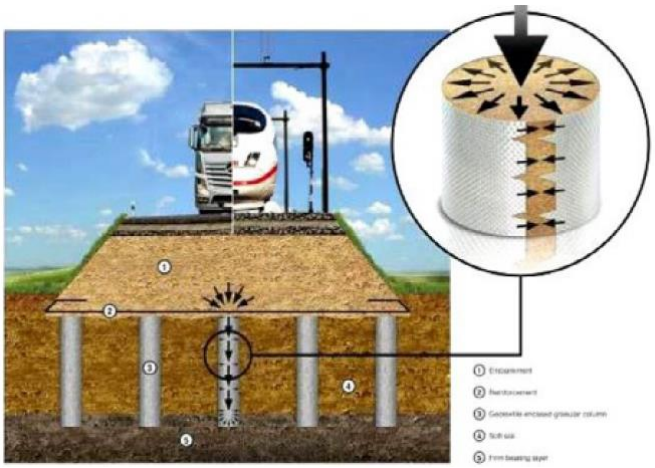

Figure 2.8. Embankment with geosynthetic on GEC (Raithel 1999, 2000 and EBGEO 2011).

2.3.1. CASE STUDIES (ALEXIEW ET AL., 2015)

Railroad embankment at waltershof, 1995

A highly-loaded railroad that goes to the harbor in Hamburg, Germany, was needed to be extended in order to solve the increasing traffic. The embankment height is 5 m and the foundation soft soil is composed by saturated clay and peat to a depth of about 5 to 6 m. The settlement of old embankment over the years was about 1.2–1.5 m. The extension of embankment (new embankment) was decided to be founded on GEC. Figure 2.9 depicts the details of the project. The diameter of GEC was 1.54 m and the area replacement ratio was in the range of 20 to 30%.

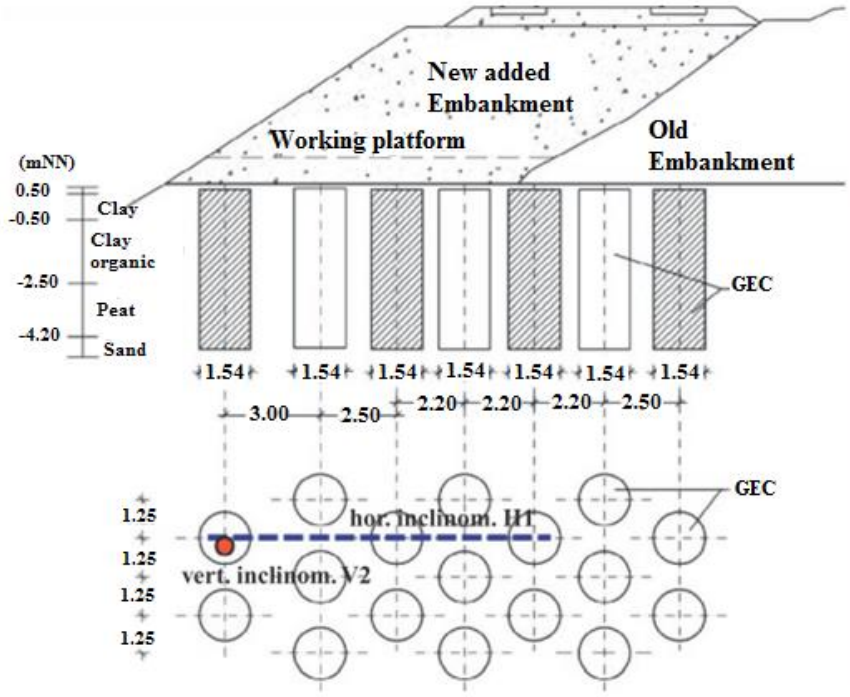

Figure 2.9. The sketch of project (Alexiew et al., 2015).

The tensile strength and stiffness of the encasement material were equal to 200 kN/m and 1800 kN/m, respectively. Since there was no encasement material, with the desired diameter, available in the market, the encasement was made using seam.

The properties of foundation soil are given in Table 2.1. Figure 2.10 shows the settlement on the top of encased columns during and after the construction of embankment for a period of about three years. The settlement after the construction when the encased columns are under both the load of embankment and the heavy train with iron ore, was measured to be about 5 cm. The increments of settlement tend to zero at the end of measuring period.

Table 2.1. Parameters of foundation soil (Alexiew et al., 2015).

Soil layer	Position (m)	γ'/γ_{sat} (kN/m^3)	k (m/s)	E_s (MN/m^2)	φ' (°)	c' (kN/m^2)
Clay	0.5 to -0.5	19/19	1E-9	2.6	29	8
Organic clay	-0.5 to -2.5	13/13	1.5E-8	0.6	25.5	16
Peat	-2.5 to -4.2	11/11	1.4E-7	0.8	20.5	8.5
Sand	-4.2	19/20	3E-5	27	35	1

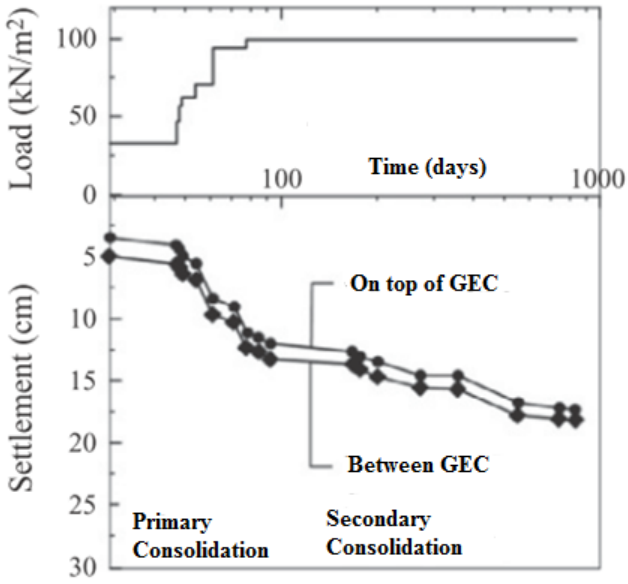

Figure 2. 10. The settlement on the GEC (Alexiew et al., 2015).

The excess pore water was measured under embankment load during the construction process. Figure 2.11 reveals three important points about the performance of GEC in dissipation of excess pore water pressure, according to the authors: (i) the maximum value obtained for the upper clay is less than the half of surface load, (ii) regarding drainage condition, the organic clay is in unfavorable position but it still consolidates quickly, (iii) The excess pore water pressure comes to reduction even before the construction ends and under increments of surface loads.

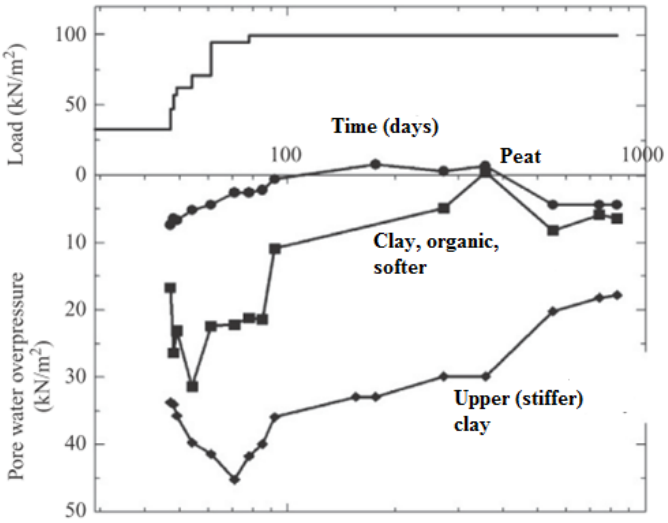

Figure 2.11. The changes in excess pore water pressure during construction of embankment (Alexiew et al., 2015).

Extension of airbus site, 2000–2002

The Airbus company needed to construct a reclamation structure at the Elbe River in Hamburg, Germany, in order to extend the site of company by approximately 140 ha.
The area extension is accomplished by using a 2.4 km long dike surrounding the polder. The location is illustrated in Figure 2.12.

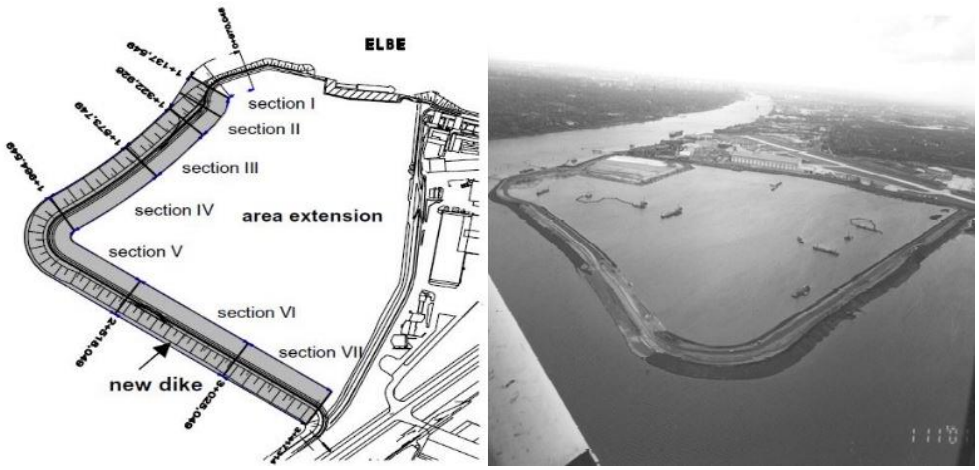

Figure 2.12. The location of dike and polder (Raithel et al., 2002).

This improvement provided the stability of the area by avoiding soft soils to move into the river zone. The dike was supported by almost 60,000 GECs with a diameter of 0.8 m. The distance between the adjacent columns has varied between 1.7 and 2.4 m (Figure 2.13). This improvement technique enabled the dike to be constructed on very soft soil having thickness of between 8 to 14 m and the undrained shear strength between 0.4 to 10 kN/m2 (Figure 2.14).

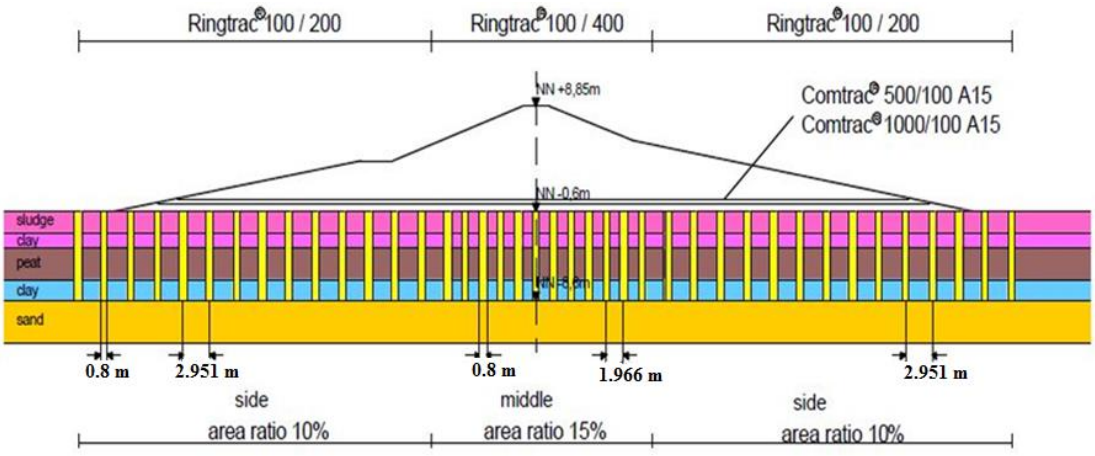

Figure 2.13. Cross section profile (Raithel et al., 2002).

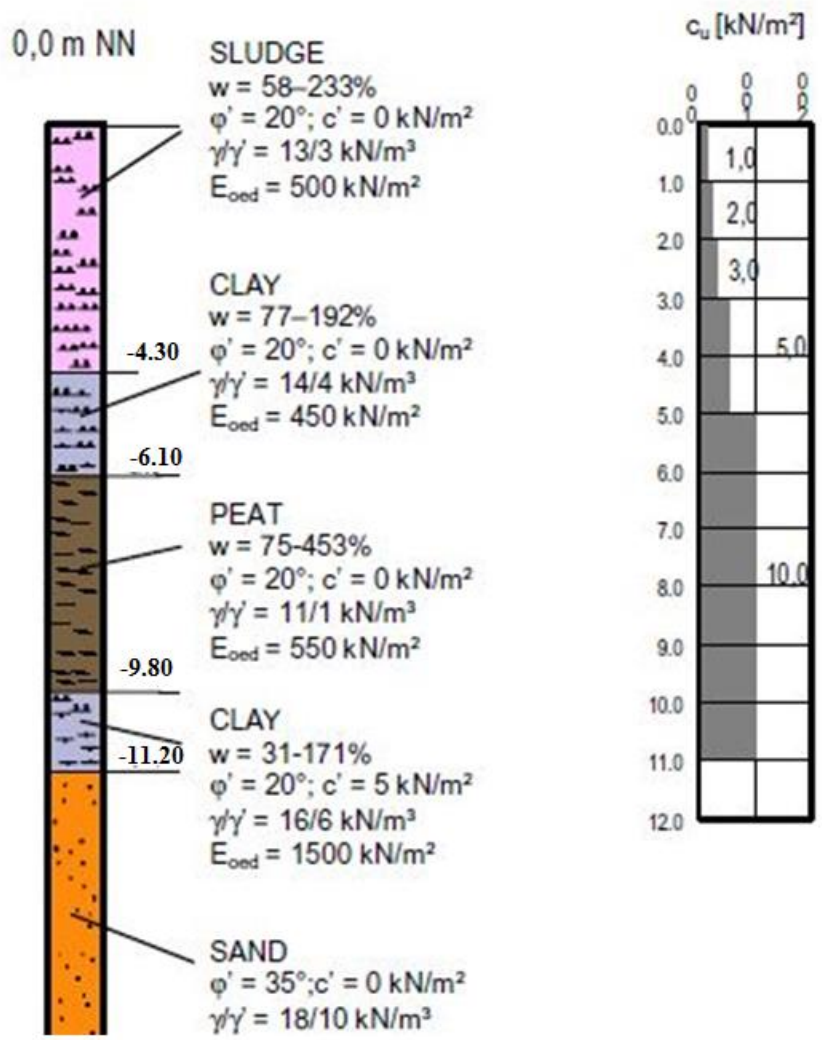

Figure 2.14. Ground strata profile (Raithel et al., 2002).

The soft soil surface along the dike line area was in different situations, from 0.8 m above sea level to 2.5 m below sea level. Displacement method was chosen as an appropriate installation method. Figure 2.15 indicates the measurements of the undrained shear strength (c_u) of soil at different depths of the soft soil before and immediately after installation of the columns. They clearly show the improvement provided by the installation method.

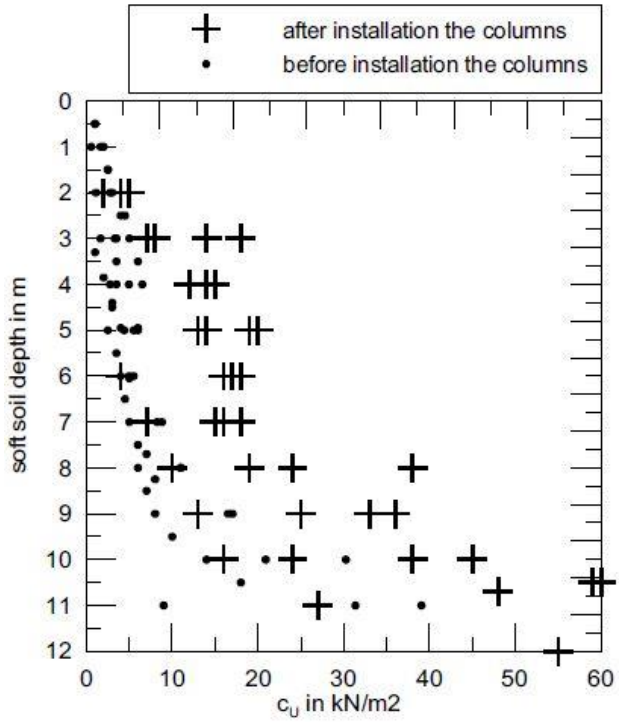

Figure 2.15. Undrained shear strength measurements (Raithel et al., 2002).

Figure 2.16 shows the settlements versus surface load applied by the construction of dike. It shows that the settlement increase tends to reduce with time, even when the surface load is increasing. It can be noticed in a very sensible form at day 300, when the surface load increases by two meter of the embankment height and the settlement reduction happens. It also can be observed that for this period the settlement tends to reach around zero.

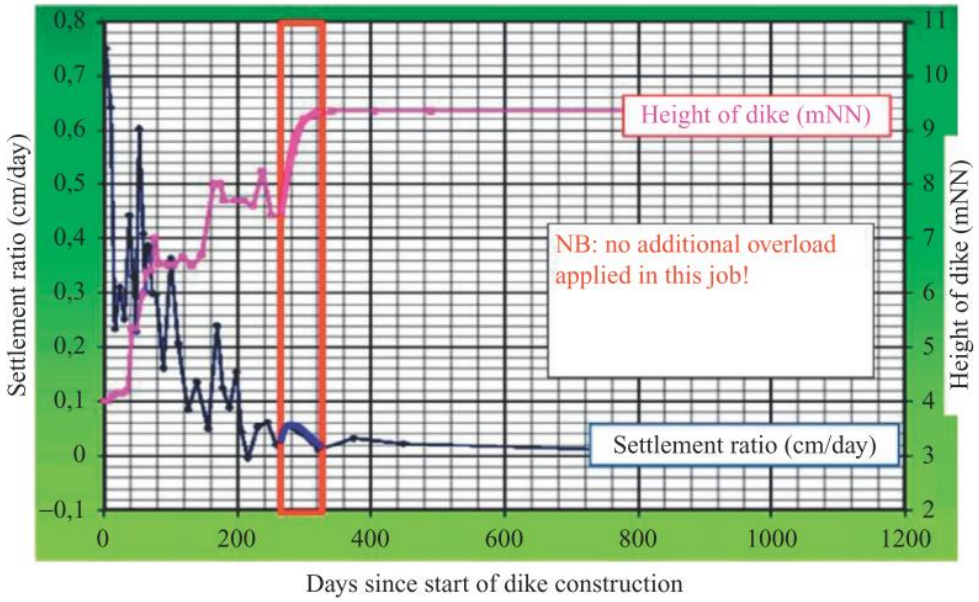

Figure 2.16. Settlement versus embankment load with time (Alexiew et al., 2015).

Railroad embankment Bothnia line, 2001–2002

In Sweden, the Bothnia line (a high-speed railway line) goes through a valley covered with soft soil to a depth of about 7.5 m. The embankment of railroad has a height of about 9 to 10 m. In order to reduce the settlement of embankment, the foundation soil was reinforced by GEC with a diameter of 0.8 m. The displacement method was used to install the columns with an area replacement ratio of 15% and the columns were installed in a triangular pattern. Figure 2.17 illustrates the cross section of embankment and columns.

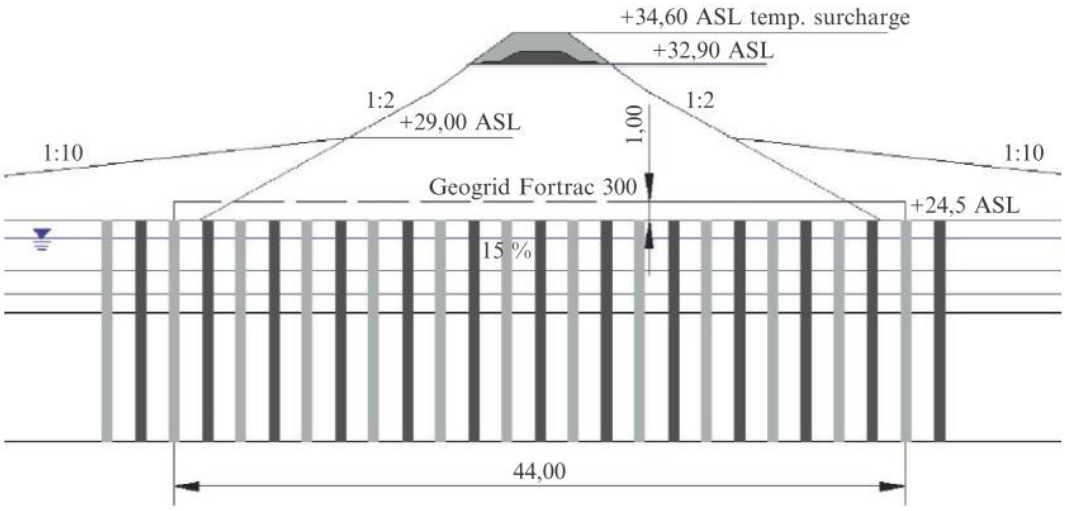

Figure 2.17. Cross section of embankment reinforced by GEC (Alexiew et al., 2015).

The foundation soil consists of different layers of clay and silt. The different layers of soil and their parameters are shown in Figure 2.18. The encasement was provided by a seamless woven geotextile. Due to the availability of coarse crushed rock in the region, the GECs were filled by this type of material. The use of crushed rock can cause damage to the geotextile during installation and compaction, which leads to reduction in the tensile strength.

In order to evaluate the reduction factor (RF_{inst}) due to installation damage, the process of installation was simulated at the Geotechnical Faculty of the University of Kassel. The outcome of tests gave an average RF_{inst} of about 1.36 and it was applied to the ring tensile strength of the encasement. In the case of sand, an average RF_{inst} of about 1.05 to 1.15 can be considered. The settlements of embankment, after its construction, were measured for a period of time of about 250 days.

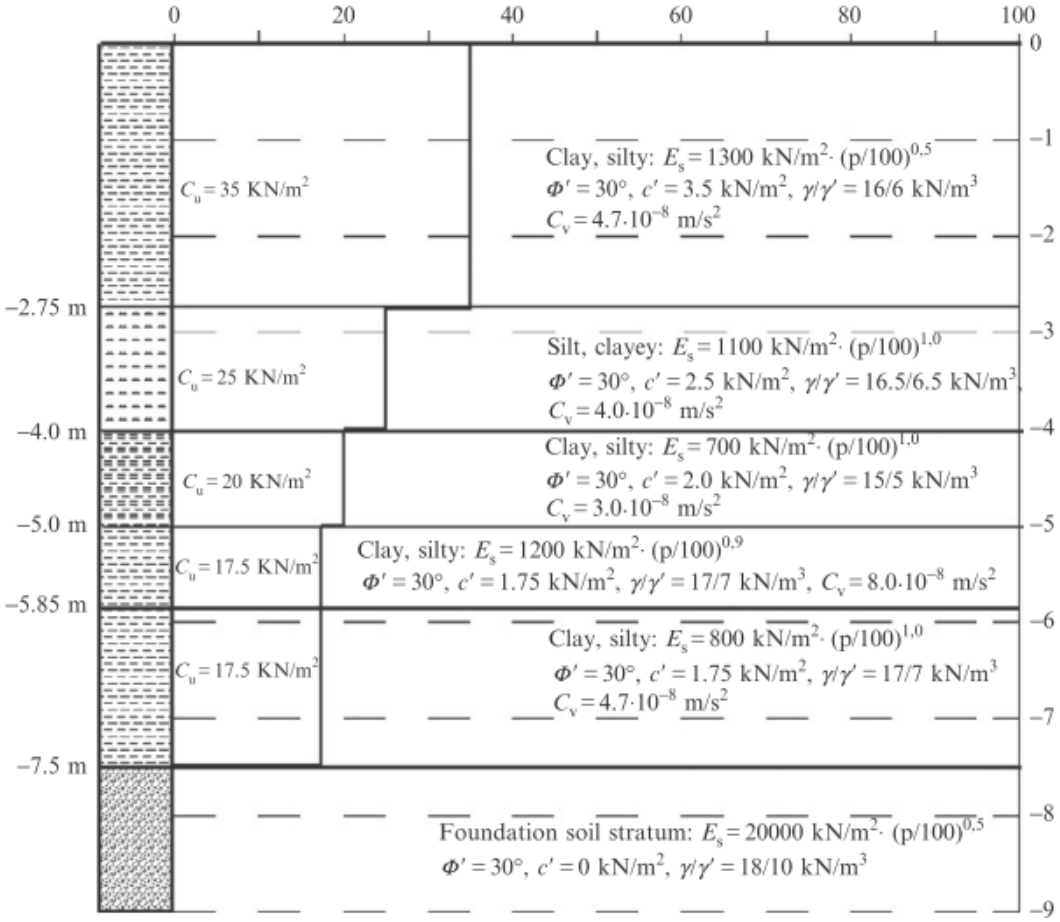

Figure 2.18. Parameters of soil layers (Alexiew et al., 2015).

In addition, the settlements were calculated regarding two different values of friction angle ($\varphi'_1 = 37.5^{\circ}$ and $\varphi'_2 = 45^{\circ}$). It was found that φ'_2 gives more reliable results. Figure 2.19 shows that almost 90% of primary consolidation settlements occurs in a period of about three months after the construction of embankment.

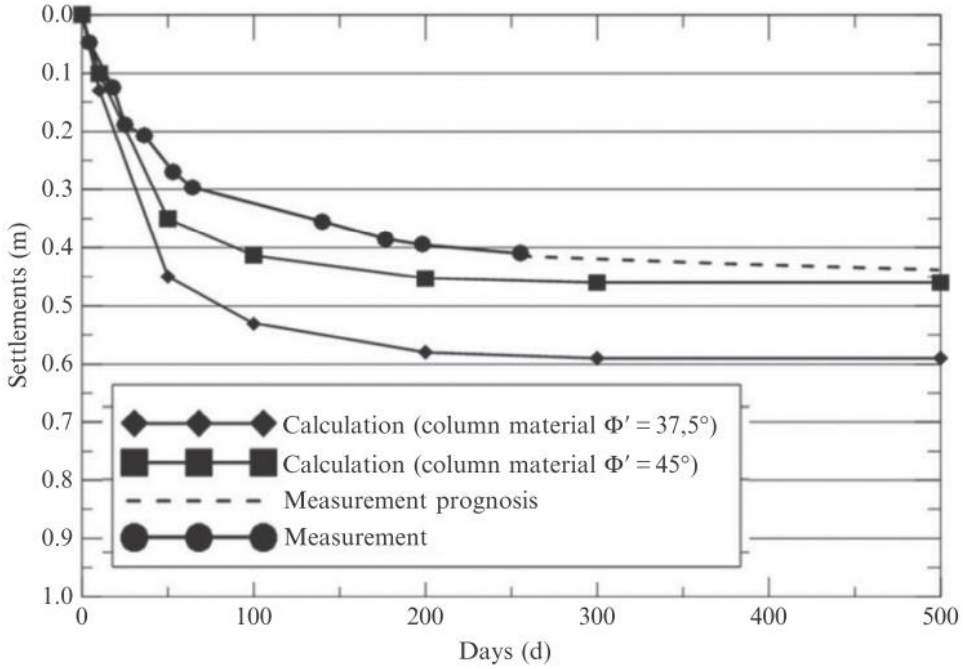

Figure 2.19. Settlement of embankment with time (Alexiew et al., 2015).

High-speed rail link, 2002

There is a high-speed railroad that connects Paris to Amsterdam that passes through hundreds of meters of a region used to be a place for waste disposal. This region is covered by a waste layer with the thickness of about 4 to 6 m that lies on a thick layer of sand. The materials of region are contaminated by oil and heavy metals. Figure 2.20 shows the cross section of project.

At the beginning two options were considered as possible solutions for improving the foundation soil. One of them was the removal of waste material and then the replacement by clean sand and the other one was using a slab supported by piles to a depth of 10 m. Additional studies found out that GEC could be a better solution respecting financial, ecological and logistic reasons.

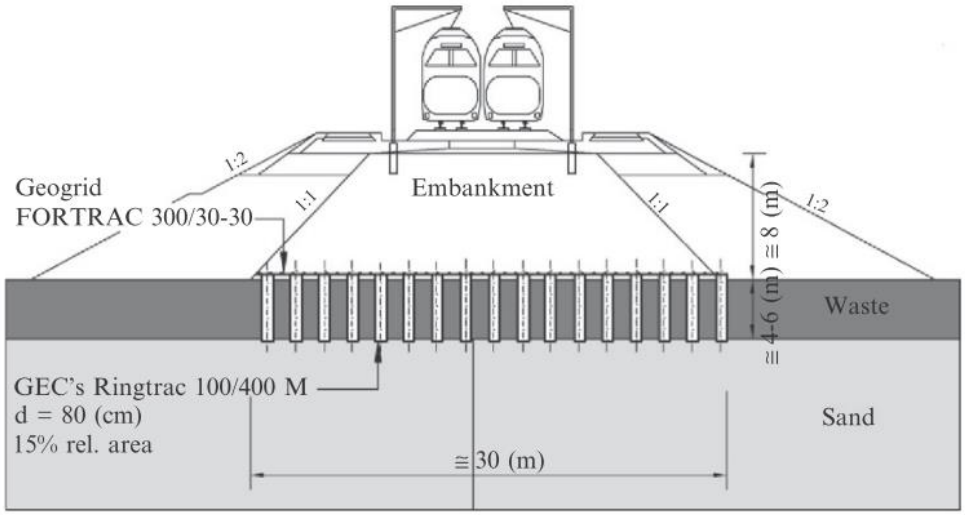

Figure 2.20. Railroad cross section (Alexiew et al., 2015).

The GECs used in this project had a diameter of 80 cm and the area replacement ratio of 15%. The encasement was produced by high chemical resistance polyvinylalcohol with the ring tensile strength of 300 and 400 kN/m. Regarding the settlements of improved area, three conditions were of concern: (i) to keep them to a limit of about 10 cm, (ii) to keep them as same as possible regardless of the extreme non-uniformity of waste material, and (iii) to accomplish a quick consolidation during and after the construction. The project was instrumented by horizontal inclinometers at the top of the GECs to measure the settlements developed by the construction of embankment (Figure 2.21 and Figure 2.22).

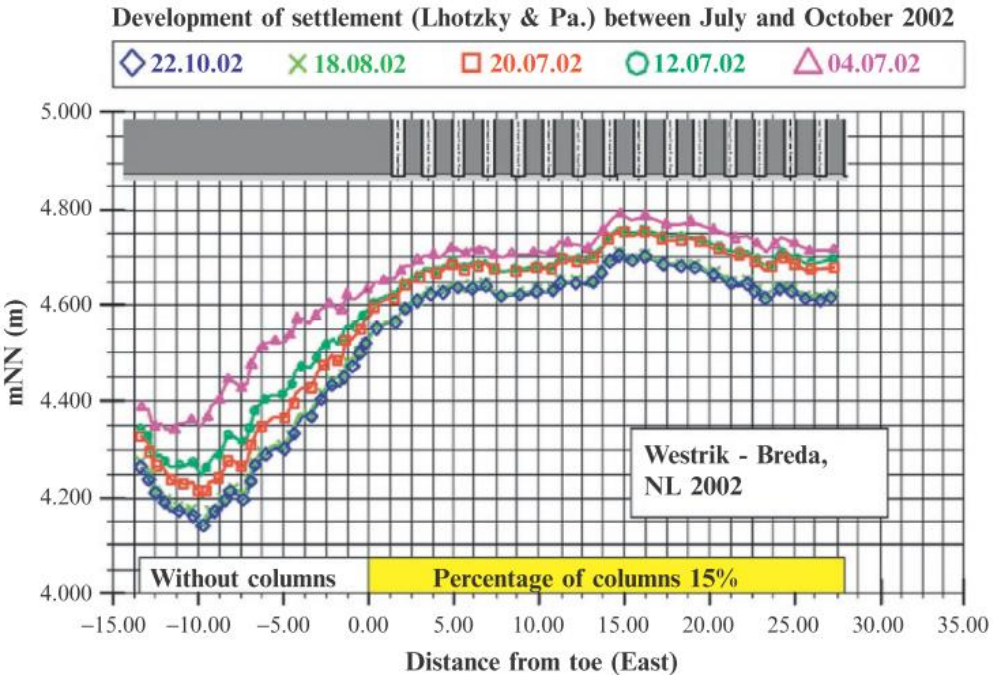

Figure 2.21. Settlement development (Alexiew et al., 2015).

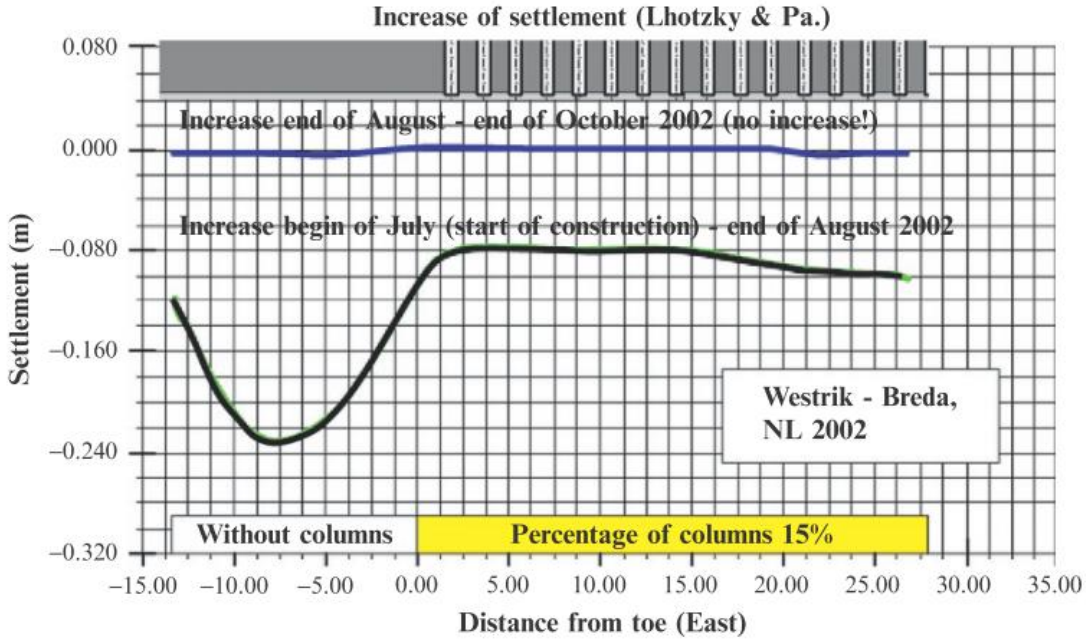

Figure 2.22. Settlement development during and after the construction (Alexiew et al., 2015).

2.3.2. ANALYTICAL METHODS

For the case of granular columns used in very soft soils, in the last years it has developed the encased column technique. For the design of this improvement technique, various analytical methods have been developed recently. At first the calculation process was recommended by Van Impe (1989) and then developed in numerical and analytical models by Raithel (1999) and Raithel & Kempfert (2000, 2005). The confinement provided by geosynthetic in the Geosynthetic Encased Columns (GEC) is considerably greater than the confinement provided by the surrounding soil and consequently the GEC suppots a greater load than the conventional granular column.

The method of Raithel (1999, adopted by EBGEO, 2011) considers the theory of elasticity and identical settlements for both granular column and surrounding soil. Moreover, this method predicts the behavior of unit cell for long-period drained condition when maximum value of bulging and settlement are obtained. The coefficient of active earth pressure ($K_{a,c}$) is applied to the column as the method considers that the column comes to an active lateral pressure condition at final stage.

As illustrated in Figure 2.23, there is an equilibrium between the loading on unit cell ($\Delta\sigma_0$) and vertical stresses shared by the column ($\Delta\sigma_{v,c}$) and surrounding soil ($\Delta\sigma_{v,s}$). In this method, the ring tensile force can be calculated by:

$$F_R = J\frac{\Delta \mathrm{r}_{\mathrm{geo}}}{r_{\mathrm{geo}}} \tag{2.2}$$

where, Δr_{geo} and r_{geo} are lateral bulging and initial radius of geotextile, respectively.

The model was developed based on the conventional calculation models used for granular columns, which are completed by the effect of geotextile encasement and uses an iterative process, by means of the Equations 2.3, 2.4 and 2.5.

$$\Delta \mathrm{r}_c = \frac{K_{a,c}.\left(\frac{1}{a_E}.\Delta\sigma - \frac{1-a_E}{a_E}.\Delta\sigma_{v,s} + \sigma_{v,0,c}\right) - K_{0,s}.\Delta\sigma_{v,s} - K_{0,s}.\sigma_{v,0,s} + \frac{(r_{\mathrm{geo}} - r_c).J}{{r_{\mathrm{geo}}}^2}}{\frac{E^*}{\left(\frac{1}{a_E - 1}\right).r_c} + \frac{J}{{r_{\mathrm{geo}}}^2}} \tag{2.3}$$

$$E^* = \left(\frac{1}{1-\nu_s} + \frac{1}{1+\nu_s}.\frac{1}{a_E}\right).\frac{(1+\nu_s).(1-2\nu_s)}{(1-\nu_s)}.E_{\mathrm{oed},s} \tag{2.4}$$

$$\left\{\frac{\Delta\sigma_{v,s}}{E_{\mathrm{oed},s}} - \frac{2}{E^*}.\frac{\nu_s}{1-\nu_s}\left[K_{a,c}.\left(\frac{1}{a_E}.\Delta\sigma - \frac{1-a_E}{a_E}.\Delta\sigma_{v,s} + \sigma_{v,0,c}\right) - K_{0,s}.\Delta\sigma_{v,s} - K_{0,s}.\sigma_{v,0,s} + \frac{(r_{\mathrm{geo}} - r_c).J}{{r_{\mathrm{geo}}}^2} - \frac{\Delta \mathrm{r}_c.J}{{r_{\mathrm{geo}}}^2}\right]\right\}.h = \left[1 - \frac{{r_c}^2}{(r_c + \Delta \mathrm{r}_c)^2}\right].h \tag{2.5}$$

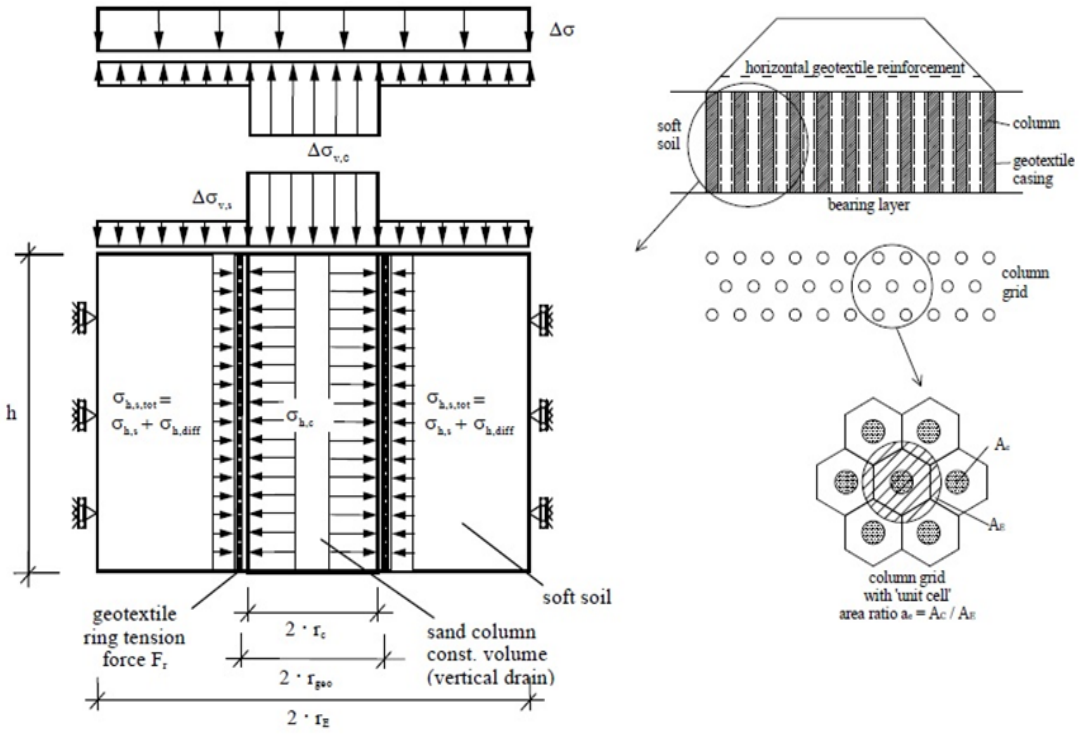

Figure 2.23. Analytical model for "Geotextile Encased Columns", simplified picture after Raithel & Kempfert (2000).

where,

$\Delta\sigma_{v,s}$: Increase of vertical stress on soft ground

$E_{oed,s}$: Oedometric modulus of soft soil

ν_s: Poisson's ratio of soft soil

$K_{a,c}$: Coefficient of active earth pressure of column

a_E: Area replacement ratio

$\Delta\sigma$: Applied stress at the top of unit cell

$\sigma_{v,0,c}$: Initial stress on the column before loading

$K_{0,s}$: Coefficient of lateral earth pressure at rest for soft soil

$\sigma_{v,0,s}$: Initial stress on soft soil before loading

r_{geo}: Radius of the surrounding geotextile

r_c: Sand cutting radius, internal to the geotextile

J: Geotextile tensile stiffness

h: Column length

Castro and Sagaseta (2011) developed an analytical method based on the unit cell concept. The soft soil was supposed as an elastic material and the column as an elasto-plastic material utilizing the Mohr-Coulomb yield criterion. In this method, encasement material was treated as an elasto-plastic material by considering a limit for tensile strength.

Zhang and Zhao (2014) developed an analytical calculation method for the design of geosynthetic-encased and non-encased granular columns. The analytical method is based on unit cell concept and as compared with the analytical methods presented by Pulko et al. (2011) and Castro and Sagaseta (2011), in the method presented by Zhang and Zhao (2014), the shear stress (slide friction) between the soil and column was taken into account. As the authors pointed out, this method may not be appropriate when high deformation is expected.

Briaud (2013) presented an analytical calculation to predict the load bearing capacity of a single encased column. The method takes into account the influence of geosynthetic tensile stiffness and the water table to estimate the bearing capacity of column. Based on the method the ultimate bearing capacity of the encased column can be calculated by the following equation:

$$P_u = k_p\left(P'_L + P_{geo}\right) \tag{2.9}$$

where,

k_p: Passive earth pressure of the column material, that is a function of friction angle of column material ($k_p = \frac{1+\sin\varphi}{1-\sin\varphi}$)

P'_L: Effective stress

P_{geo}: Pressure contributed by the encasement, obtained by following equation:

$$P_{geo} = E\frac{\Delta r}{r_0^2} \tag{2.10}$$

where,

E: Geotextile tensile stiffness

Δr: Lateral variation

r_0: Radius of the column

Additional information on the method is presented by Briaud (2013).

2.3.3. EXPERIMENTAL STUDIES

Alexiew et al. (2003) recommended that encased granular column should be installed with an area replacement ratio of 10-20% having diameter of about 0.8 m and installing based on a triangular arrangement with axial distance of 1.7-2 m.

Sharma et al. (2004) carried out a series of laboratory tests on layered granular columns reinforced with horizontal strips of geogrid. The tests were performed on single sand columns of 60 mm in diameter and 300 mm in length (Figure 2.24). The number of geogrid strips and the distances between adjacent strips were different in every model test. The results confirmed the influence of horizontal strips of geogrid on the improvement of bearing capacity and the reduction of lateral bulging.

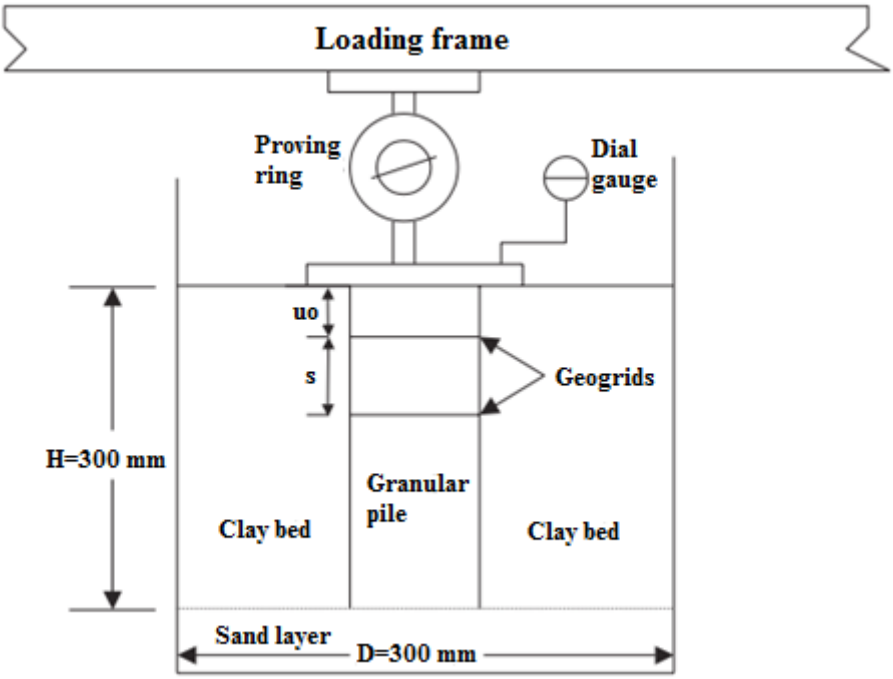

Figure 2.24. Sketch of the load test (Sharma et al., 2004).

Gniel & Bouazza (2009) conducted a series of small scale tests on encased granular column improved soft soil. The cylinder steel cell used in the tests was of 550 mm height and 150 mm internal diameter (6 mm steel wall thickness). They tested columns with 50.5 mm in diameter and 310 mm in length, to investigate the behavior of geogrid partially encased granular column. They concluded that, by increasing the length of encasing for both isolated single column and

group column, in case of partially encased column tests, the results show a steady decrease in vertical strain (Figure 2.25). The bulging occurred directly underneath the base of encasement. According to the methodology, an important rise in column stiffness and more reduction in column strain was achieved for fully-encased columns compared to clay behavior alone.

Figure 2.25. Small scale tests (Gniel & Bouazza, 2009).

Murugesan and Rajagopal (2009) implemented three series of laboratory tests and numerical simulation on encased granular column by varying the diameter of the columns (50 mm, 75 mm and 100 mm). The cylindrical cell used in the tests was of 210 mm diameter and 500 mm high. They concluded that the geosynthetic encasement enhances the bearing capacity of the column and stress-strain curve of the column indicates linear behavior and didn't show any failure unlike the conventional granular columns.

The behavior of geosynthetic-encased column was also analyzed by Araujo et al. (2009) for specific case of stabilization of embankments on a porous collapsible structured unsaturated soil as shown in Figure 2.26. They used different column material (sand and gravel) and different types of geosynthetics (woven geotextile and geogrid) with internal measurements of the strain inside the column by means of Strain Gauges (SG). The behavior of both conventional (sand and gravel) columns and encased (geotextile-encased sand and geogrid-encased gravel) columns were investigated by means of in-situ loading. Throughout testing, the local soil collapse was induced by injection of water from the top of the granular column to investigate the casing influence on the column behavior. The authors reported that depending on the materials used, a significant increase in bearing capacity for encased columns when comparing conventional columns can be obtained. In addition, the influences of foundation collapse by using geosynthetic-encased granular column can also be reduced.

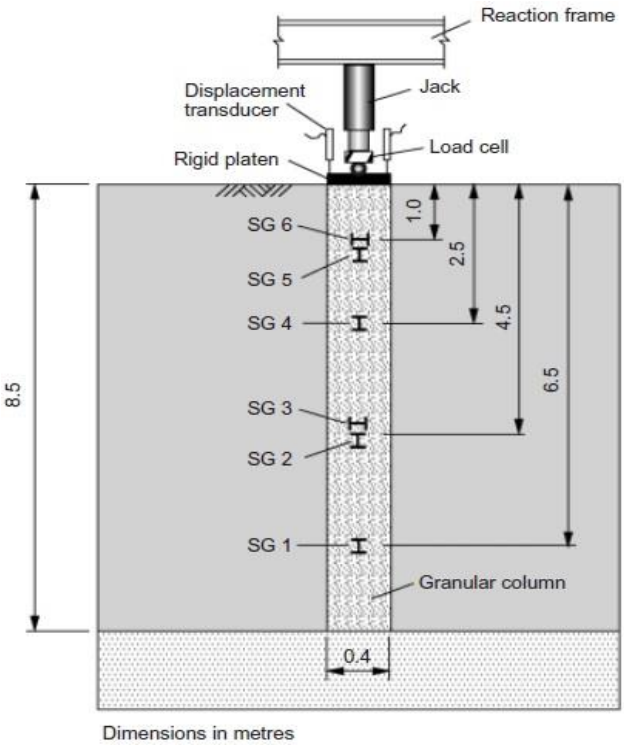

Figure 2.26. Schematic of the load test on granular columns (Araujo et al., 2009).

Yoo and Lee (2012) investigated the deformed shape, carrying capacity and settlement reduction of a geogrid-encased column (GEC) using field-scale load tests. Also, the influence of the geogrid encasement length and column strain was investigated. The tests were conducted on columns with two different lengths (L = 5.4 m and 8 m), and 0.76 m in diameter. In addition, isolated GEC behavior was compared to Rammed Aggregate Pier (RAP) and conventional granular column behavior.

RAP is an exclusive installation procedure using helical auger for excavation that after placing column content in stages, employs vertical impact ramming energy, resulting in good strength and stiffness. The authors reported that the encasement provided an additional confinement that reduced the settlement of soft soil and increased the stiffness of the column. Furthermore, the bulging of the encased column has occurred directly underneath the base of the encasement for the case of partially-encasement. They also stated that for both full-encasement and partially-encasement of granular column the improvement of column performance was fund to be significant.

Elsawy (2013) studied embankment construction over Bremerhaven clay using full scale unreinforced and reinforced with ordinary and geogrid-encased granular columns by means of

numerical analyses using PLAXIS software. The granular columns were simulated with a diameter of 1.0 m and length of 6.0 m. The results for long-term consolidation analyses indicated that granular column increases bearing capacity of the clay and accelerate the dissipation of excess pore water pressure. As expected, once the granular column is encased, relevant improvement occurs in the performance of granular column. The numerical analyses also showed that the higher stress concentration ratio in the granular columns contributes meaningfully to the acceleration of consolidation process.

Ali et al. (2014) investigated the behavior of GECs using different geosynthetic arrangement. In this study, model tests were carried out on long floating and end-bearing single and groups of columns with and without reinforcement. The tests were performed to evaluate the relative improvement in the failure stress of the composite ground due to different types of reinforcement as shown in Figure 2.27. The exhumed deformed column shapes were used to understand the failure mechanism for different types and configurations of reinforcement. Authors reported that geogrid was the best geosynthetic type for encasement for end-bearing columns; for floating columns, geotextile and geogrid were similarly worthy for laminated columns using horizontal discs of geosynthetic and encasement patterns.

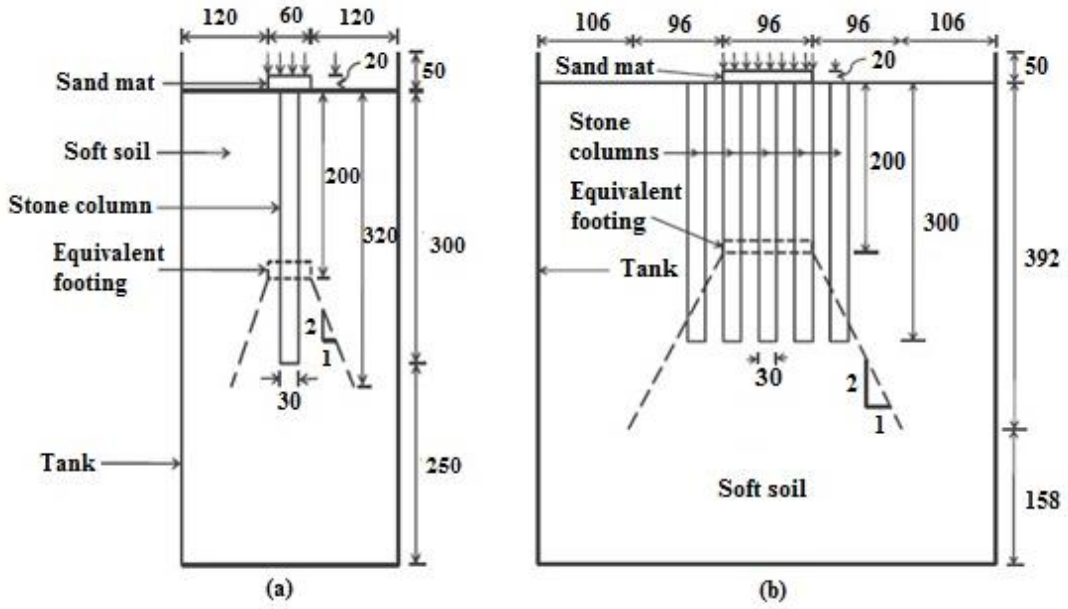

Figure 2.27. (a) Schematic view of the single granular column foundation and (b) schematic view of foundation with group of granular columns. All dimensions are in millimeters (Ali et al., 2014).

Chen et al. (2015) presented laboratory tests and numerical simulations of an embankment reinforced with geosynthetic-encased column. The results of the study showed that the encased column failure was caused by the columns bending. The stability of the embankment was evaluated by 2D and 3D simulations. Based on the obtained results, they came to a conclusion that 3D simulations provided closer estimations to the laboratory tests than 2D simulations.

In recent years there have been various studied on the performance of the encased columns considering column length, column arrangement and influence of encasement (Miranda & Costa, 2016; Castro, 2017; Mohapatra et al., 2017; Hong et al., 2017). However, additional studies are necessary.

2.4. INSTALLATION METHOD

2.4.1. REGULAR INSTALLATION METHODS

For column installation, two common methods (replacement or displacement method) may be used. These methods are depicted in the following parts.

The replacement method uses an open-bottom PVC/steel pipe (casing) equal in diameter to the GEC. The casing is pushed down to the underlying rigid layer. The soil within the pipe is withdrawn using a helical auger to form a cavity. The geosynthetic is then placed inside the pipe and the cavity is filled with the granular material. Granular column content broadly consists of either sand or gravel. When the cavity is totally filled, the pipe is pulled out. To achieve the desired relative density of the column material, the column material can be compacted by vibrating the pipe as long as the pipe is dragged out. The replacement method installation is shown in Figure 2.28.

In displacement method pipe is pushed down with/without vibration to the rigid layer. The casing tip has two small traps which are closed through driving, resulting in displacement of the surrounding soft soil. Then, the geosynthetic is placed in the casing and is filled up inside. Finally, the pipe is pulled out and the two small traps are opened due to the weight of the column content above it. This installation method is shown in Figure 2.29. The installation of the displacement method is most widely used for construction of GEC in very soft soils.

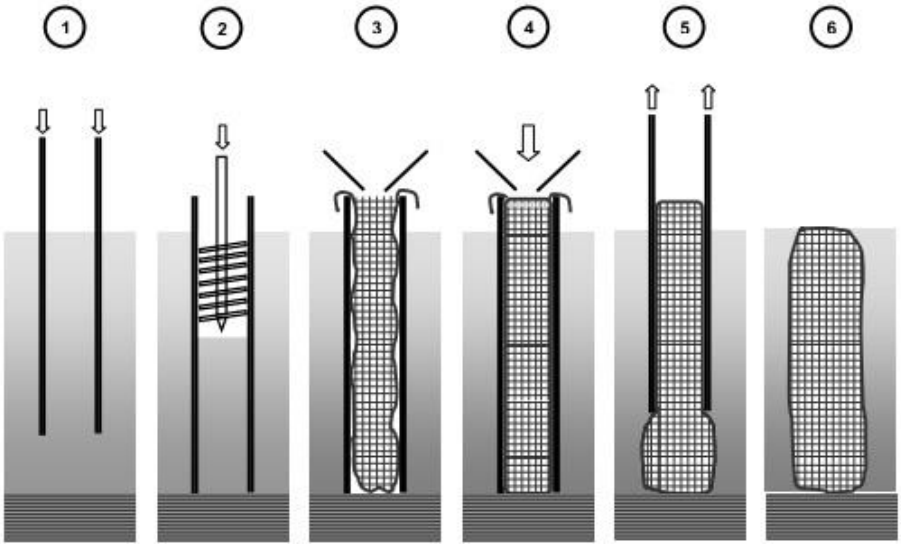

Figure 2.28. Replacement method (Gniel, 2009).

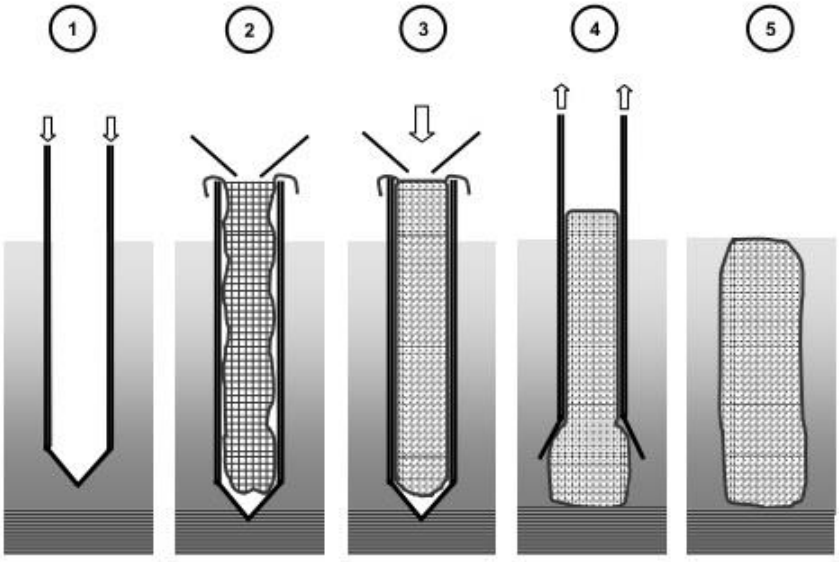

Figure 2.29. Displacement Method (Gniel, 2009).

2.4.2. SPECIFIC INSTALLATION METHODS

The other installation method, cited by researchers (Ali et al., 2012, 2014; Hong et al., 2015) for laboratory tests, is called cast-in place method (Figure 2.30). In this method, the steel/PVC pipe is placed at the center of a box then the remolded clay is placed in regular small stages to avoid air void. After placing the surrounding soil, the column is formed in layers to reach certain value of relative density.

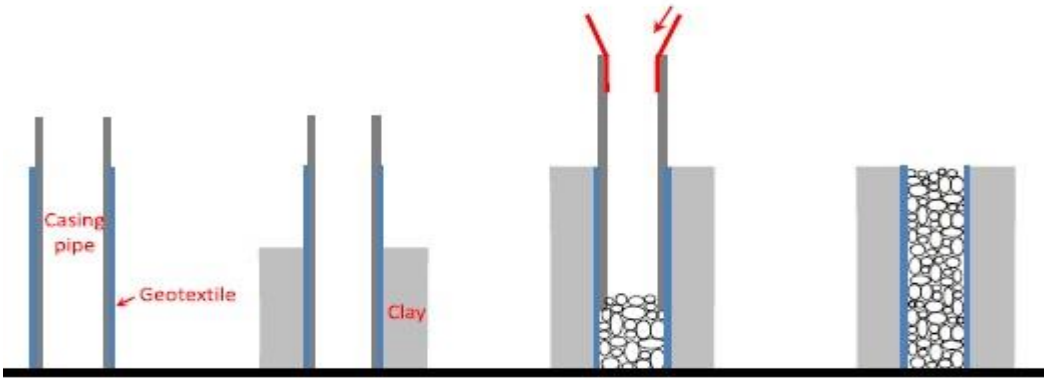

Figure 2.30. Cast-in place method (Hong et al., 2016).

2.5. NUMERICAL SIMULATIONS

After the laboratory tests have been completed, the results were analyzed using back analysis. Numerical analyses were performed using the Finite Element Method (FEM), which is nowadays widely used. Most of the input parameters of the program were defined through laboratory test results.

2.5.1. FINITE ELEMENT METHODS PROGRAM

The PLAXIS (2D and 3D) program was used to analyze the results obtained from laboratory tests with a very friendly graphical user interface. The program allows the use of different types of soil models, construction in stages, possible excavations, the use of beam elements to simulate piles, application of vertical drains, the use of geosynthetic elements to simulate reinforcements, interface elements, besides generating initial pore pressure and excess pore pressure due to the construction (Brinkgreve et al., 2016).

The program consists of two panels: input and output. The first panel models the problem, where its geometry, boundary conditions, material properties and elements that facilitate the analysis such as beam elements, interface, geotextile and vertical drains elements. In addition, the input panel generates the mesh that the user can choose the type of global refinement (very coarse, coarse, medium, fine and very fine) or refine around a point, structural members or further refine along a line of geometry.

The problem can be simulated by 6 or 15-noded in PLAXIS 2D and by 10-noded in PLAXIS 3D. These number mean that the model with higher number of nodes can produce greater number of nodes (applicable for displacement and pore pressure, etc.) and of stress points (applicable for stress-strain curve and pore pressure, etc.). In other words, the higher number of nodes can produce higher level of accuracy.

The type of constitutive model must be defined for all soil types. PLAXIS has various constitutive models for different types of soils (Mohr-Coulomb, Soft-Soil model, Hardening-Soil model, Cam-Clay model) and rocks (Hoek-Brown model).

The program also allows to run User-Defined (UD) soil models. This ability allows users to program their specific models using FORTRAN program.

Mohr-Coulomb model is a linearly elastic perfectly plastic. This model can be used for a first approximation of soil behavior, since it uses a constant stiffness for each type of material. Nevertheless, such a model may be useful in identifying plastic regions. The model based on both Hook's law (linear elastic) and Mohr-Coulomb failure criterion.

Modified Cam-Clay model is used to simulate clays. The overall connection between volume change and pressure in clay can be expressed using the concept of normal consolidation line (NCL) and over-consolidation line (OCL). Passing the intersection with additional stress increase makes the stress state move down along the normal consolidation line. This has similar characteristics to the stress-strain curve of an elasto-hardening plastic model. Hence, the initial linear elastic region of the over-consolidation line can be corresponded to the hardening plastic region of the normal consolidation line.

The material properties of the soil are generally obtained from the one-dimensional consolidation test, such as the Compression index (C_c) and Swelling index (C_s). The compression index and swelling index are related to the Normal consolidation line slope λ and Over-consolidation line slope κ by the following equations.

$$\lambda = \frac{C_c}{2.303} \qquad 2.11$$

$$\kappa = \frac{C_s}{2.303} \qquad 2.12$$

Soft-Soil model was developed to simulate highly compressible soils, such as normally consolidated clays, clayey silts and peats. This model is based on the Cam-Clay model. Some features of this model are:

- Stiffness dependent on the stress level;
- Distinction between primary loading and unloading-reloading;
- Ability to take into account the stress history;
- Failure according to the Mohr-Coulomb criterion.

The modified compression index (λ^*) and modified swelling index (κ^*) are the principal parameters of this soil model. They can be calculated by following equations:

$$\begin{cases} \lambda^* = \dfrac{\lambda}{1+e} \\ \lambda^* = \dfrac{C_c}{2.3(1+e)} \end{cases} \qquad 2.13$$

$$\begin{cases} \kappa^* = \dfrac{\kappa}{1+e} \\ \kappa^* \approx \dfrac{2C_s}{2.3(1+e)} \end{cases} \qquad 2.14$$

In the soil properties of PLAXIS, it is also necessary to define the properties of the interface. This is done by means of the definition of the resistance of the material, which can be rigid, in case the interface has the same resistance of the surrounding soil or manual, where it can be taken into account with the interface resistance reduction factor (R_{int}) using values smaller than one. The program also allows the definition of interface permeability.

For simulation of reinforcement elements, the program has the geogrid element in which the only required input parameter is the tensile stiffness in one direction (EA_1) for isotropic behavior and the tensile stiffness in two directions (EA_1, EA_2) for orthotropic behavior. Thus, this type of element does not resist compression or bending. Defining the geometry and boundary conditions and generating the initial stresses and the mesh, the program at the final

step executes the calculation in the input panel. In this step, it is necessary to choose the type of calculation that will be performed according to the type of analysis that is needed to be done.

PLAXIS has five types of analysis. The first type is plastic (plastic analysis), which is used in the analysis of elastoplastic deformations where it is not necessary to include the effects of excessive deformations. This type of analysis is used in several applications in geotechnical engineering.
The second type is the consolidation analysis that is that usually applicable when there need to analyze the time dependent development of excess pore water pressure in a saturated clay type soil. The third one is the safety analysis that can calculate safety factor. Safety factor is calculated as a function of shear strength parameters as following equation:

$$SF = \frac{\tan \varphi_{input}}{\tan \varphi_{reduced}} = \frac{c_{input}}{c_{reduced}} = \frac{S_{u,input}}{S_{u,reduced}} \qquad 2.15$$

where,
φ: Friction angle;
c: Cohesion;
S_u: Undrained shear strength.

The fourth type is dynamic analysis that is related to those problem which are involved with dynamic loadings. The final type of analysis is fully coupled flow-deformation that considers simultaneously the development of deformations and pore pressures in a saturated or partially saturated soil as a result of time-dependent changes of the hydraulic boundary conditions. Thus, this type of analysis can be considered for dams and embankments that are subjected to tidal waves.

PLAXIS Output panel is capable to graphically display the post-processing results. In this part of the program, several types of results can be shown graphically. In addition, there can be selected a cross section and ask the program to draw some kind of displacement, deformation or stress along that section. In this panel, user is able to draw the curves of deformation and excess pore water pressure versus time and also many other results that can be drawn out of the results.

3. METHODOLOGY

In this research, the performance of geosynthetic reinforced granular columns was studied by means of a three-stage approach. This includes (a) large-scale laboratory analysis of reinforced column; (b) numerical simulation of the large-scale tests; (c) full-scale numerical modelling to examine the behavior of encased column group.

3.1. MATERIALS

The following part presents the physical properties and behavior of the materials chosen for utilize in large-scale laboratory tests. This part includes the properties of the collected soil and the materials that have been used as the column contents and three types of geotextile (G-1, G-2, and G-3) that were used as the column reinforcement. The three different types of materials used as the column content were sand, gravel, and Construction Waste (CW). Sand is a typical type of material for geotextile encased column but, in this study, it was decided to use other type of materials in order to find the efficiency of these materials for improvement in the performance of the technique. The use of CW can lead to important economic and environmental benefits. It preserves both energy and resources.

3.1.1. COLLECTED SOIL

To study the behavior of geosynthetic reinforced columns, a very soft soil was necessary to have a better understanding on the proficiency of encased granular column. The soft soil samples were desired to be homogeneous and behave as a reliable material.

Since the size of the test box was quite large, therefore, there was needed to prepare 5 to 7 tons of soil. The collected soil was spread out on a thick plastic sheet and was turned over for 10 days in order to become dry. After dying, the soil was sieved to by the sieve No.10 (2 mm).

Particle size distribution of the soil, with and without dispersing agent, is presented in Figure 3.1. Before sieving the soil was smashed manually but yet there were many tiny clusters that affect the particle size distribution curve. By pulverizing the soil mechanically or using

dispersing agent, it can be possible to get rid of the tiny clusters. The soil parameters derived from the curve (Figure 3.1a) are presented in Table 3.1.

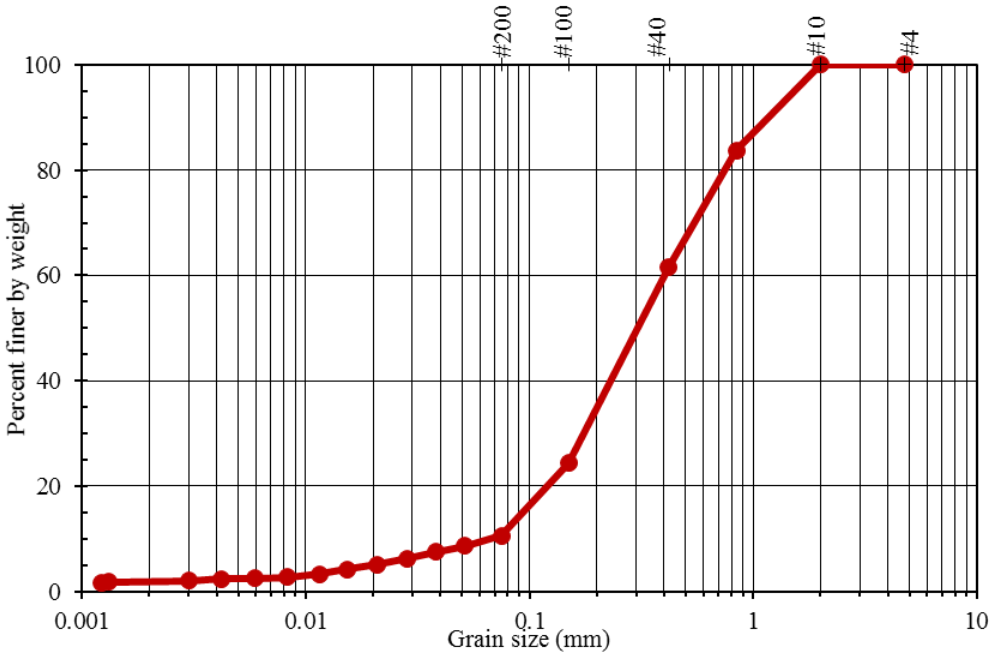

(a)

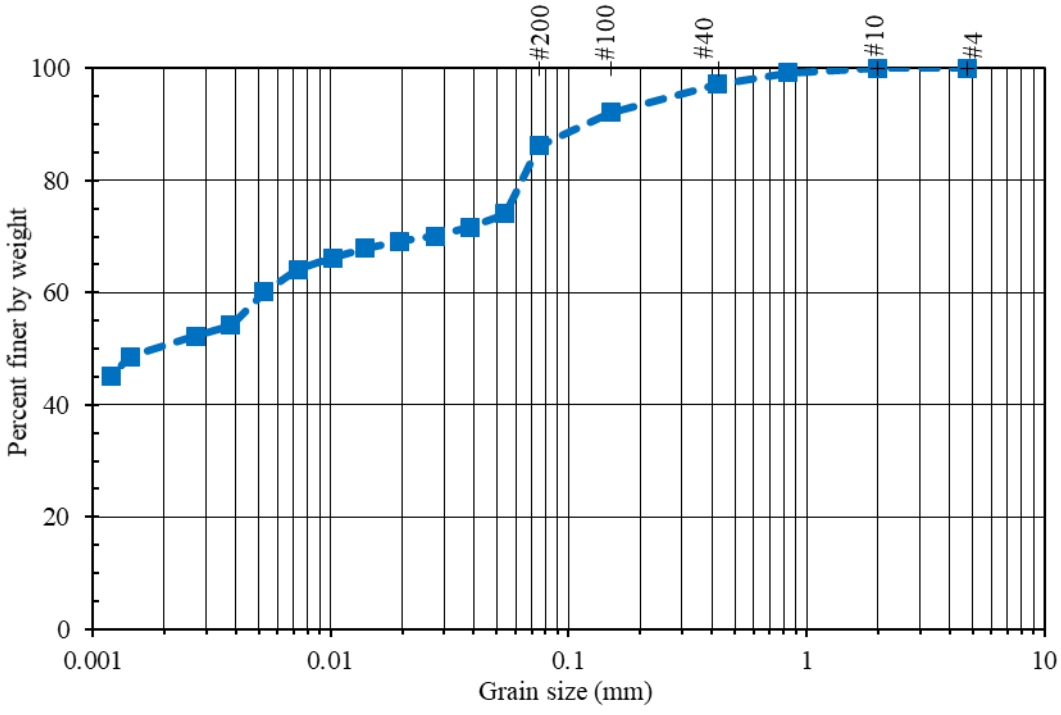

(b)

Figure 3.1.Particle size distribution of the soil: (a) without dispersing agent and (b) with dispersing agent.

Table 3.1. Soil parameters.

Parameters	Value
C_u (-)	5.5
C_c (-)	1.05
D_{50} (mm)	0.304
D_{10} (mm)	0.073
D_{30} (mm)	0.175
D_{60} (mm)	0.401

In order to obtain a very soft soil condition, bentonite was added to the collected soil (Mollins et al.,1995). The liquid limit (w_L) and plastic limit (w_P) of the soil without bentonite and mixed with 4% bentonite were measured based on Brazilian Standards NBR-6459/ABNT (1984) and NBR-7180/ABNT (1984), respectively. These limits, specific gravity (G_s), void ratio (e) and dry unit weight (γ_{dry}) for the soil are available in Table 3.2.

Table 3.2. Properties of the soil used in model test.

Soil parameters	Value		
	without bentonite	4% bentonite	bentonite
w_L (%)	39	60	495
I_P (%)	10	21	435
G_s (-)	2.68	2.7	2.76
e (-)	1.27	1.23	1.1
γ_s (kN/m^3)	26.75	27.05	28.5

The study aimed at investigating the excess pore water pressure caused by the column installation method (displacement method) and loading tests of the reinforced column. One of the most important factors to decide about the percentage of bentonite addition was the permeability of the soil. This unsaturated soil, as shown in particle size distribution section, is almost a sandy soil. For determination of permeability (k), based on NBR-13292/ABNT (1995) and NBR-14545/ABNT (2000), the constant and falling head permeability tests were carried out for the soil before and after bentonite addition, respectively. The permeability of the soil before and after adding bentonite is shown in Table 3.3.

Table 3.3. Permeability of the soil.

Permeability	Value	
	without bentonite	4% bentonite
Calculated by average (cm/s)	2.23×10^{-3}	4.93×10^{-5}
Calculated by average at 20°c (cm/s)	1.94×10^{-3}	4.2×10^{-5}

An important factor of this study was to install encased granular columns in a homogeneous soil with low undrained shear strength. Since the projects that have applied encased column as the ground improvement, were dealing with extremely soft soils (Raithel et al., 2004; Alexiew et al., 2015), in this study undrained shear strength was aimed to be less than 5 kPa.

To reach the desired undrained shear strength soil sample was mixed with water as long as sample obtains a uniform and consistent paste to reach a water content of about 60%. The percentage of water content was determined by trial and error.

Consolidation test (Figure 3.2) of the soil was carried out in order to find compression index (C_c) and swelling index (C_s). The test results offered C_c and C_s to be 0.47 and 0.03, respectively.

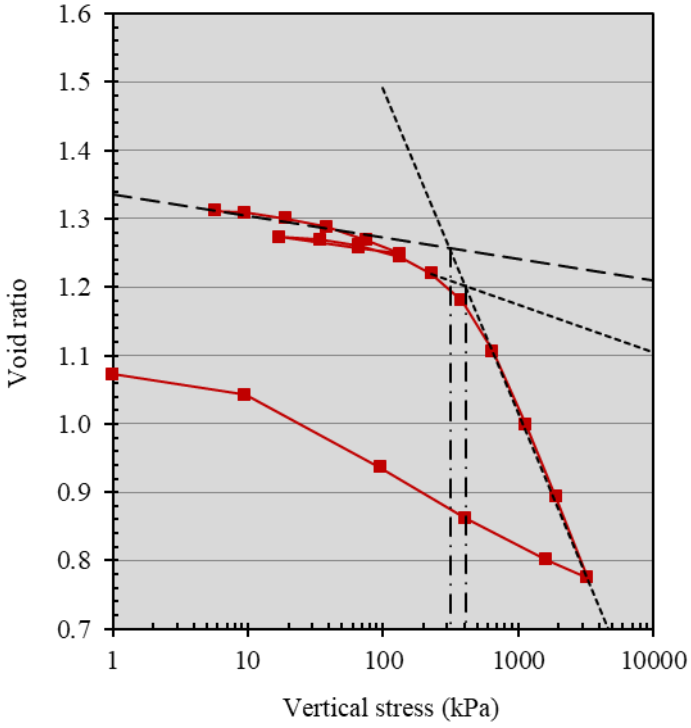

Figure 3.2. Consolidation test of soil.

3.1.2. COLUMN MATERIALS

Sand is a common material to use as the column material for geotextile encased column. The particle size distribution of the sand used in the tests is shown in Figure 3.4-a. As it was mentioned before, for evaluating the capability of other coarse-grained materials such as gravel and CW, it was utilized these two types of material for forming the granular column (Figure 3.3).

(a) (b)

Figure 3.3. Column materials: (a) gravel and (b) CW.

Desired size of gravel was commercially available (gravel 00) and its particle size distribution is depicted in Figure 3.4-b. The very need of using construction waste (CW) has resulted in environmentally-friendly projects that support the reuse of this type of materials. The main importance is to encourage construction projects to reuse large quantities of CW and on the other hand to reduce the costs of the projects. CW, typically, presents a variety of materials with different sizes. To achieve the desired size, all the materials were sieved by the sieve NO. 3/4". The particle size distribution of CW is shown in Figure 3.4-c. Table 3.4 presents the parameters of the column materials.

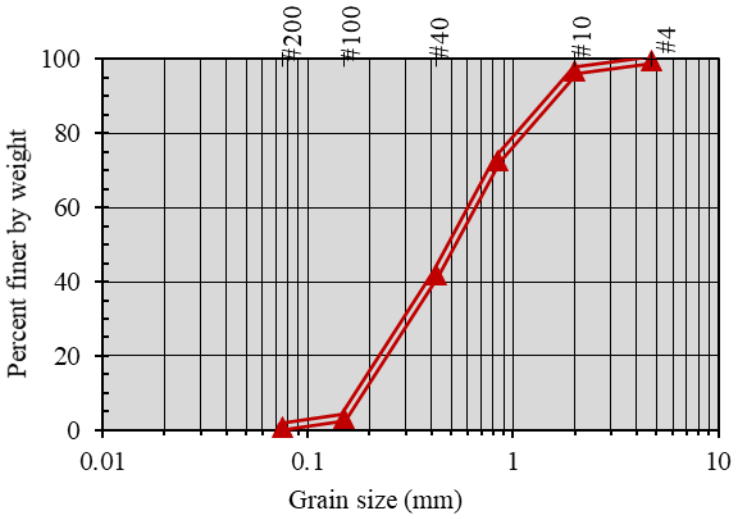

(a)

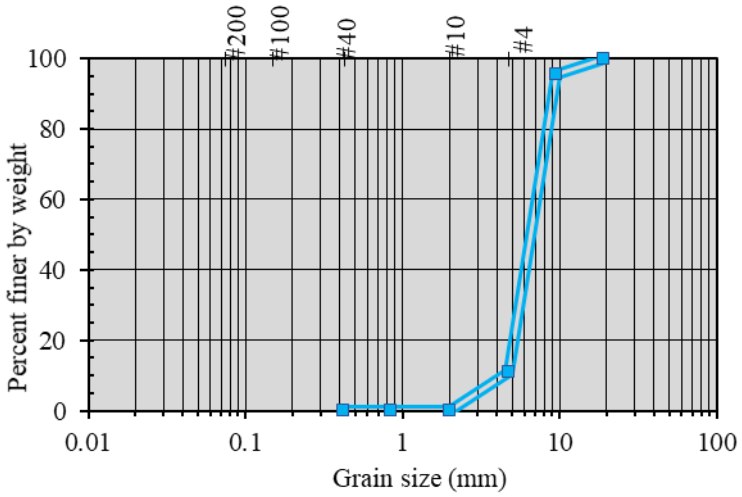

(b)

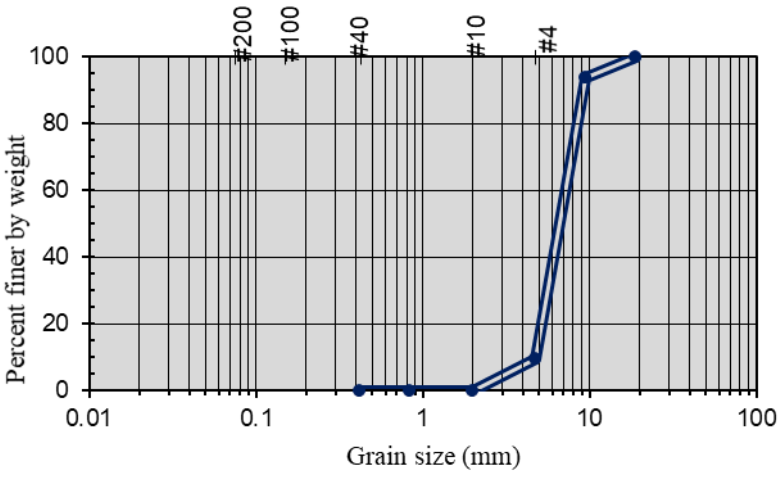

(c)

Figure 3.4. Particle sized distribution of column materials: (a) sand, (b) gravel and (c) CW.

Table 3.4. Parameters of particle size distribution.

Parameters	Sand	Gravel	CW
C_u (-)	3.51	1.6	1.5
C_c (-)	0.825	0.98	0.92
D_{50} (mm)	0.50	6.55	6.64
D_{10} (mm)	0.179	4.44	4.78
D_{30} (mm)	0.305	5.56	5.64
D_{60} (mm)	0.63	7.11	7.21
e_{max} (-)	0.87	0.74	0.76
e_{min} (-)	0.6	0.41	0.45
G_s	2.65	2.66	2.65

Based on the installation method, granular column commonly has a relative density ranging between 50% and 100% (Ali et al., 2012). In order to obtain the unit weigh of the sand, gravel CW columns, three samples of each type were prepared by three different geotextile types (G-1, G-2, and G-3). The geotextiles were sealed at the bottom by non-woven geotextile as shown in Figure 3.5. Then the columns of about 40 cm in high and 15 cm in diameter (section 3.5), were filled by sand, gravel, and CW in stages. Based on the weight and volume obtained from these small column, the values of relative density of 82% for the sand and 85% for the gravel and CW were obtained.

Figure 3.5. Use of non-woven geotextile to seal the bottom of encasement.

Direct shear tests by standard apparatus of this test, were carried out to determine the friction angle of sand, gravel and CW. Due to the grain size of the gravel and CW that may affect the results of the tests, in addition, it was decided to utilize the apparatus of medium scale direct shear test (samples of 300 mm x 300 mm x 175 mm) that was available in the laboratory of geotechnical department as shown in Figure 3.6. The test results for sand, gravel and CW are shown in Figure 3.7.

Based on the desired value of relative density, samples were prepared. The normal stresses, for the shear tests, were equal to 50 kPa, 150 kPa, 250 kPa and 350 kPa. The friction angle of each type of material is presented in Table 3.5. For each test the samples were prepared based on the desired relative density which was measure based on the volume and weight of the material (gravel and CW) obtained from smalls columns tests (section 3.5).

In case of using gravel or CW, there could be some damages to the geotextile encasement during the process of compaction and vibration of the column to reach desired relative density. These damages can affect the performance of geotextile and consequently reduce the bearing capacity of the encased column.

Figure 3.6. Apparatus of medium scale direct shear test.

Table 3.5. Peak friction angle of the column materials.

Test type	Standard direct shear test			Medium scale direct shear test	
Material	sand	gravel	CW	gravel	CW
Friction angle (˚)	40.5	44	43	43	42

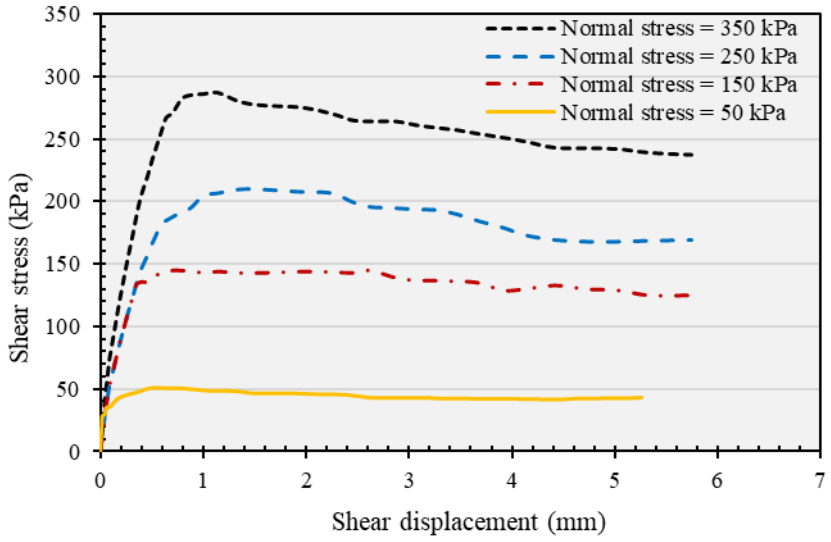

(a)

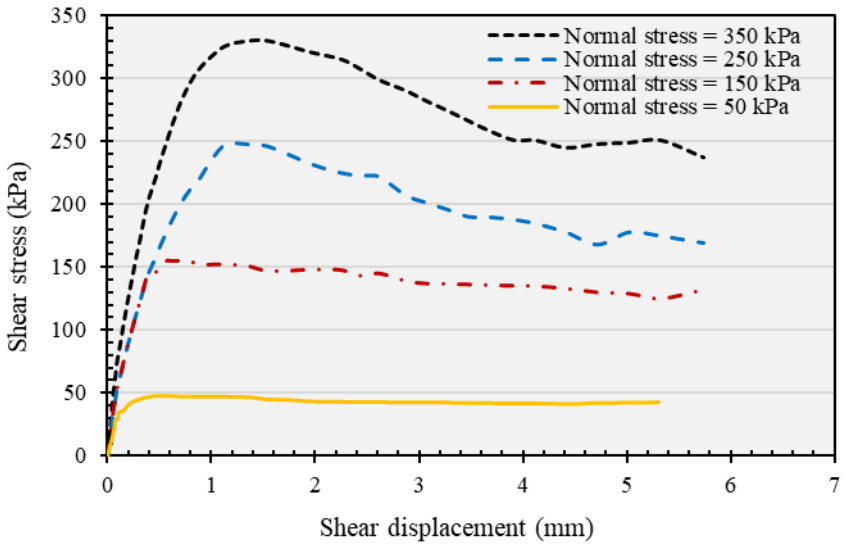

(b)

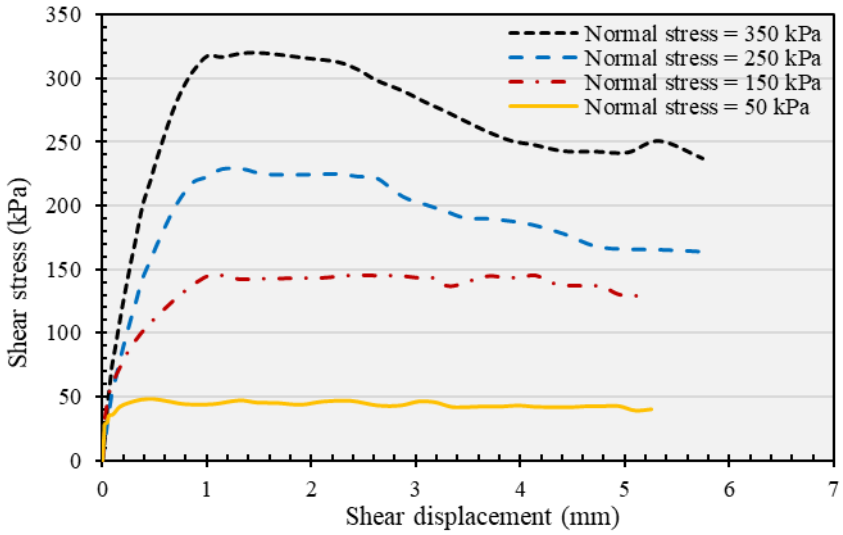

(c)

Figure 3.7. Direct shear test: (a) sand, (b) gravel and (c) CW.

3.1.3. GEOTEXTILE

A key challenge in model studies working with geosynthetic materials is selection of appropriate materials. In order to have similar behavior between the prototype and model, similarity analysis can be used to reach scaling factor. Baker et al. (1991) widely explained the similarity analysis. The relationship provided by Baker et al. (1991), assume scaling factor (λ) to be calculated as:

$$\lambda = \frac{f_P}{f_m} \qquad (3.1)$$

where f_P and f_m are physical measures that are related to the prototype and the model, respectively. In case of GEC, scaling factor can be determined as the ratio of the diameter of prototype divided by the diameter of model ($\lambda = D_p / D_m$).

Three types of woven geotextile were selected to study the effects of geosynthetic stiffness and strength on the performance of the encased column in very soft soil. This study aimed to reach model test results compatible with prototype results. To this end, the scaling factor was used to choose the properties of the geosynthetic materials utilized in the tests. The diameter of encased columns employed in the projects reported by Raithel et al. (2002, 2004), Alexiew et al. (2003) and Araujo et al. (2009) was 0.4-1 m and the model test diameter was selected to be 0.15 m. Thus, the scaling factor (λ) was calculated to be approximately 2 to 7.

Considering the scaling factor and the tensile strength/stiffness of the woven geotextile materials that are available in market (tensile strength = 10 – 500 kN/m and tensile stiffness = 50 – 2000 kN/m), the tensile strength and the tensile stiffness of the model can be varied approximately between 1.5 to 85 kN/m and between 8 to 335 kN/m, respectively.

Three types of woven geotextile (G-1, G-2 and G-3) were chosen. G-1 has the highest values because it´s a reinforcement used for real cases of GEC with a diameter of 40 cm. The properties of the geotextile materials are given in Table 3.6.

Table 3.6. Properties of woven geotextile.

Properties	Woven geotextile		
	G-1	G-2	G-3
Tensile strength (kN/m)	100	55	35
Tensile stiffness (kN/m)	950	366	233
Maximum strain (%)	6	15	15
Thickness (mm)	0.6	0.6	0.4
Mass per unit weight (g/m^2)	360	272	163
Polymer type	Polyvinyl Alcohol	polypropylene	polypropylene

Since the desired diameter of geotextile sleeves (15cm) was not commercially-available, it was necessary to prepare them using seam. Generally, three types of stitching seam (butterfly seam, J-seam and flat/prayer seam) may be employed to prepare sleeves. In order to prepare test samples for the laboratory experiments in general accordance with NBR-13134/ABNT (1994), each sample should be approximately 250 mm wide with a stitch interval in the center for the seam. The sample should be cut at the both sides of sample (shaded areas) to accomplish a final width of 200 mm as shown in Figure 3.8.

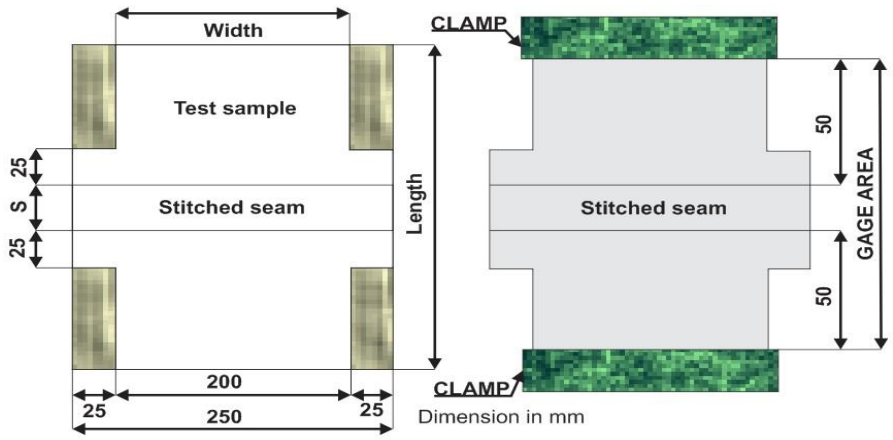

Figure 3.8. Sample test preparation for wide strip tensile tests.

In butterfly seam type, as shown in Figure 3.9-a, both parts of the geotextile are folded in different sides. In other words, geotextile edges are folded separately and then sewing is applied to the folded edges. For the J-seam type, as shown in Figure 3.9-b, geotextile edges are folded together at the same side and the flat seam type, Figure 3.9-c, is simple sewing of geotextile edges.

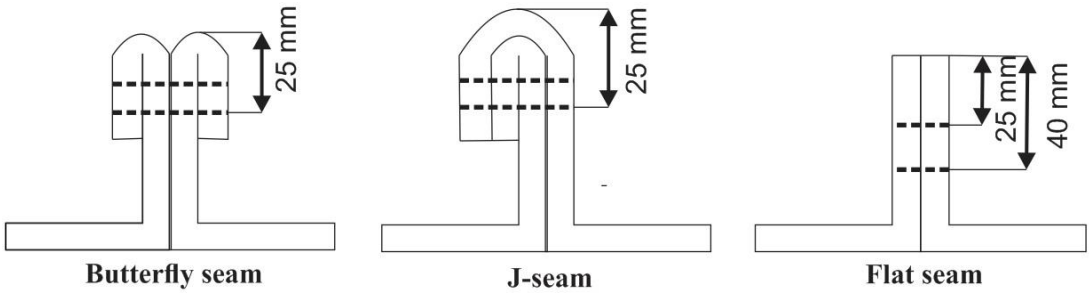

(a) (b) (c)

Figure 3.9. Seam types for sewing.

For G-1, both butterfly and flat seam, were employed to evaluate the efficiency of sewing and its effect on the tensile strength and stiffness. By conducting the test of sewn seam strength on the samples, it was found that the butterfly provided a stronger seam. The results of the tests are presented in Table 3.7.

Table 3.7. Seam properties of G-1.

Properties	Seam type	
	Butterfly	Flat
Ultimate tensile strength of seam (kN/m)	30	12
Strain at ultimate tensile strength (%)	22	10
Stiffness at 5 % strain (kN/m)	120	100
Ultimate strain (%)	50	21

According to the results of seam tests, properties of G-2 and G-3 are presented in Table 3.8. The G-2 and G-3 were prepared by the company using the flat seam. The test results of the G-1, G-2 and G-3 are shown in Figures 3.10, 3.11 and 3.12, respectively.

Table 3.8. Seam properties of geotextiles.

Properties	Geotextile type	
	G-2	G-3
Ultimate tensile strength of seam (kN/m)	16	8
Strain at ultimate tensile strength (%)	16	15
Stiffness at 5 % strain (kN/m)	107	53.4
Ultimate strain (%)	30	27

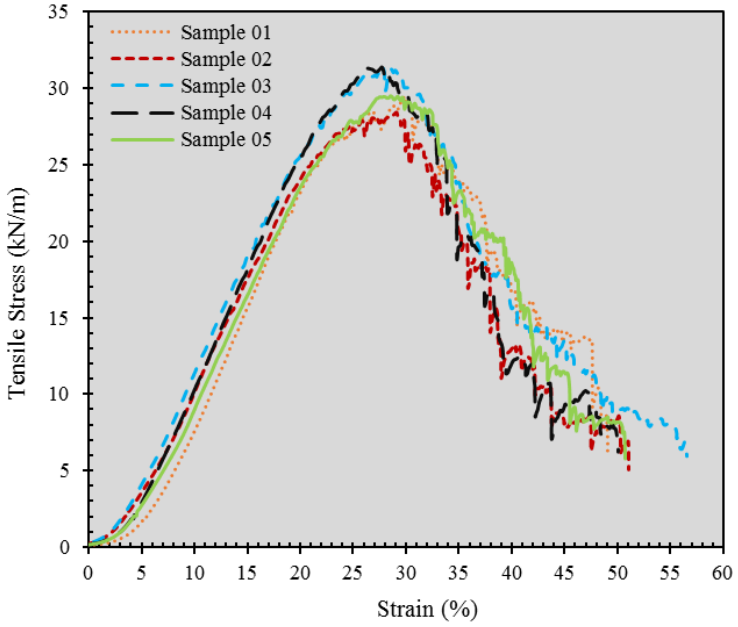

Figure 3.10. Test results of butterfly seam for G-1.

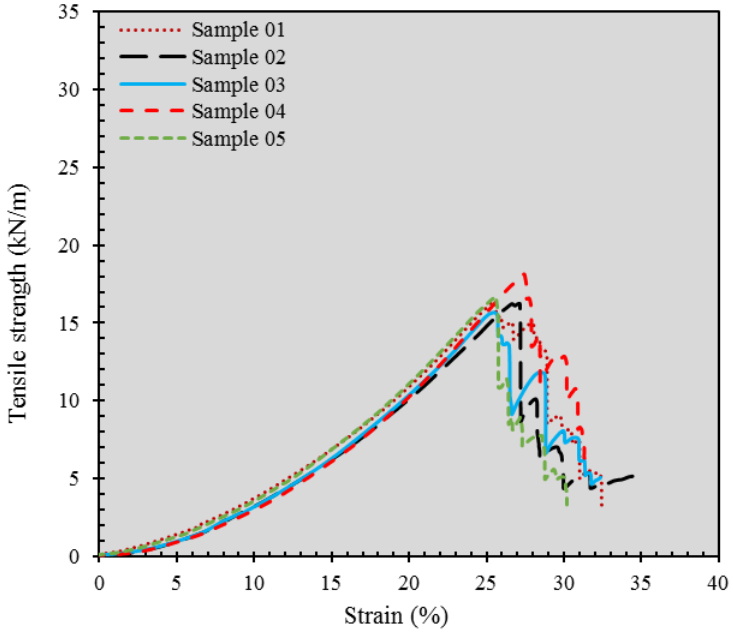

Figure 3.11. Test results of flat seam for G-2.

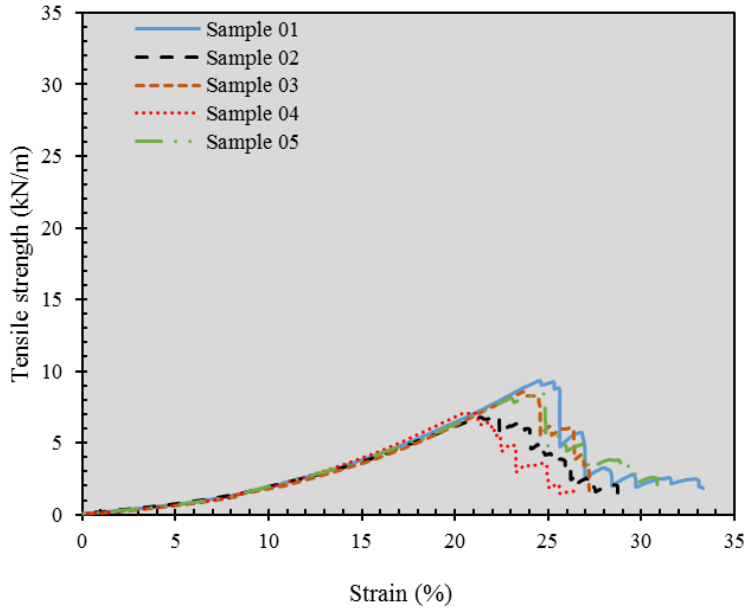

Figure 3.12. Test results of flat seam for G-3.

The seam strength efficiency can be calculated by following equation:

$$S_E = \frac{T_{\text{seam}}}{T_g} \times 100\ (\%) \qquad (3.2)$$

where T_{seam} and T_g are wide width seam strength (NBR 13134/ABNT - 1994) and wide width geosynthetic strength without seam (NBR 12824/ABNT - 1993). The G-1 butterfly and flat seams represented the seam strength efficiency of about 12.6% and 10.5%, respectively. This value for the G-2 and G-3 was measured to be about 29% and 23%, respectively.

3.2. SOIL PASTE AND BOX PREPARATION

Firstly, the soil was mixed with the 4% of bentonite in a large mixer that usually is used to make concrete. The water was added to the soil mixture little by little and this process was continued until the water content was reached to approximately 60%. The soil paste was mixed as long as the paste becomes uniform. The inside parts of the box were completely cleaned and a film of silicon grease was applied to them in order to limit the friction between the wall and soil sample.

In order to monitor the pore water pressure during the tests, it was necessary to provide an undrained condition. To this end, thick plastic sheets were totally covered the inner sides of the box and the overlapping parts of the sheets were covered by duct tape. The plastic sheet was also fixed at the bottom of box by duct tape (Figure 3.13). The plastic sheets also reduce the friction between the soil and the box sides.

Figure 3.13. Preparation of the box for the tests.

After preparing the soil paste, it was folded in large plastic sheets for about 24 hours to let the water content become uniform throughout the soil paste. Then, it was placed in the box in layers of 20 cm thick by manually molding. It was attempted to avoid the air voids as much as possible (Figure 3.14).

Figure 3.14. Placing the soft soil into the box.

3.3. COLUMN INSTALLATION

For installation of the geotextile encased column, by conducting some tests on the small columns with 40cm in length and 15cm in diameter, it was found that relative density can play an important role on the stress-strain behavior of the GEC. Since there was no possibility of providing efficient vibration to the column by regular installation methods (section 2.4), it was decided to construct the column in layers of 20 cm and provide vibration by hand after placing each layer to control desired volume in order to reach desired relative density. After preparation of the column, it was placed in a PVC pipe which was sealed at the bottom by geomembrane. Then the pipe was pushed into the soft soil until the bottom of the box. When the column reached to the desired depth, the pipe was carefully removed (Figure 3.15). In order to keep the column being perpendicular to the base of the box, it was utilized a wood casing at the top of the soil surface as shown in Figure 3.16. The preparation of the column material and the column installation method are shown in Figure 3.17.

(a) (b)

Figure 3.15. Installation of Column: (a) pipe insertion and (b) pipe removal.

Figure 3.16. Use of the wood casing for pipe insertion.

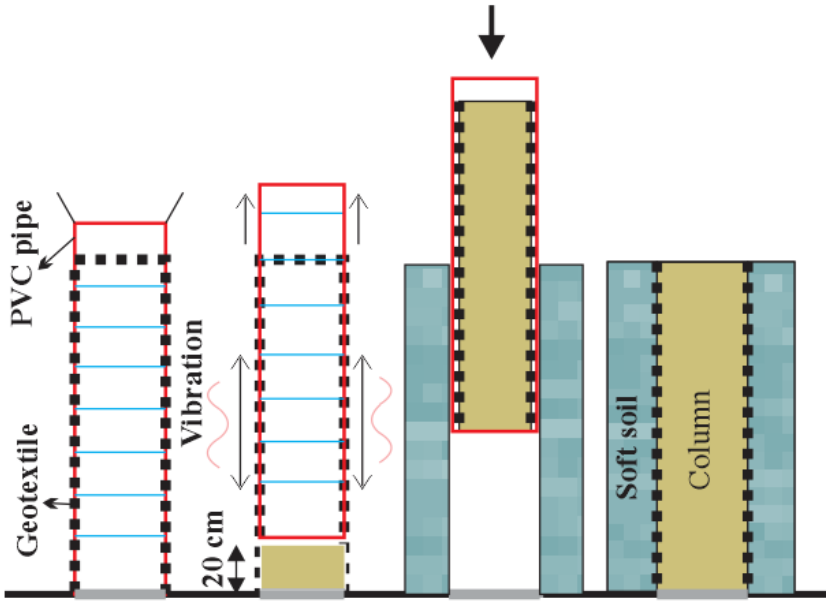

Figure 3.17. Column preparation and installation procedures.

3.4. INSTRUMENTATION

To observe excess pore water pressure, due to the installation method and loading test, inside the soft soil, six piezometers were employed. Three pressure cells were installed horizontally at the column side to observe lateral earth pressure around column. To monitor the stress-strain behavior of the GEC, four displacement transducers and a load cell were used. Figure 3.18 shows the exact position of each instrument used in the tests.

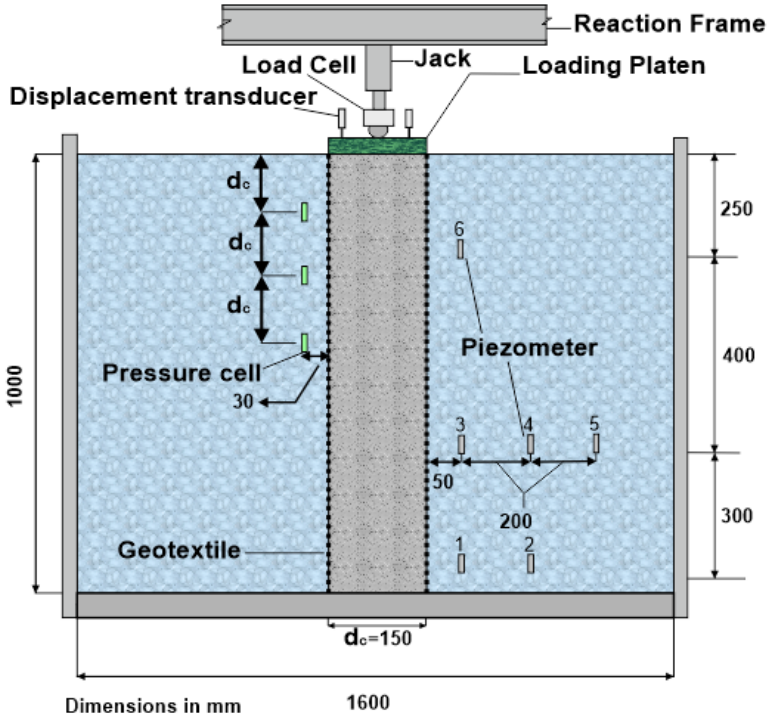

Figure 3.18. Schematic of the load test on GEC.

In order to facilitate the understanding of this type of soil improvement, it was employed a set of instruments to monitor the column and soil behavior during the column installation and loading tests. At the very beginning, it was needed to calibrate all the instruments. Calibration needs to be done in an appropriate way by taking into account the very specifications of instruments which are to be used.

3.4.1. ACQUISITION SYSTEM

The very first equipment in any monitoring instrumentation is the acquisition system. It works as the brain of research as it collects all the information that are reported by each instrument to a specific canal. In other words, commonly, all the instruments are electric devices which report electrical signals to the acquisition system, and it interprets all these signals to the practical units to make sense out of them. Based on the type of instrument, there must be applied a specific configuration to the canal in which the desired instrument is to be connected.

In this study, each canal of the acquisition system was configured based on the requirements and characteristics of the desired instrument. Figure 3.19 shows the acquisition system used for interpretation of the instruments outcome. It offers 16 canals to be connected with desired

instruments. The system allows readings of DC or AC voltage signals in single mode up to ± 10V.

The configuration of each type of instruments (full bridge, half bridge and one quarter bridge, etc.) depends on the instructions provided by its company. For instance, generally, for load cell the configuration should be set based on the full bridge specifications that is shown in Figure 3.20.

Figure 3.19. Acquisition system.

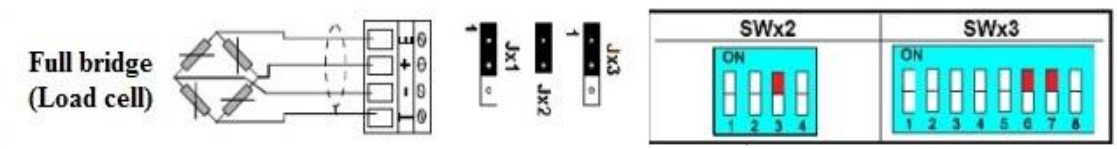

Figure 3.20. Configuration of the full bridge connection for load cell (Lynx manual, 2005).

3.4.2. LOAD CELL

A load cell was employed to measure the load transferred to the top of the column. It was calibrated by using a calibrated compression machine as shown in Figure 3.21. In order to do this, the load cell outcomes were registered by means of acquisition system for certain amounts of loading then the results were plotted in a graph to check out the preciseness of results. Figure 3.22 shows the two types of load cells (LC-1 and LC-2) with different loading capacity. The maximum capacity of LC-1 and LC-2 is about 300 kN and 20 kN, respectively (calibration appendix A).

Figure 3.21. Calibration of load cell.

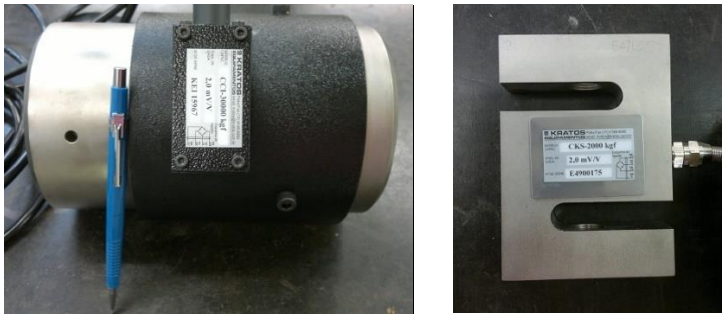

(a) (b)

Figure 3.22. Load cells: (a) LC-1 and (b) LC-2.

3.4.3. DISPLACEMENT TRANSDUCER

For the sake of measuring vertical displacement on the top of column, four displacement transducers were calibrated. The calibration was conducted using level measuring tool, compression machine (capable of moving manually), magnetic measuring stand and dial gauge. Before starting the calibration of displacement transducer, dial gauge was calibrated using micrometer. The displacement transducer and the dial gauge were fixed to the lateral supports of the compression machine, then both of them were leveled. By moving the arm of compression machine and reading the dial gauge, the corresponding value for the displacement transducer were recorded by data logger. As shown in Figure 3.23, this procedure was continued

for regular intervals until reaching enough points that represent appropriate calibration of instrument (calibration appendix B).

Figure 3.23. Calibration of Displacement transducer.

3.4.4. PRESSURE CELL

Three pressure cells were calibrated in this study. Generally, in calibration of pressure cell two important effects should be considered. Firstly, normal stress distribution at the surface between the pressure cell and the soil should be uniform. Secondly, based on the design method, when the pressure cell deflects, an arching type phenomenon may develop. Thus, calibration requires to occur in the same type of soil to be used in the tests (very soft soil). Since the cells were calibrated in very soft soil ($S_u < 15$ kPa) the probability of having the arching phenomenon was miniscule. The calibration was carried out inside a small box (Figure 3.24).

The soil was prepared and placed inside the box in two layers. The pressure cell was placed at the surface of the first layer before placing the second layer. Since the pressure cell is sensitive to the density and resistance of the soil, it was conducted vane shear test to measure the undrained shear strength of the soil. To apply uniform stress at the top of second soil layer, normal stress was applied by water pressure through a rubber bag (calibration appendix D).

(a)

(b) (c)

Figure 3.24. (a) Pressure cell calibration, (b) pressure application system and (c) air/water interface.

3.4.5. PIEZOMETER

Six electric piezometers (2.7 cm in diameter and 17 cm in length) were calibrated using pressure controller machine. The pressure controller machine was capable of providing constant water pressure ranging from -100 to 350 kPa with resolution of 1 kPa. The calibration could be carried out by applying increments of water pressure and recording piezometer output by acquisition system (Figure 3.25). Based on the information provided by the company, the precision and linearity of piezometers are about 0.25% and 0.5%, respectively.

Before installation, piezometers should be appropriately prepared. To this end, a large bucket was filled with water and piezometer was totally submerged in water. A small quantity of washed sand was placed at the bottom of a small bag of non-woven geotextile then the bag was submerged in the bucket. After placing the piezometer, inside the bag was filled with washed sand as shown in Figure 3.26 (calibration appendix C).

Figure 3.25. Calibration of piezometer.

During the tests there were no registration for piezometer 6 and 5, therefore, it was desided to understand if the size of piezometers could affect the results. To this end, piezometers were connected to laboratory tubings which were closed by porous stones at the other side (Figure 3.27). Then the side of laboratory tubings with porous stones were installed at the same depths of piezometers. The results did not show any difference for the piezometers 5, but piezometer 6 captured some miniscule changes.

Figure 3.26. Piezometer preparation.

Figure 3.27. Porous stone installed into laboratory tubing.

3.4.6. PREPARATION

After preparing the large sample, it was left for 5 days in a controlled condition for water content equalization. During this five-day period, soft soil surface was totally covered by plastic sheets to avoid water content loss (Figure 3.28).

(a) (b)

Figure 3.28. (a) Soft soil surface and (b) soil surface covered by plastic sheets.

3.5. SMALL COLUMNS

For running the large scale test, it was needed to determine the bearing capacity of encased column. To this end, it was decided to conduct the compressibility test on the small samples of encased columns with 15 cm in diameter and 40 cm in length. As show in Figure 3.29, for three types of geotextile (G-1, G-2, and G-3) samples were prepared and tested. Figure 3.29 shows just G-1 and G-2 because G-2 and G-3 are of same appearance.

In order to measure the bearing capacity of small columns, six samples of each type of geotextile were tested. The average bearing capacity of G-1, G-2, and G-3 for the cased of sand column was measured to be 43.15 kN, 23.34 kN, and 13 kN, respectively.

Figure 3.30 indicated the deformation of small columns during the loading test. The failure of seam occurred at a distance of 10 cm from the top of column. Figure 3.31 shows the load-settlement curves of the column for these three types of geotextile.

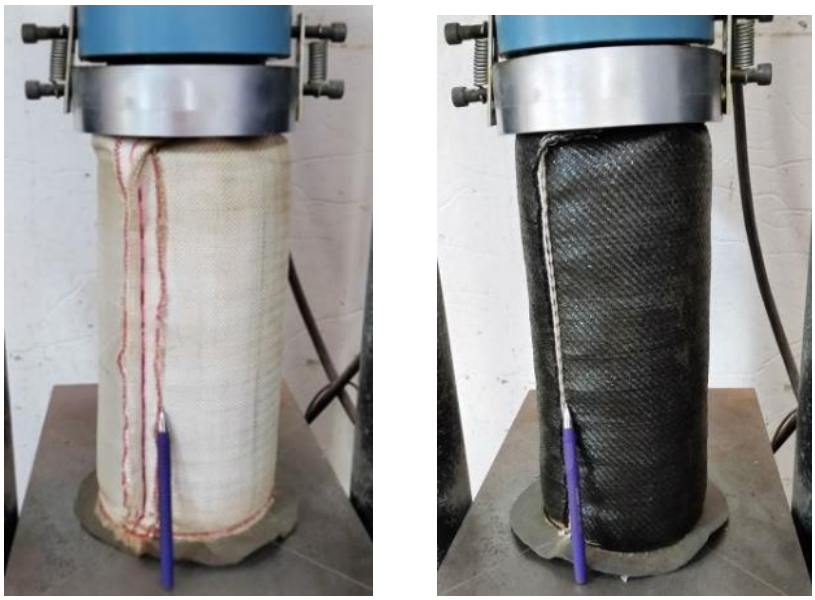

(a) (b)

Figure 3.29. Compressibility test (a) G-1 and (b) G-2.

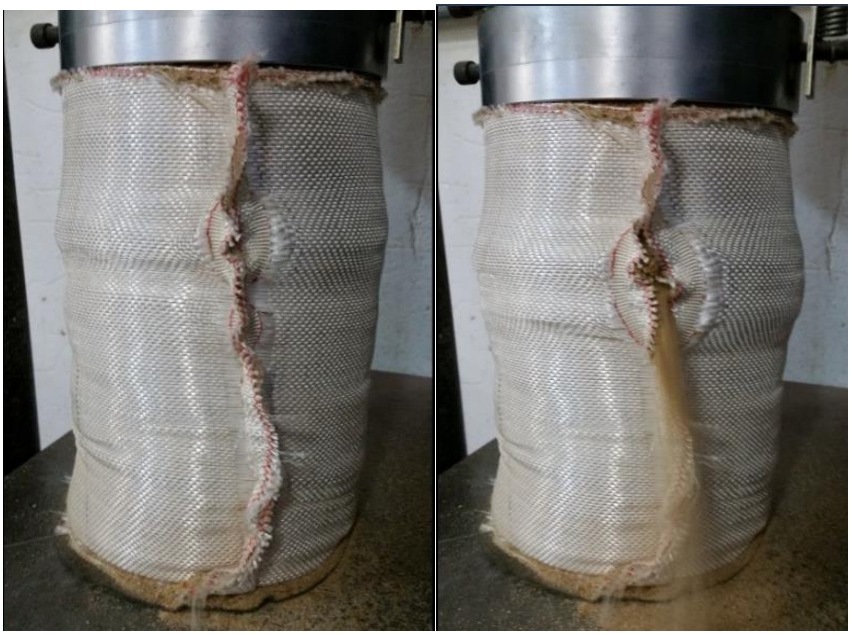

Figure 3.30. Failure of the small columns due to loading at seam.

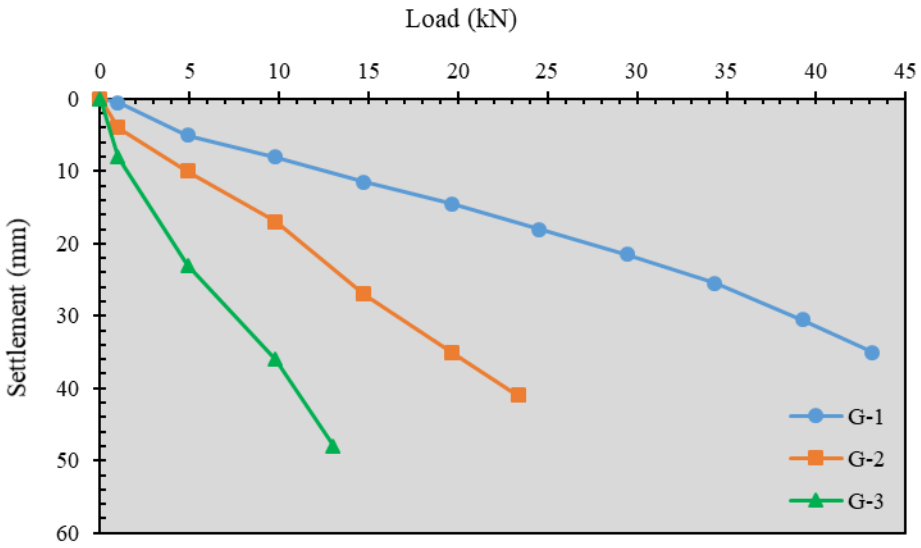

Figure 3.31. Loading test on small columns.

3.6. LARGE COLUMN LOADING AND TEST COMPLETION

The footing area was chosen to be equal to the surface area of encased column (Figure 3.32). Loading was applied on the encased column in regular stages. After each stage, loading was reducing because of column vertical deformation until the readings of the displacement transducers remain in a stable situation. Therefore, it was relevant to record the output of the transducers after each load increment for a short period time of about 20-30 minutes. The loading was continued until the maximum of load bearing capacity was reached (column failure).

After the test completion, the column content was carefully removed until half the column. The upper half of the column was filled with plaster and left for 24 hours, then soft soil around the encased column was removed and the column was exhumed.

Figure 3.33 shows the footing area after the test completion. As it can be seen the water level came above the column surface after the loading test.

Figure 3.32. Footing area of the loading tests.

(a) (b)

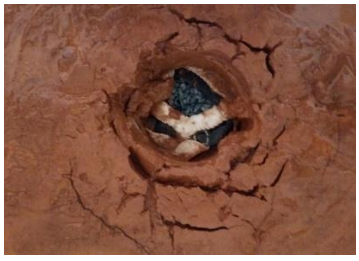

(c)

Figure 3.33. Footing area after loading test: (a) loading platen situation, (b) column surface after removing the loading platen and (c) column surface after removing water.

4. OBTAINED RESULTS OF MODEL TESTS

4.1. SETTLEMENT AND BEARING CAPACITY

Two of the most important factors in design of geotechnical structures are the absolute and differential settlements. The GECs are used to improve the behavior of very soft soils. In any type of improvement method two important limit states should be considered. First, the ultimate limit state which means that the structure must not collapse or become unstable under any conceivable loading. Second, the serviceability limit state which designates that the settlement must be within tolerable limits to avoid the structure being impaired. This shows the significance of load-settlement tests for any kind of foundation system.

The footing area was chosen to be equal to the surface area of encased column and loading was applied on the encased column in regular stages. After each stage, loading was reducing because of column vertical deformation until the readings of the displacement transducers remain in a stable situation. Due to the large measured values of displacement for each loading stage, it was relevant to record the output of the transducers after each load increment for a short period of time of about 20-30 minutes in order to avoid transducers reach its maximum measurement capacity before the column failure. The loading was continued until the ultimate load bearing capacity was achieved and column failed. After the test completion, the column content was carefully removed until half the column. The upper half of the column was filled with plaster and was left for 24 hours, and then soft soil around the encased column was removed in order to exhume the column.

In this study the loading tests, for different column materials and encasement, were compared to each other based on a constant settlement value (50 mm) that was assumed to be equal to 5% of the column length (1 m).

4.1.1. CONVENTIONAL COLUMN

In order to have a better understanding of the influence of geotextile encasement on the behavior of column, conventional columns (sand, gravel, and CW) were tested. Since the higher portion of bearing capacity of conventional columns is due to the confinement provided by the surrounding soil, in case of a very soft soil, they are not expected to support much of the surface

load. As shown in Figure 4.1, all three types of material (sand, gravel, and CW) showed very low performances.

Since for conventional columns the surrounding soil provides confinement to the column content that makes it capable to support surface loads, the undrained shear strength of surrounding soil plays an important role in its the bearing capacity.

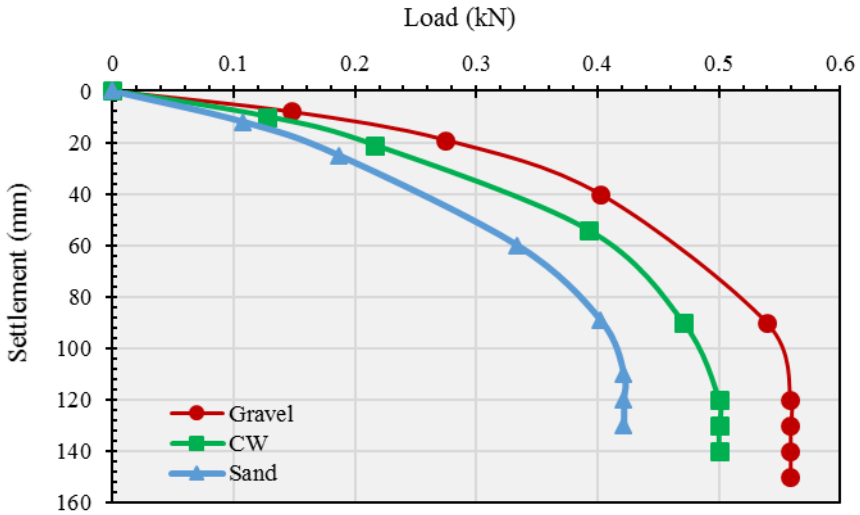

Figure 4.1. Settlement behavior of conventional columns under loading.

4.1.3. ENCASED SAND COLUMN

One of the most popular material for geotextile encased column is sand. This could be for two reasons. First, it may be easier to achieve the rate of desired compaction; and, second, it may cause less damage to the encasement material by comparing it with coarser materials such as gravel.

The results of the load-settlement curve for encased sand column, as shown in Figure 4.2, clearly show the importance of the geotextile tensile stiffness and strength on the behavior of the encased column. In other words, by increasing the value of tensile strength and stiffness of column the load bearing capacity of encased column increases and settlement on the top of the column decreases.

For instance, the bearing capacity corresponding to the settlement value (50 mm) for G-2 is approximately twice of that for G-1 and this scenario continues almost all along the curves. The results of G-1 indicate grater bearing capacity and less settlement than G-2 and G-3.

Figure 4.3 illustrates the exhumed encased sand column 24 hours after the completion of test. It can be seen that the upper part showed lateral bulging. This will be discussed in other section. It just illustrates G-1 and G-2 because G-2 and G-3 had the same appearance.

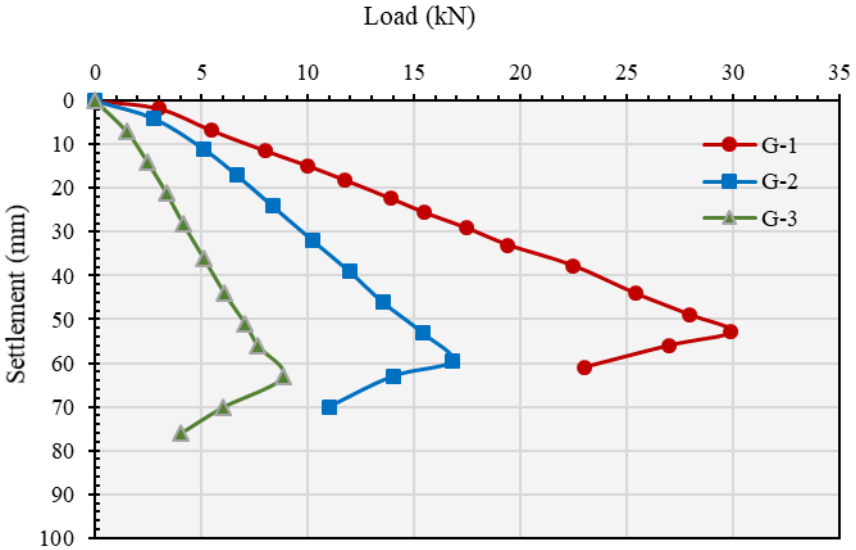

Figure 4.2. Settlement behavior of encased sand column under loading.

(a) (b)

Figure 4.3. Encased column after loading test: (a) G-2 and (b) G-1.

Figure 4.4 shows the comparison between the measured and calculated ultimate bearing capacity of the encased column. The calculated procedure is presented by Briaud, (2013). The results were compared for three types of geotextile (G-1, G-2, and G-3) that were used in this study. The results of analytical method, generally, show a good agreement with those of load testing on the column. There are slight variations between the results. The variations for G-1, G-2, and G-3 were measured to be 0.13 % (the values are almost identical), 6.6%, and 6.17%, respectively.

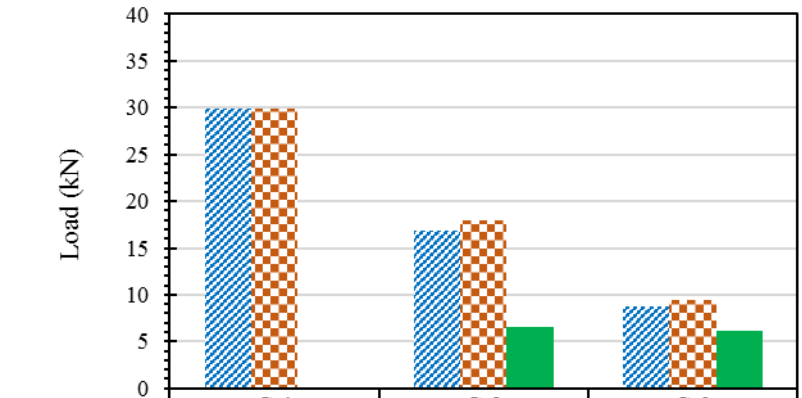

	G-1	G-2	G-3
Measured	29.91	16.8	8.82
Calculated	29.95	17.99	9.4
Variation (%)	0.13	6.6	6.17

Figure 4.4. Ultimate bearing capacity for different types of geotextile for encased sand column.

4.1.4. ENCASED GRAVEL COLUMN

Gravel can be used as an alternative to sand, since it may offer greater friction angle which could increase the bearing capacity of the column. For this study, it was decided to evaluate the performance of encased gravel column compared with encased sand column. Figure 4.5 indicates the loading test on encased gravel column. As it was predicted, gravel improved the bearing capacity of the column.

By comparing the ultimate bearing capacity of gravel and sand columns, the improvement of bearing capacity for G-1, G-2, and G-3 was measured to be 12%, 16.7%, and 22.2%, respectively. It seems that the higher percentage of improvement was contributed to the geotextile with lower value of tensile stiffness.

The settlement obtained for the maximum bearing capacity of the gravel column indicated an increase of about 15% comparing with that of the sand column for G-1. This increase of settlement was calculated to be 10.9% and 9.5% for G-2 and G-3, respectively. This is probably due to gravel breakage and will be discussed in other section latter on.

On the other hand, by comparing the bearing capacity of encased sand and gravel (G-1) obtained for settlement value (50 mm), it was concluded that both encased sand and gravel (G-1) presented almost the same values of bearing capacity.

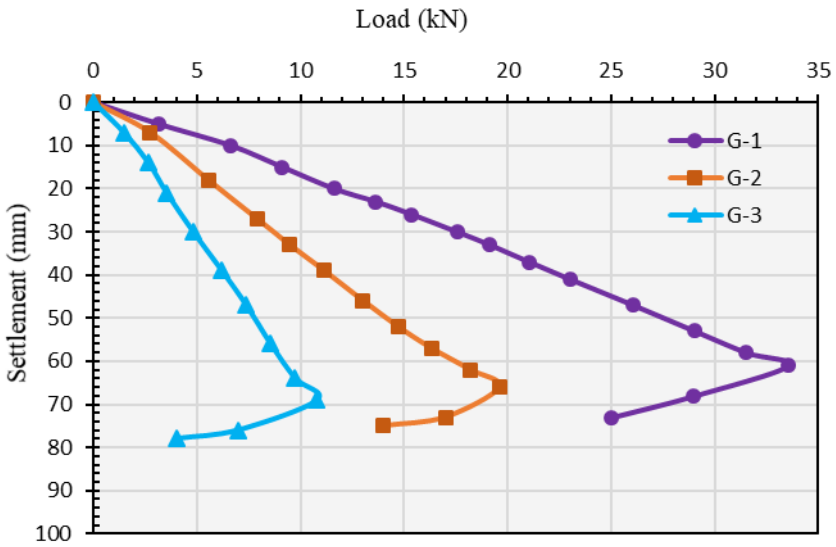

Figure 4.5. Settlement behavior of encased gravel column under loading.

Figure 4.6 outlines the results of ultimate bearing capacity obtained from the loading tests and analytical calculations. The values obtained by analytical calculation reveal some differences for G-3 but when it comes to G-1 and G-2, these differences become greater. The variations for G-1, G-2, and G-3 were measured to be 16.9%, 19.8%, and 14%, respectively. For the case of gravel as a filling material, obtained values by the tests could be influenced by the material breakage.

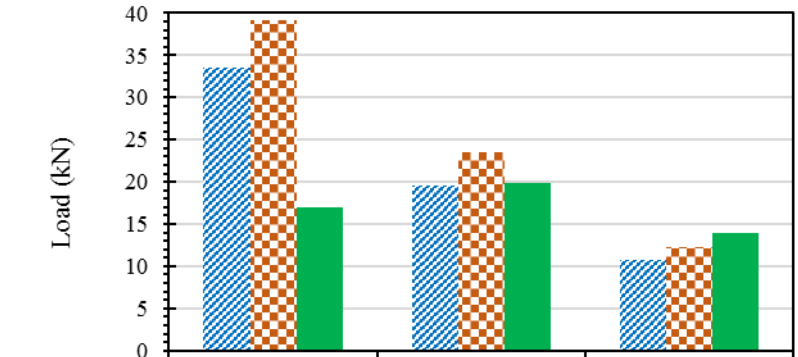

	G-1	G-2	G-3
Measured	33.5	19.61	10.78
Calculated	39.17	23.5	12.3
Variation (%)	16.9	19.8	14

Figure 4.6. Ultimate bearing capacity for different types of geotextile for encased gravel column.

4.1.5. ENCASED CW COLUMN

Reuse of construction materials can represent important environmental and economic benefits. It also preserves both resources and energy. Thus, Construction Waste (CW) was considered to be used as column material in order to evaluate the efficiency of using this kind of material.

The results of loading tests for the settlement value (50 mm) show reduction of the bearing capacity of CW column by comparing it with that of sand column (Figure 4.7). The reduction can be expressed in percentage for G-1, G-2, and G-3, which were measured to be about 25%, 12%, and 14%, respectively. On the other hand, by comparing the results with those of gravel column, it can be concluded that gravel column provides higher values of the bearing capacity.

The other important factor in the column behavior is the total settlement of the column. The growth of settlement for G-1 compared with that of sand column, reaches to a value of about 40% which could affect the design parameters in large scales if there are some limitations for the settlement of desired construction. By measuring the growth value of settlement for G-2 and G-3 to be about 36% and 40%, respectively, it could be concluded that the settlement should be verified to be within tolerable limits in case of using CW column. For both cases (bearing capacity and settlement), the results could be influenced by the breakage of column materials. This will be discussed in other sections.

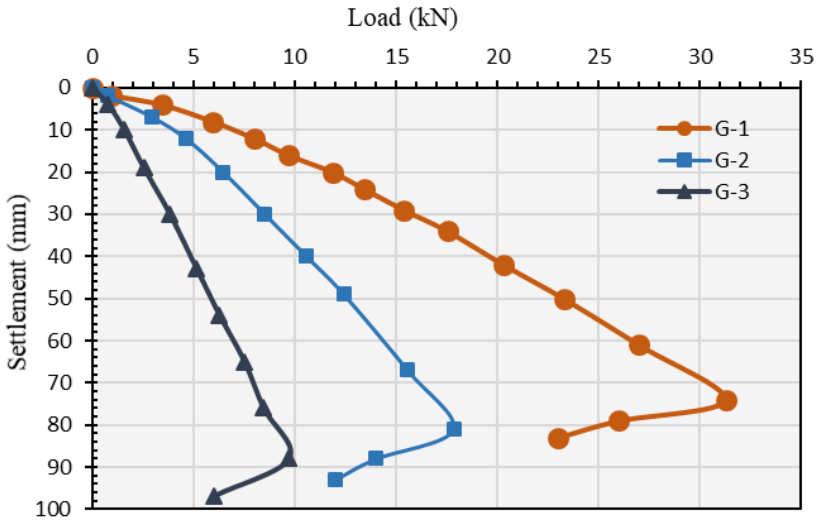

Figure 4.7. Settlement behavior of encased CW column under loading.

Figure 4.8 shows the result of ultimate bearing capacity measured by analytical and experimental methods for CW columns. As it can be seen, there are some differences between them. It can be deduced that, generally, the analytical method suffers from slight overestimations since almost all values obtained from experimental tests (for encased sand column, encased gravel column, and encased CW column) are less than those from analytical calculations. The variations for G-1, G-2, and G-3 were measured to be 12.34%, 18.32%, and 13.8%, respectively.

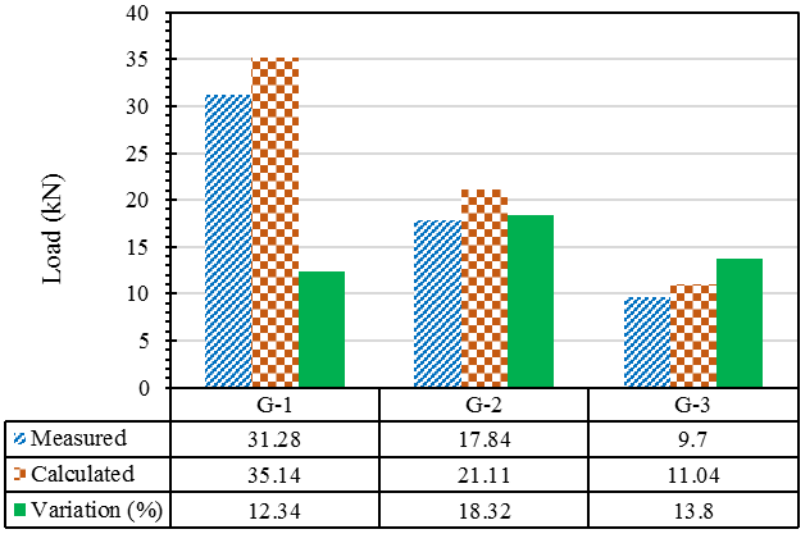

	G-1	G-2	G-3
Measured	31.28	17.84	9.7
Calculated	35.14	21.11	11.04
Variation (%)	12.34	18.32	13.8

Figure 4.8. Ultimate bearing capacity for different types of geotextile for encased CW column.

Figure 4.9 indicates the ultimate bearing capacity obtained from the loading tests. It clearly shows the very important role of encasement and the tensile stiffness and strength of the geotextile in improvement of the ultimate bearing capacity of column. Conventional columns (Con.Column) are suffered from very small bearing capacity. For instance, the ultimate bearing capacity of conventional sand column was improved by a factor of about 71 (G-1), 40 (G-2), and 21 (G-3). On the other hand, the bearing capacity obtained for the settlement value (50 mm, 5% of the column length) shows that the encased sand columns presented better performance compared to the encased gravel and CW columns (Figure 4.10).

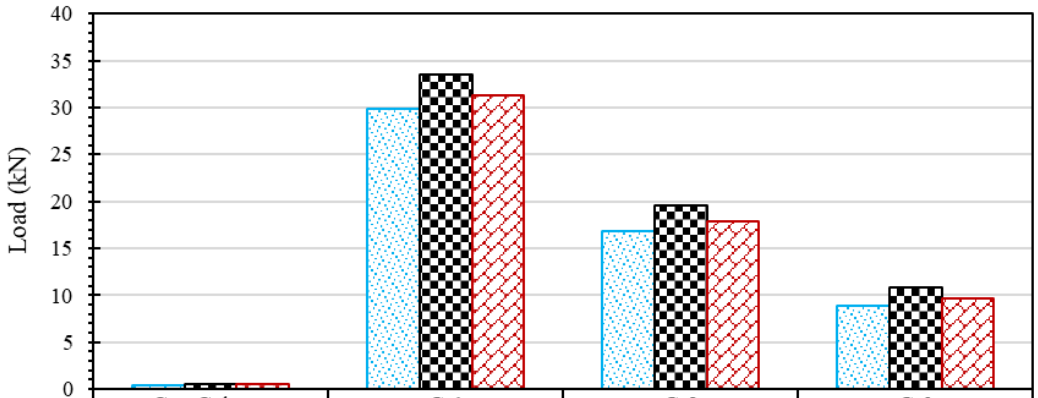

	Con.Column	G-1	G-2	G-3
sand	0.42	29.91	16.8	8.82
gravel	0.56	33.5	19.61	10.78
CW	0.50	31.28	17.84	9.7

Figure 4.9. Ultimate bearing capacity of the encased and conventional column.

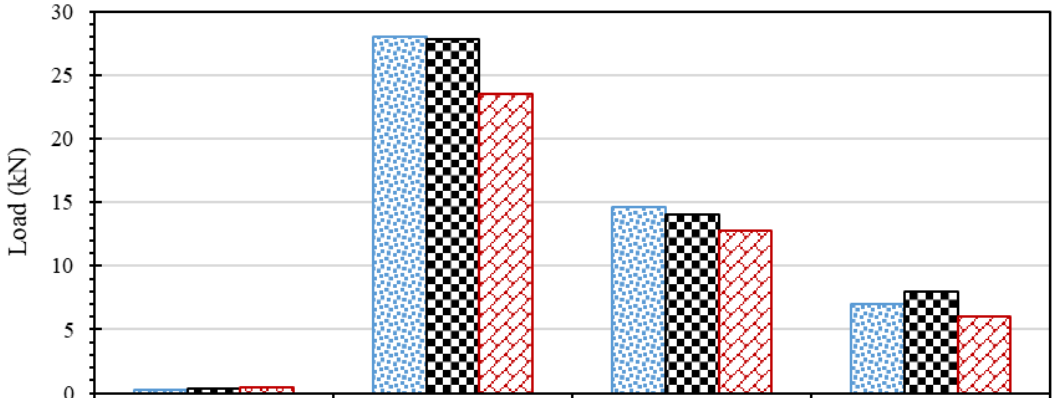

	Con.Column	G-1	G-2	G-3
sand	0.3	28	14.6	7
gravel	0.36	27.8	14	8
CW	0.44	23.5	12.8	6

Figure 4. 10. Bearing capacity at the settlement value (50 mm).

4.2. LATERAL BULGING

Geotextile encasement provides a confinement around column and this confinement affects the lateral bulging and restricts its value. In order to measure the lateral bulging of encased column, after the loading test, the column materials were excavated to the half of column height. Then the cavity was filled by plaster and was left to rest for 24 hours. The day after, the column was exhumed carefully in order to measure the lateral bulging all along the column.

The maximum value of lateral bulging for G-1 was measured to be 8.5 mm (in term of radius) at the depth of 15 cm below the soil surface (Figure 4.11-a). The depth of the excessive lateral bulging is approximately twice the diameter of encased column. This is in agreement with the experimental results of Greenwood (1970) and Hughes et al. (1975) who presented that the excessive lateral bulging of a conventional granular column takes place in the upper half of column above a depth of around four times the diameter of column. Beneath the depth of excessive lateral bulging ($\approx 2d_c$), the column experiments a slight uniform lateral bulging to the bottom of column.

The lateral bulging for G-2 shows a slight increase all along the column, when compared to that of G-1. The excessive lateral bulging, similar to G-1, was occurred approximately at a depth of about two times the diameter of column. As shown in Figure 4.11-b, the maximum value of lateral bulging was measured to be 11.95% of the radius of column ($\frac{\Delta r_c}{r_c} * 100 = 11.95\%$) at the depth of 17.5 cm.

It is relevant to mention that the lateral bulging of columns was not symmetric and also the tensile stiffness and strength of the geotextile did not influence the depth of excessive lateral bulging. It can be concluded that the failure mechanism of encased column is similar to that of conventional column in terms of lateral bulging.

That maximum value of lateral bulging for G-3 was measured to be 9.4 mm at a depth of about 16.5 cm (Figure 4.11-c). The other specifications of the lateral bulging along the column are similar to those of G-1 and G-2.

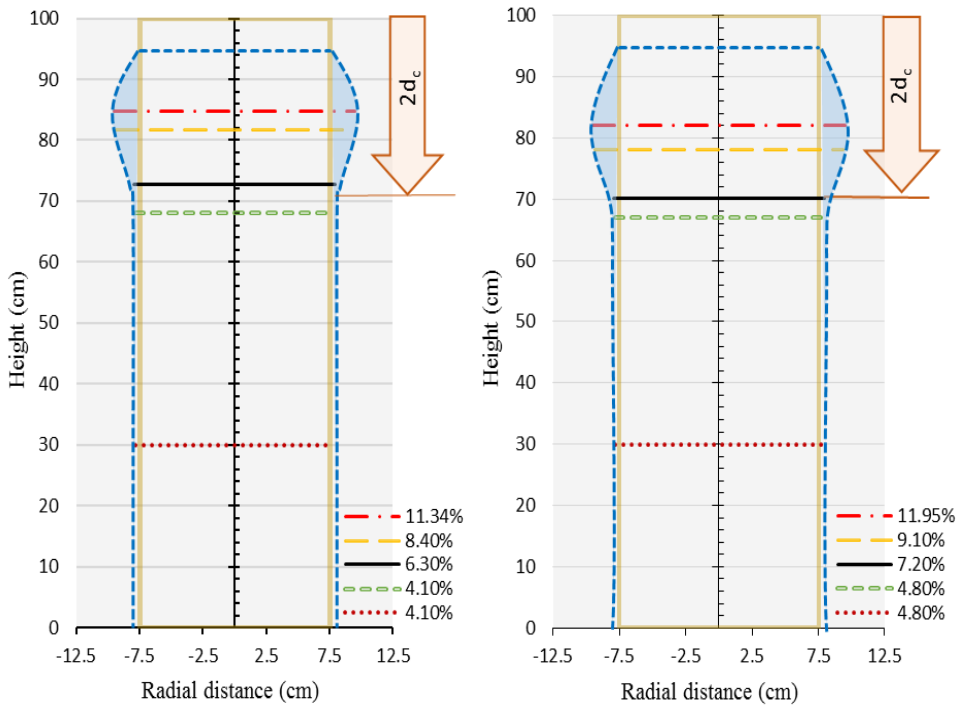

(a) (b)

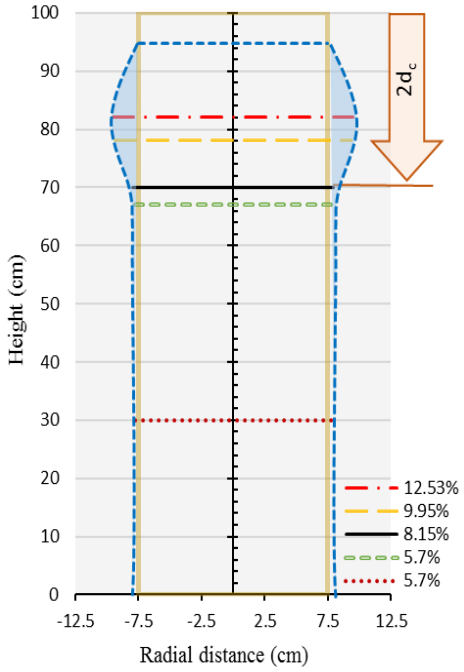

(c)

Figure 4.11. Lateral bulging for different depths: (a) G-1, (b) G-2 and (c) G-3.

The ring tensile force of geotextile can be calculated by measuring the value of lateral bulging of column and tensile stiffness of geotextile. The maximum value of ring tensile force has

occurred approximately at the same depth for three types of geotextile (G-1, G-2, and G-3). By measuring the ring tensile force, there could be a general understanding on the hoop forces at any stage of loading and also at the stage of column failure. These values are of importance because they can characterize the geotextile type based on the hoop forces.

Since the encasement of granular column are in tubular form, the ring tensile force can be presented as a basic characterization of geotextile that can give a comprehension on the bearing capacity of encased column. As shown in Figure 4.12, the maximum tensile force has occurred at the upper half of the column, as expected. It can be observed that the encasement, depending on the geotextile tensile stiffness, undergoes some levels of the ring tensile force all along the column. When the column is loaded to fail, it happens to experiment the yield hoop force at a depth of about 1 to 2 times the diameter of column.

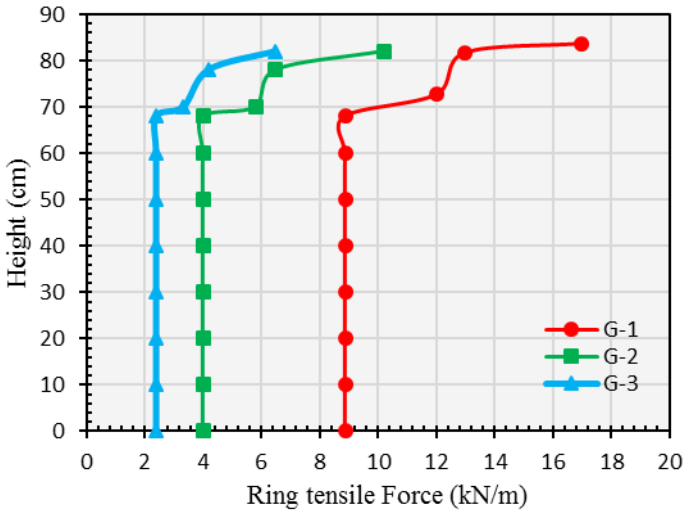

Figure 4.12. Tensile force distribution versus height for sand columns.

4.3. LATERAL EARTH PRESSURE

Beside the column, there were installed three pressure cells at different depths of 15 cm, 30 cm, 45 cm. Since the maximum value of bulging occurred at a depth of about 15-18 cm, only the pressure cell which was installed at 15 cm (d_c=15 cm) in depth was affected by the lateral bulging of the column and no output was registered for the pressure cells located at the depths of 30 cm and 45 cm. As it was shown in Figure 4.13-a, due to the greater lateral bulging of G-2, its values of lateral pressure were bigger than those of G-1 for encased sand column.

Consequently, the ultimate value of coefficient of lateral earth pressure achieved for G-2 is grater that that of G-1 (Figure 4.13-b). The results that are presented in Figure 4.13 were obtained for the first two tests because thereafter pressure cells have broken and it was not possible to measure the lateral pressure during the tests.

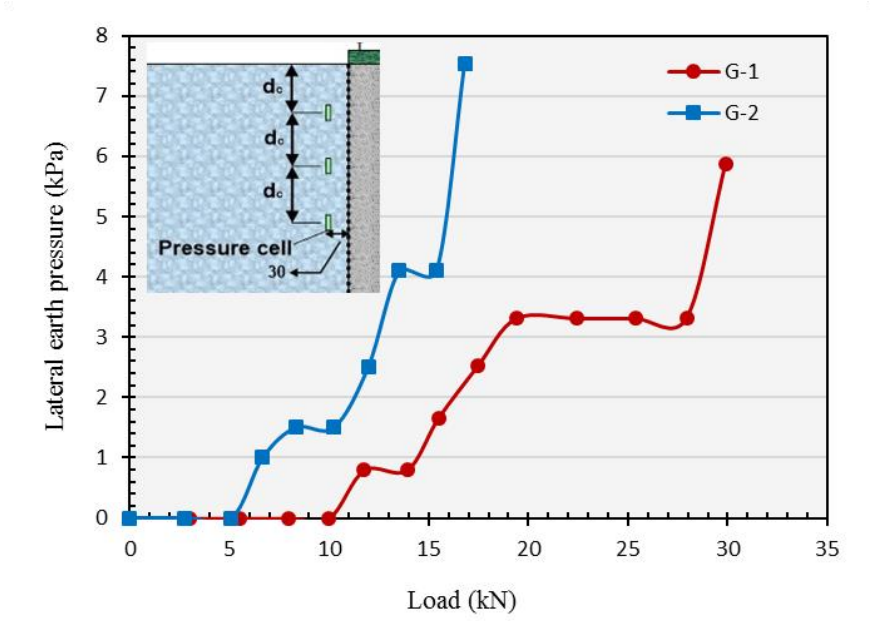

(a)

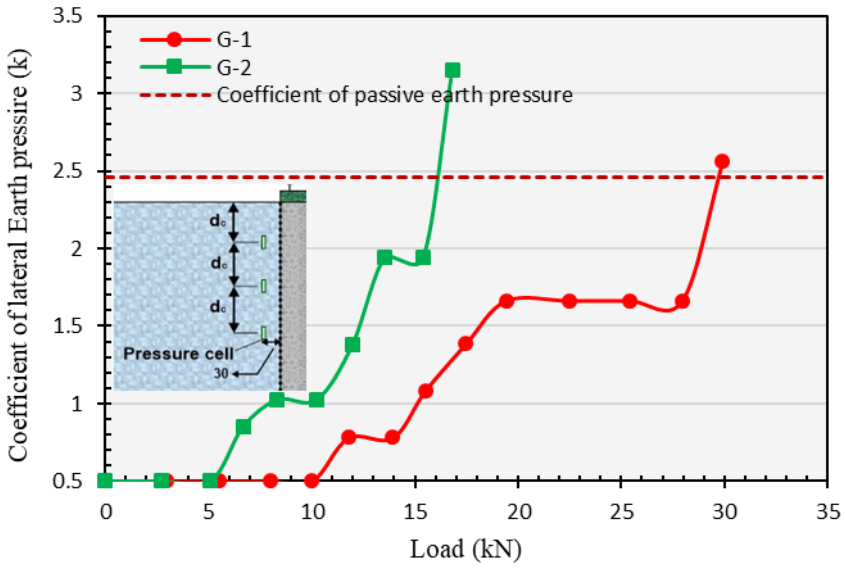

(b)

Figure 4.13. (a) Lateral pressure beside the column and (b) coefficient of lateral earth pressure (at depth of 15 cm) for encased sand column.

Commonly, displacement method is used as the installation method of encased granular columns in very soft soils because the process of other methods like replacement method can cause some difficulties and may not be so efficient.

The displacement method is carried out either by static or jointly by static and by dynamic installation method that cause a cylindrical soil densification (smear zone) around the column which may be considered by changing the value of the coefficient of lateral earth pressure (K). As reported by Priebe (1976) and Gäb et al. (2008) this coefficient can be assumed as K=1. Goughnour and Bayuk, (1979) assumed this coefficient as $K_0 < K < K_p$, where K_0 and K_p are the coefficient of earth pressure at rest and the passive earth pressure of the soil.

The columns were installed using displacement method. Due to this installation method high amount of soil, at the zone of installation, was displaced by the column materials. It was interested to measure the lateral pressure imposed to the soil during column installation. Figure 4.14 shows the maximum value of lateral pressure at a distance of 30 mm the next to the column. It can be seen that in both pressure cells installed at depths of 30 cm and 45 cm, the K value was reached to about 7.5.

As mentioned before, the results that are presented in Figure 4.14 were obtained for the first two tests because thereafter pressure cells broke and it was not possible to measure the lateral pressure during the tests.

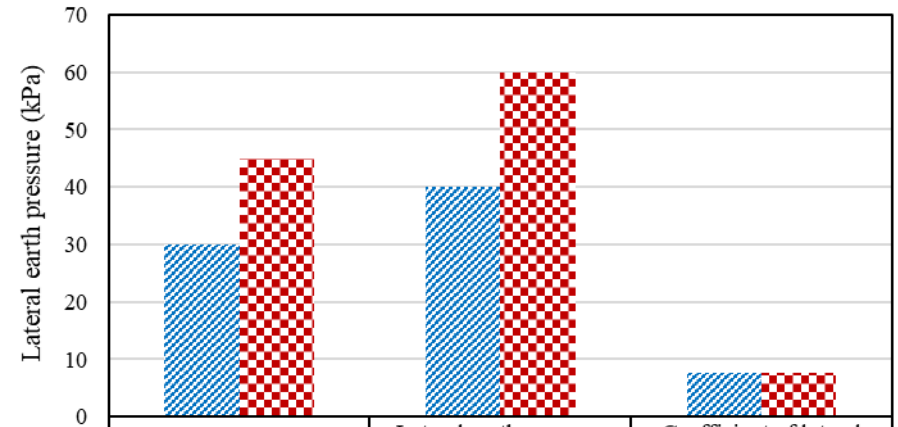

	Depth (cm)	Lateral earth pressure (kPa)	Coefficient of lateral earth pressure
Series1	30	40	7.52
Series2	45	60	7.52

Figure 4.14. Lateral earth pressure due to column installation method.

4.4. SMEAR ZONE AND UNDRAINED SHEAR STRENGTH

In this study, the smear zone was of interest to check the validations of assumptions that were mentioned before. In order to reach that, there were various measurements of the smear zone diameter right after the installation the column. It was observed that, for a column with 15 cm in diameter, the smear zone diameter has varied between 27 to 28 cm. Thus, it may result that in case of very soft soil, the smear zone can be measured as 1.8 to 1.9 the diameter of the column. Figure 4.15 illustrates the appearance of soil suction on the soil surface after installation.

(a)

(b)

Figure 4.15. Appearance of soil suction on soil surface; (a) encased sand column and (b) encased gravel column.

In addition of the surface appearance of smear zone, vane shear tests were carried out to ensure the real diameter of this zone. The vane shear tests also proved that in a diameter of 1.8 to 1.9 the column diameter, the soft soil offers higher values of undrained shear strength compared with the soil that is located in undisturbed zone. Its relevant to mention that all the vane shear test results have been corrected using Bjerrum's (1972) correction factor.

These tests were performed before the installation of column, right after the installation, and after dissipation of excess pore water pressure around the column. They have been implemented at the depths of 20, 40, 60,80 cm in four sides of the column by means of laboratory vane shear test apparatus. By using the extension rod (Figure 4.16), the tests were able to be carried out at desired depths. Figure 4.17 shows the location of vane shear tests that were carried out at four directions of the column.

Since the tests were involved with the very soft soil that may affect the results of the vane shear test due to the adhesion (friction) between the rod and the soil, before implementation of the principal tests, the value of this adhesion was measured. For all the tests the values of friction were subtracted.

Figure 4.16. Extension rod for vane shear test.

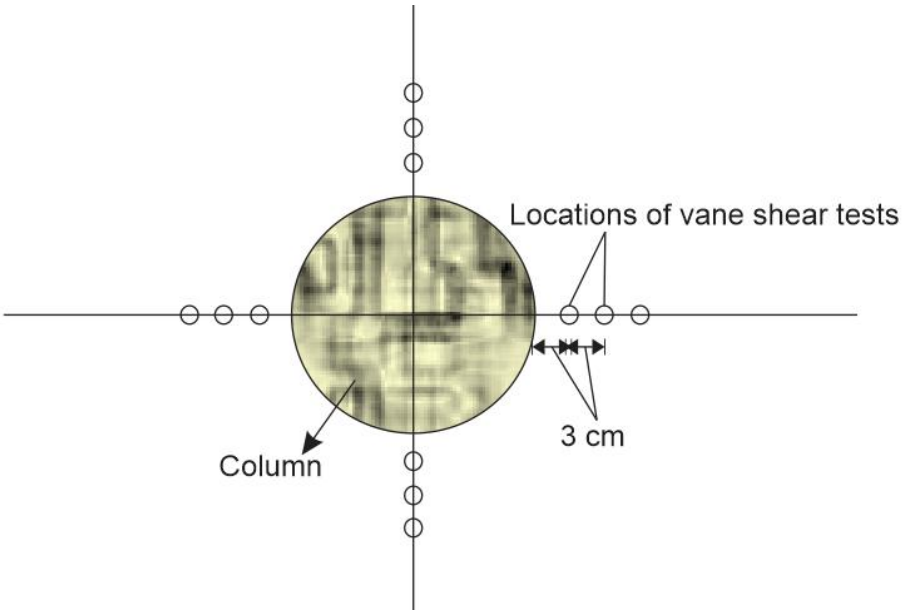

Figure 4.17. Locations of vane shear tests at four sides of column.

Figure 4.18 depicts the values of undrained shear strength for six sets of tests that were carried out. These sets of test were carried out for both encased and conventional columns. In order to evaluate the preciseness of the results, the standard deviation for any set of tests was measured. Based on the results, generally, it can be concluded that the preciseness of the vane shear tests may reduce by depth. For the tests of the friction between the rod and the soil, the standard deviation varied from 6% (depth of 20 cm) to 18% (depth of 80 cm).

Maximum standard deviations were measured for the depth of 80 cm. For the tests before the installation of column, after installation, and after dissipation of the excess pore water pressure, the maximum standard deviation was measured to be 34%, 37%, and 46%, respectively.

On the other hand, the minimum standard deviations were measured for the depth of 20 cm. These values were measure to be 18% (before installation), 17% (after installation), and 35% (after dissipation).

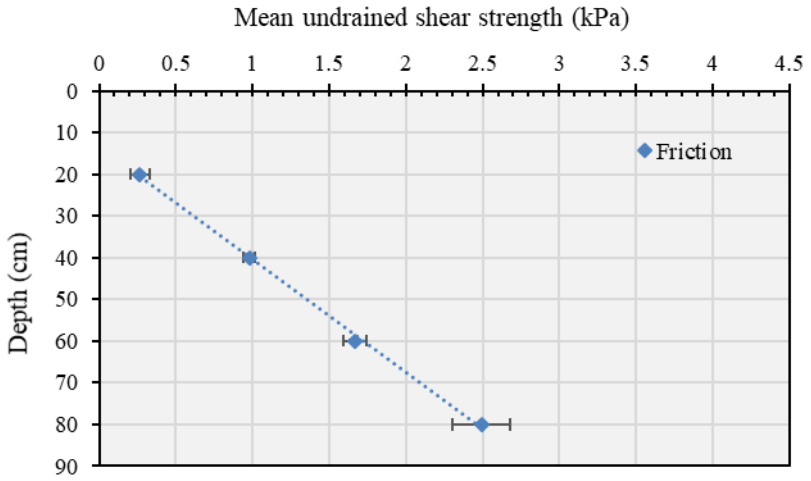
Mean undrained shear strength (kPa)
0
0.5
1
1.5
2
2.5
3
3.5
4
4.5
Depth (cm)
0
10
20
30
40
50
60
70
80
90
Friction

(a)

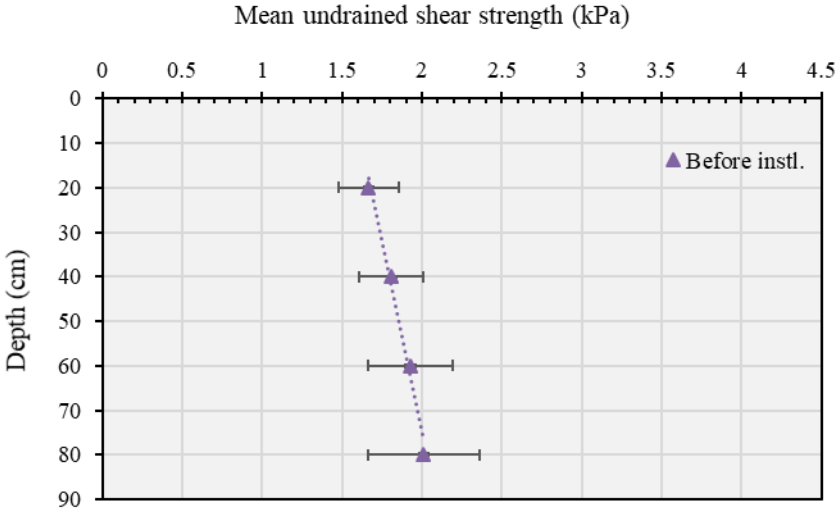
Mean undrained shear strength (kPa)
0
0.5
1
1.5
2
2.5
3
3.5
4
4.5
Depth (cm)
0
10
20
30
40
50
60
70
80
90
Before instl.

(b)

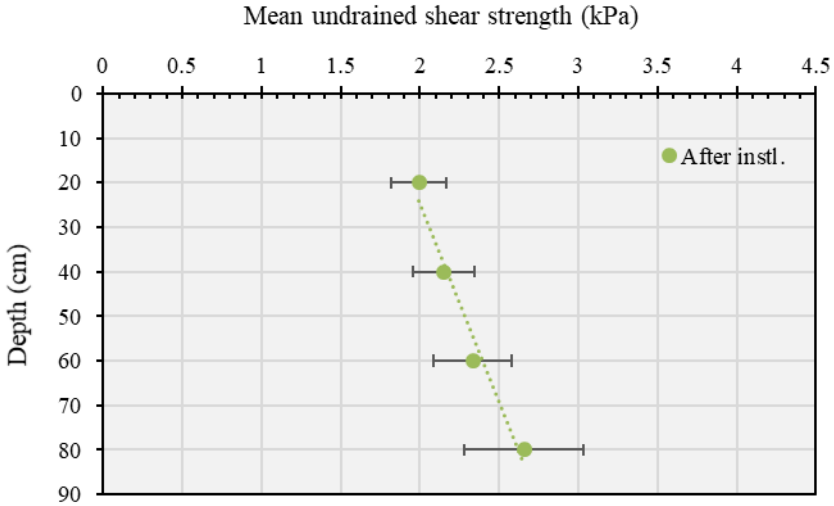
Mean undrained shear strength (kPa)
0
0.5
1
1.5
2
2.5
3
3.5
4
4.5
Depth (cm)
0
10
20
30
40
50
60
70
80
90
After instl.

(c)

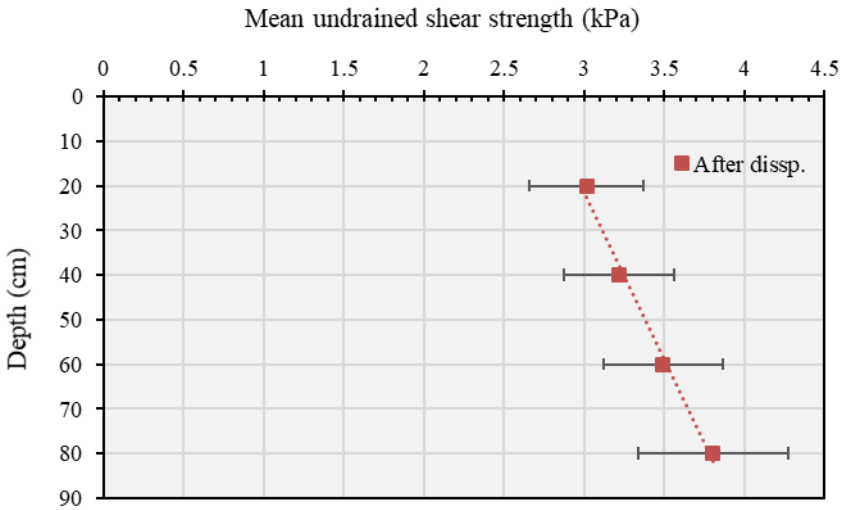

(d)

Figure 4.18. Standard deviation of the vane shear test results: (a) friction, (b) before installation, (c) after installation and (d) after dissipation of excess pore water pressure.

As shown in Figure 4.19, when comparing the results of undrained shear strength before and after the installation of column, it can be concluded that, by considering the standard deviation for each depth, the displacement method did not improve significantly the shear strength of the soil that is located inside the smear zone.

It seems that only after the dissipation of excess pore water pressure around the column, the shear strength of smear zone increased. Raithel et al. (2002) showed that after installation of the encased column, the undrained shear strength of adjacent soil has grown by 300%. They did not specify if the tests were carried out right after the installation or later.

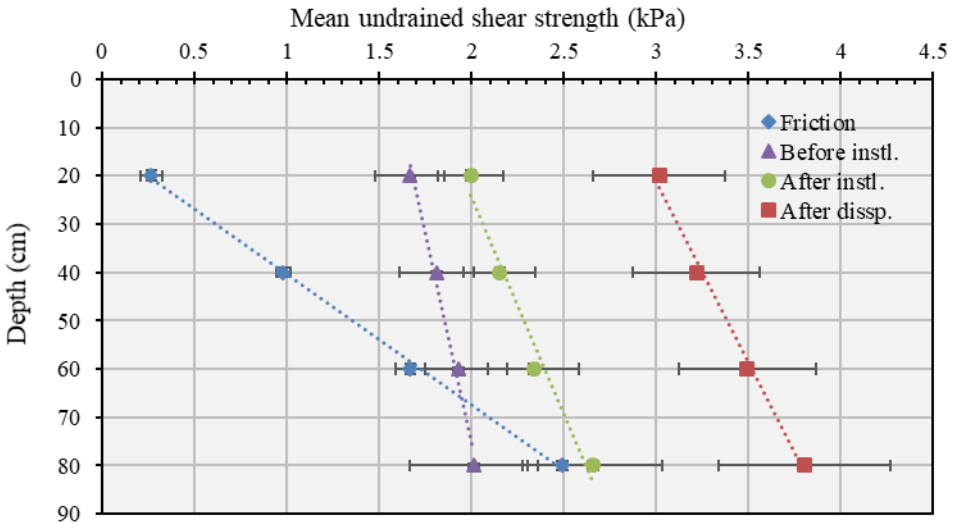

Figure 4.19. Undrained shear strength for different sets of tests.

4.5. EXCESS PORE WATER PRESSURE

Since the tests were running in an undrained condition, it was employed six piezometers in different depths to monitor the changes of excess pore water pressure during the tests. Piezometers were installed with small distances from the column. Figure 4.20 outlines the position of piezometers. Figure 4.21 show the hydrostatic pressure inside the soil for each piezometer. These value approved that the soil was at 100% of saturation.

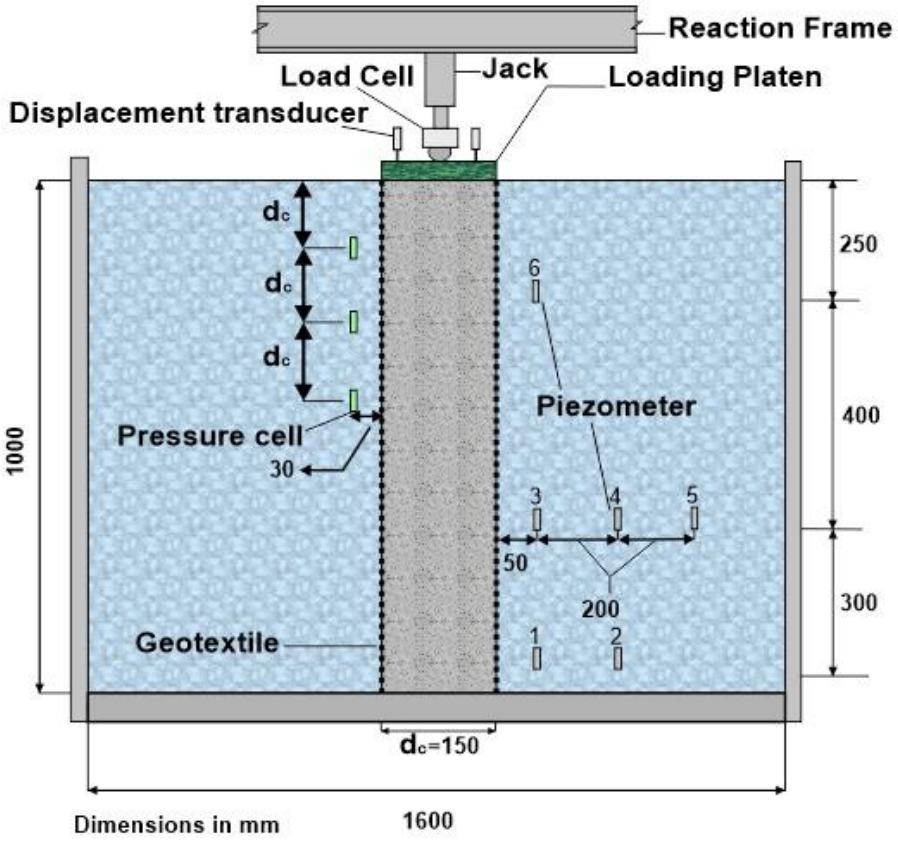

Figure 4.20. Schematic of the load test on GEC.

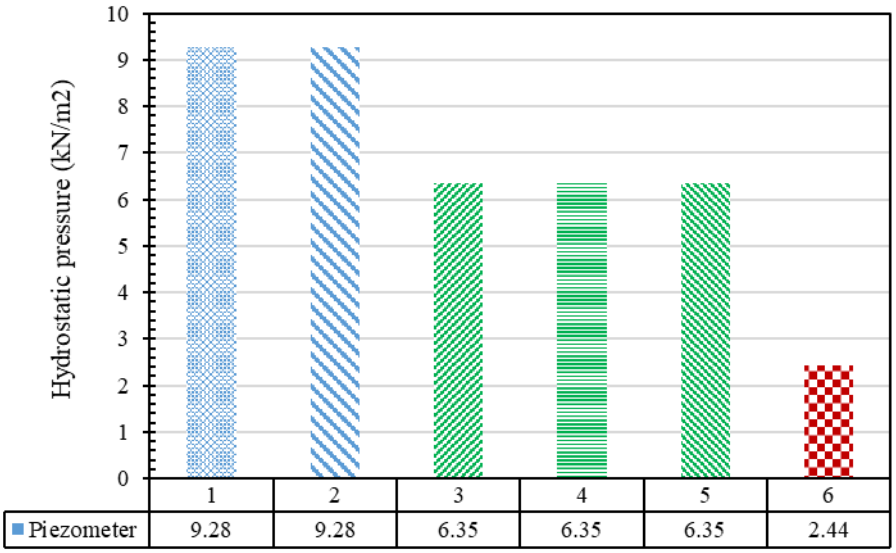

Figure 4.21. Hydrostatic pressure inside soil paste.

The excess pore water pressure around the column was imposed by the displacement method in which the PVC pipe causes displacement of the soil at the installation area. Thus, the results

of excess pore water pressure measurements for both encased and conventional column were quite similar.

Figure 4.22 indicates the values of excess pore water pressure during the installation of column. Firstly, it can be noticed that the values of excess pore water pressure have increased during the installation when the drainage is not permitted due to the PVC tube that has surrounded the column. Then, the results have showed the dissipation of the excess pore water pressure after removing the PVC tube. As shown, the maximum value of excess pore water pressure was registered for the piezometer number 1, which is at the bottom of the box and close to the column. The minimum value was registered for the number 6, which is close to the soil surface (drainage boundary). For the piezometer number 5, there was no registration for the changes of excess pore water pressure.

Taking into account the piezometers number 1, 3, and 6 which are closer to the zone of column installation, it can be concluded that the excess pore water pressure rises by a value of about 160% from the number 6 to number 3. The difference between the number 3 and 1 shows a growth of about 160% for the excess pore water pressure.

To sum up these values, it can be concluded that the excess pore water pressure rises by a value of about 160% for each 30 to 40 cm of depth for the piezometers that are at the closest distance to the column. These piezometers are almost inside the smear zone of the column, that's why they were more affected by the installation process.

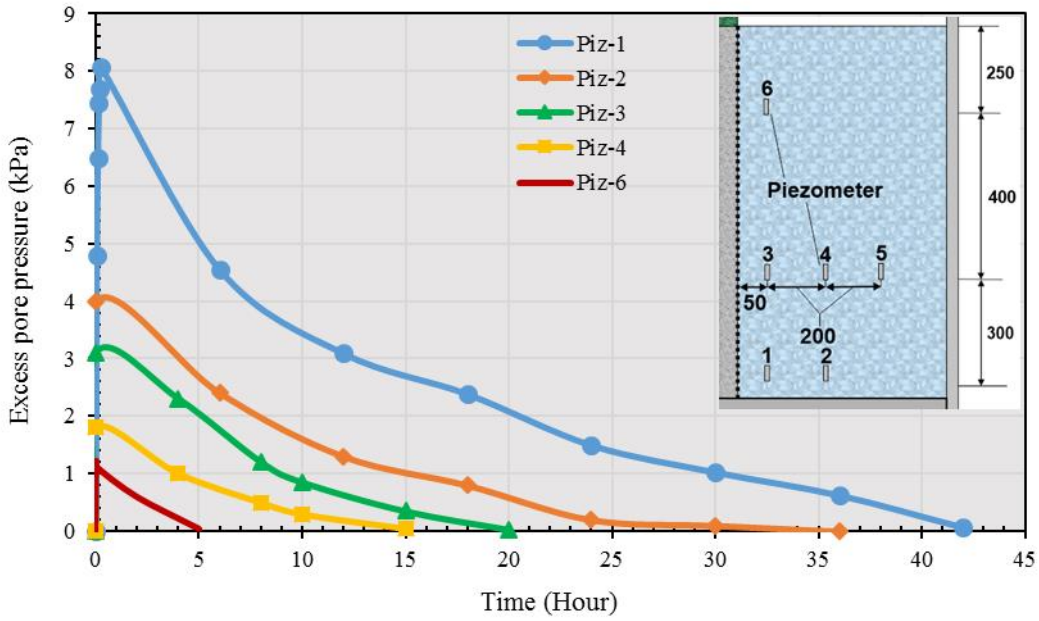

Figure 4.22. Dissipation of excess pore water pressure.

On the other hand, for the piezometers number 4 and 2, which are out of smear zone, it also has shown that they have been influenced by the installation method. The value of excess pore water pressure grows by a value of about 122% from the number 4 to 2.

Comparing the results in the horizontal direction for the piezometers number 1 and 2 which were installed at the same depth but at different distances from the column, as long as getting away from the smear zone, the value of excess pore water pressure showed a reduction by a value of about 50% for 20 cm in horizontal distance for the studied case. This reduction for the number 3 and 4, which are also at the same depth, was measured to be 40%.

The measurements of undrained shear strength out of smear zone did not show any increase in the soil strength but the values of excess pore water pressure reveals that still out of smear zone, the soil is affected by the installation process.

For the real case of encased column, the displacement method can cause the excess pore water pressure to increase. Thus, for a thick layer of soft soil, when it gets deeper, the displacement method charges drastically greater values of excess pore water pressure to the surrounding soil.

Since the loading was just applied on the column, during the tests, there was no registration for the excess pore water pressure and the lateral bulging of the column did not influence it. The reason of that can be due to the drainage process which was already started before the loading of the column.

4.6. FAILURE MECHANISM

One of the important parameters for the performance of the column is the friction angle of the column material. When the system is under loading, the column takes the bearing capacity from the confinement provided by geotextile and its internal friction angle. Once loading passes tolerable limits of the bearing capacity, the column fails at the seam which has the weakest tensile stiffness. The failure mechanism of the column can be presented as in Figure 4.23. There can be three different zones.

a) Zone 1: Active zone, in which the column materials experience Triaxial Compression (TC);
b) Zone 2: Radial shear zone, in which the column materials undergo Direct Simple Shear (DSS);
c) Zone 3: Passive zone, in which the soil is affected by Triaxial Extension (TE).

Since the encased columns were failed by lateral bulging, it can be concluded that zone 2 is of major importance. Thus, the column failure can be explained by Coulomb's soil model which is the basis of direct simple shear test. The model states that soil fails by forthcoming frictional sliding along a plane.

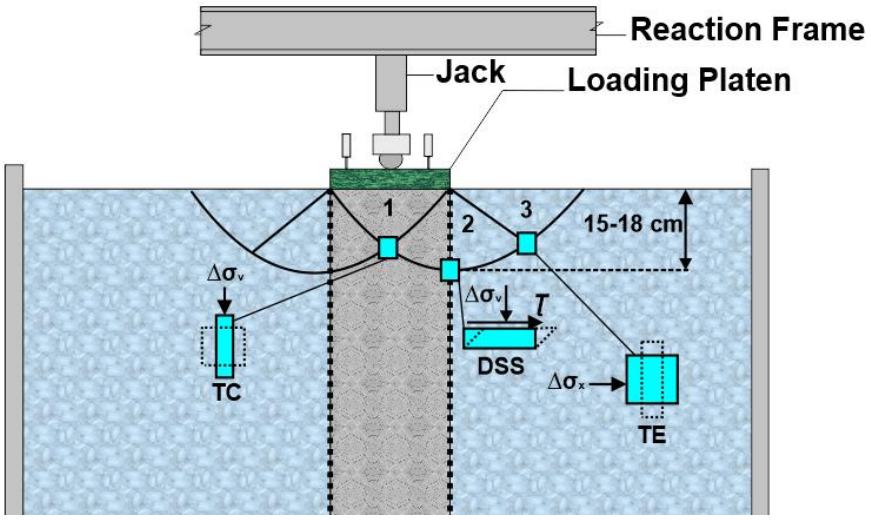

Figure 4.23. Failure mechanism of encased column.

As the settlement of the encased gravel column and the encased CW column were greater than that of sand column, these columns were sieved after the loading test to evaluate the breakage of the column materials. In order to do that, the columns were divided in five sections, as shown in Figure 4.24. For each section, the particle breakage index proposed by Marsal (1967) was calculated.

Figures 4.25 and 4.26 show the particle size distribution of the encased gravel and CW column before and after the loading tests for G-1.

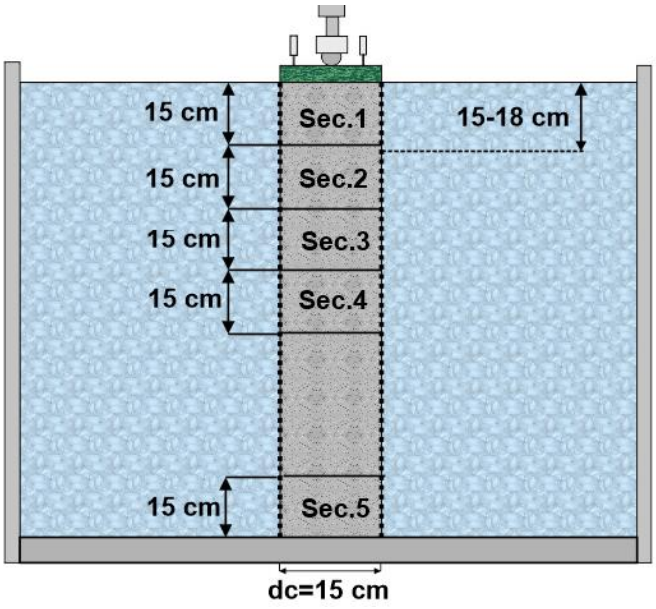

Figure 4.24. Sections of the column for sieving.

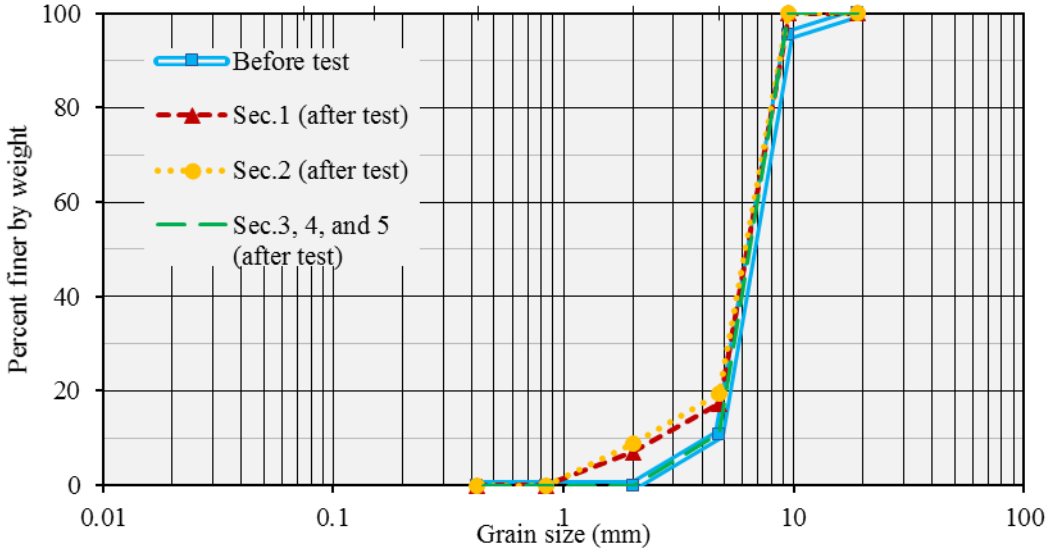

Figure 4.25. Particle size distribution of gravel before and after loading.

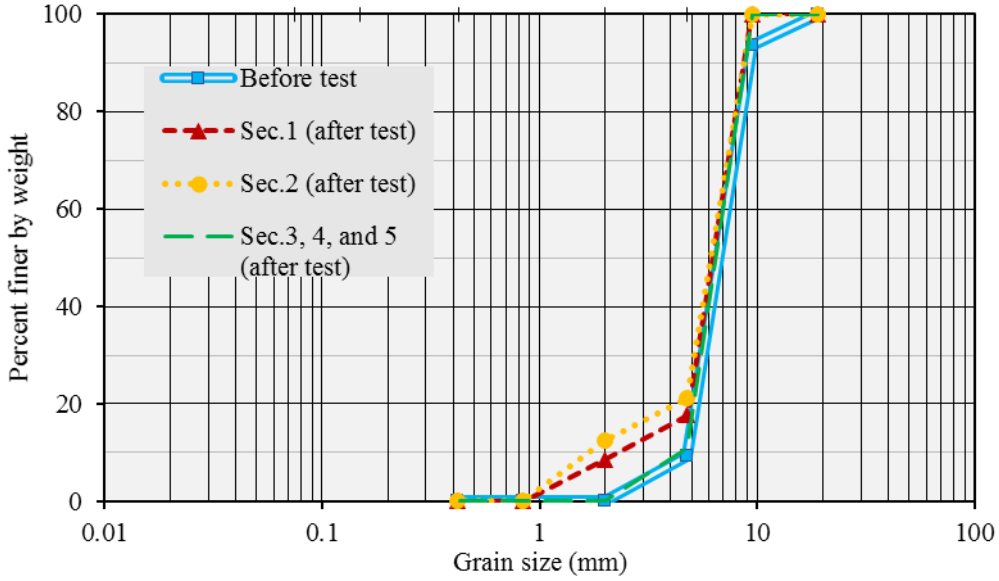

Figure 4.26. Particle size distribution of CW before and after loading.

The results of particle sized distribution of column materials revealed some differences for the sections 1 and 2 compared to those of before loading test. The sections 3, 4, and 5 did not show any significant differences. In order to have a better understanding on the column materials that were located in the sections 1 and 2, the particle breakage index was calculated for each section.

Marsal (1967) presented an equation to measure the particle breakage index of coarse-grained materials. In the proposed calculation, the particle size distribution curve is plotted for initial

and final state. The differences (ΔW) can be obtained between the percentages retained on each sieve before (W_{ki}) and after (W_{kf}) the loading application. This index is expressed as a percentage which indicates the percentage of weight of the particles that have been broken and is defined as follows:

$$B_g = \sum_{1}^{n} \left(\Delta W_{ki} - \Delta W_{kf} \right) \tag{4.3}$$

The results of B_g for the encased gravel and CW column are presented in Table 4.1. It appears that for both gravel and CW column the index for section 2 is greater than that of section 1. It seems that the section 2 is more involved with the frictional sliding of the column materials that's why it present higher value of the breakage index.

By comparing the average results of B_g, it can be calculated that the higher value of B_g presented by encased CW column is due to non-uniformity of the CW texture and its weakness to compression. Commonly, CW consists of all the materials used in the construction that some of them present high value of shear strength (e.g., pieces of concrete), while on the other hand some of them may present low shear strength (e.g., pieces of tile).

The particle breakage index for G-3 was calculated to be less than 4% for both gravel and CW columns. As it can be seen in the table, G-1, which has highest values of tensile strength and stiffness, caused the columns to have higher values of B_g.

By considering the values of lateral bulging and average of B_g, it can be concluded the G-1 presents lower value of lateral bulging and higher values B_g by comparing to those of G-2 and G-3.

Table 4.1. Particle breakage index for the encased gravel and CW column.

Geotextile	Column type	Section	Particle breakage index – B_g (%)	Average of B_g (%)
G-1	Encased gravel column	Sec.1	14.11	15.89
		Sec.2	17.67	
	Encased CW column	Sec.1	17.18	20.94
		Sec.2	24.7	
G-2	Encased gravel column	Sec.1	6.82	7.04
		Sec.2	7.27	
	Encased CW column	Sec.1	8.11	9.34
		Sec.2	10.58	
G-3	Encased gravel column	Sec.1	1.34	1.55
		Sec.2	1.77	
	Encased CW column	Sec.1	2.65	3.3
		Sec.2	3.95	

4.7. NUMERICAL SIMILATION (BACK ANALYSIS)

Numerical simulations using Finite Element Method (FEM) were carried out, regarding the back analysis of the loading tests. To this end, it was applied on the top of the column the settlement achieved in the loading tests and the load needed to reach certain levels of settlement was estimated.

The model test was simulated using axisymmetric model type for 2D analysis and for 3D analysis a quarter-model of the geometry has been used. Boundary conditions of the model (Figure 4.27) allow it to have displacements in vertical direction and the horizontal displacements at the sides were restricted (roller boundary condition). At the base, displacements in both vertical and horizontal directions were restricted as the column and the surrounding soil were placed on rigid layer.

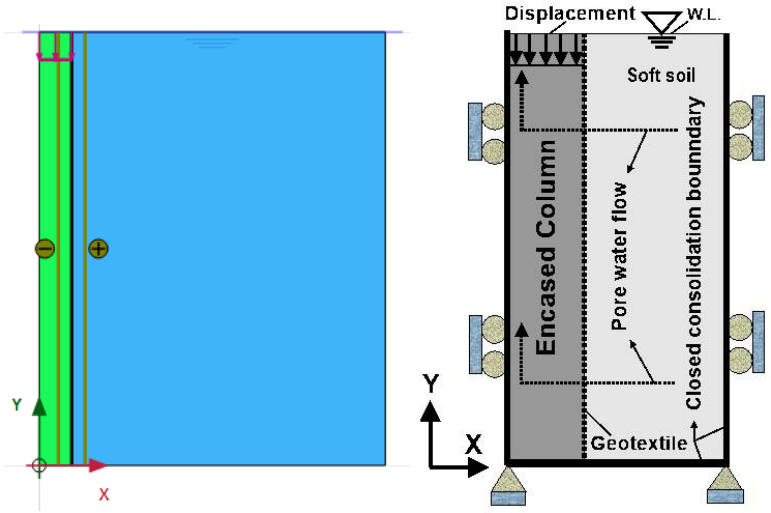

(a)

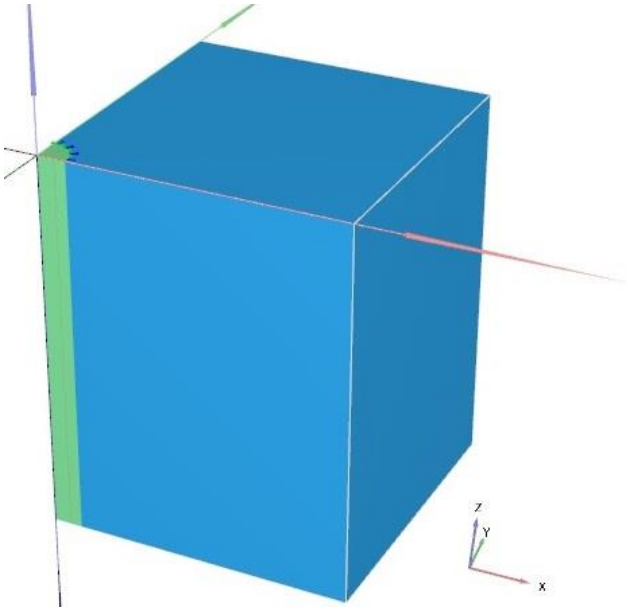

(b)

Figure 4.27. Axisymmetric modeling of the large scale tests: (a) 2D modeling and (b) 3D modeling.

The parameters of the surrounding soil and the columns (sand, CW, and gravel) are presented in the Table 4.2. Mohr-Coulomb soil model was used for predicting the behavior of column materials (sand, gravel, CW). This model utilizes a total of five parameters; Young's modulus (E'), Poisson's ratio (v), effective cohesion (c'), effective friction angle (φ'), and dilatancy angle (ψ) to evaluate the performance of the materials.

Soft soil model was used for the very soft surrounding soil. This model uses both compression and swelling indices and also Mohr-Coulomb failure parameters. It requires modified compression index (λ^*), modified swelling index (κ^*), effective cohesion (c'), effective friction angle (φ'), and dilatancy angle (ψ) to be determined. Modified compression and swelling indices can be determined by following equations:

$$\lambda^* = \frac{C_c}{2.3(1+e)} \quad 4.4$$

$$\kappa^* = \frac{2C_s}{2.3(1+e)} \quad 4.5$$

Table 4.2. Material parameters used in numerical modeling.

Material Properties	Soft clay	Sand column	Gravel column	CW column
	Soft soil	Mohr-Coulomb (MC)	Mohr-Coulomb (MC)	Mohr-Coulomb (MC)
γ_{sat} (kN/m^3)	17	20	20	19
E' (kPa)	-	80,000	80,000	35,000
ϕ' (^{o})	25	40.5	43	42
Ψ (^{o})	0	10	12	11
ν'	-	0.3	0.3	0.3
λ^*	0.088	-	-	-
κ^*	0.011	-	-	-
K_0	0.57	0.35	0.32	0.33
OCR	1	-	-	-

Where: γ_{sat} = Saturated unit weight, E' = Young's modulus, φ' = Effective friction angle, ψ = Dilatancy angle, ν' = Poisson's ratio, λ^* = Modified compression index, κ^* = Modified swelling index, K_0 = Lateral earth pressure at rest, *OCR* = Over consolidation ratio.

4.7.1. CONVENTIONAL COLUMN

Figure 4.28 shows the results of numerical analyses and the loading tests. By comparing the results of the numerical analyses and experimental tests, it can be concluded that the numerical results are almost in reasonable agreement with those of the loading tests. On the other hand, the 2D-results suffers from some deviations for sand column while when it comes to 3D-results, the deviations are almost less visible. Young's modulus of the columns was obtained by back analysis.

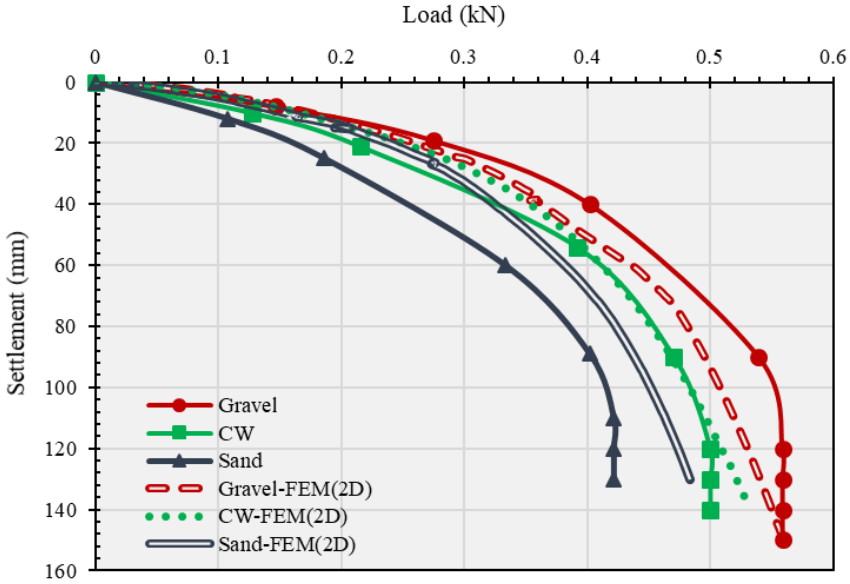

(a)

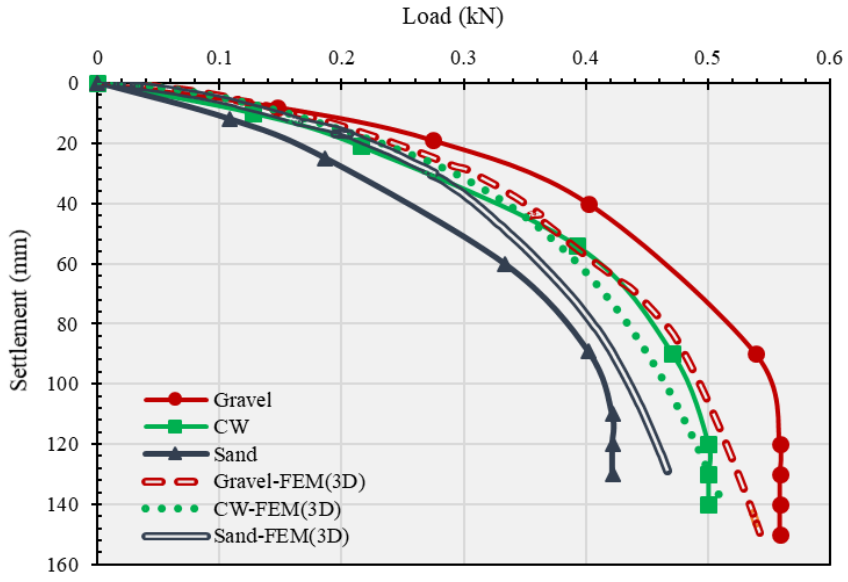

(b)

Figure 4.28. Back analysis results of the loading tests: (a) 2D analysis and (b) 3D analysis.

4.7.2. ENCASED SAND COLUMNS

The results of the numerical analyses for encased sand column shows a good agreement with those of the loading tests for G-1 and G-3 (Figure 4.29). For G-2, it can be seen that the initial part of the curves, result from the loading test and numerical results, shows slightly larger difference comparing with those of at the end of curves. This can be due to some kind of the settlement of the column material for the first steps of loading. Generally, it can be deduced that numerical results are pretty close to those of the loading test. The maximum underestimation was measured for G-2 where it happens to be 8% and 10% for 2D and 3D results, respectively.

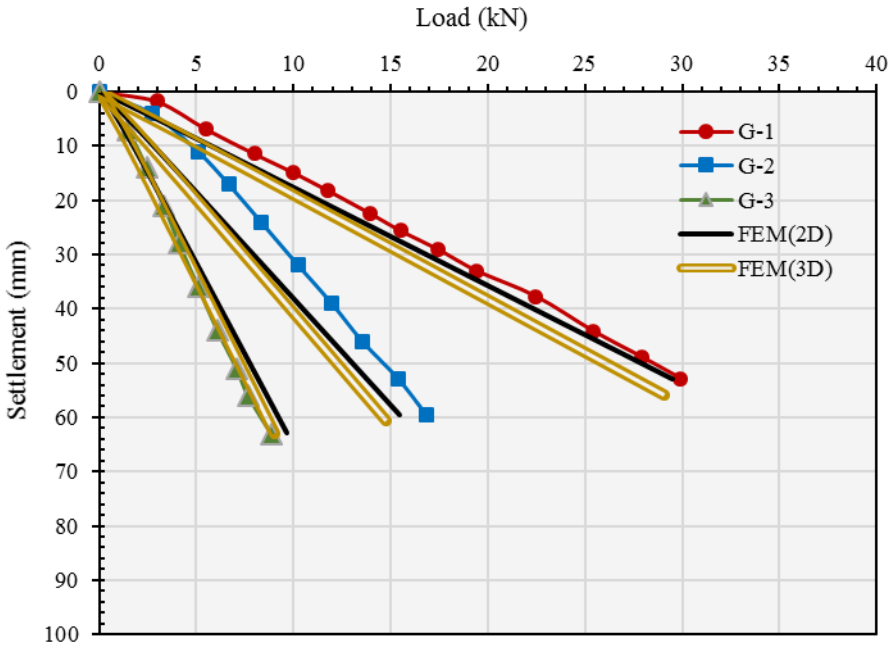

Figure 4.29. Comparison of the loading tests and numerical results for encased sand column.

4.7.3. ENCASED GRAVEL COLUMN

Figure 4.30 illustrates that the numerical results are in a very good agreement with those of the loading tests for G-1 at the initial part of curve, but from the middle part of the curve it starts to show some differences. At the end part of the curve it happens to have almost 13% and 5.5% overestimation of the load bearing capacity for 2D and 3D results, respectively. It seems to have the same scenario for G-3 as the overestimation value was measured to be almost 12.9% and 8.5% for 2D and 3D results, respectively, as the 3D-results are almost in a little better agreement

with those of the loading tests. The numerical results are in good agreement with those of the loading tests for G-2. Some differences can be due to the gravel breakage.

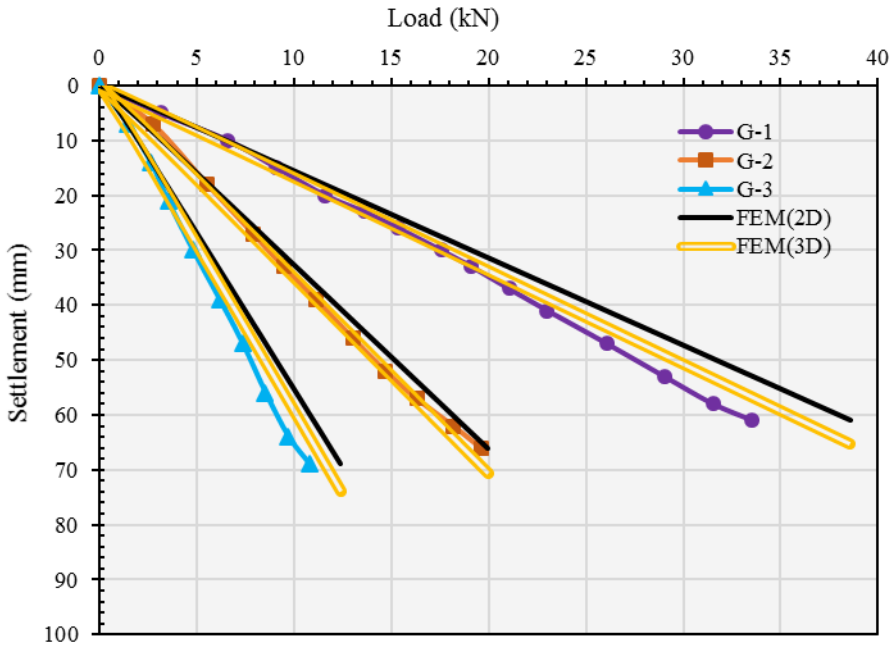

Figure 4.30. Comparison of the loading tests and numerical results for encased gravel column.

4.7.4. ENCASED CW COLUMN

The numerical results presented a straight line but the loading test results show some curvatures for G-1 and G-2 (Figure 4.31). The differences between the numerical results and those of the loading test, at the initial to middle part of the curve, happen to be grater by comparing with those of the end part. In other words, at the initial to middle part, for the same level of loadings the variation between the values of settlement obtained from the numerical and test results is greater than that of the end part.

The numerical results at a level of about 67% of the total settlement, have started to show some differences in the prediction of load bearing capacity for G-3. For a total settlement of 88 mm, the value of the load bearing capacity obtained from numerical results show almost 20% and 12% overestimation by comparing to those of the loading test for 2D and 3D results, respectively. These differences can be due to the CW breakage.

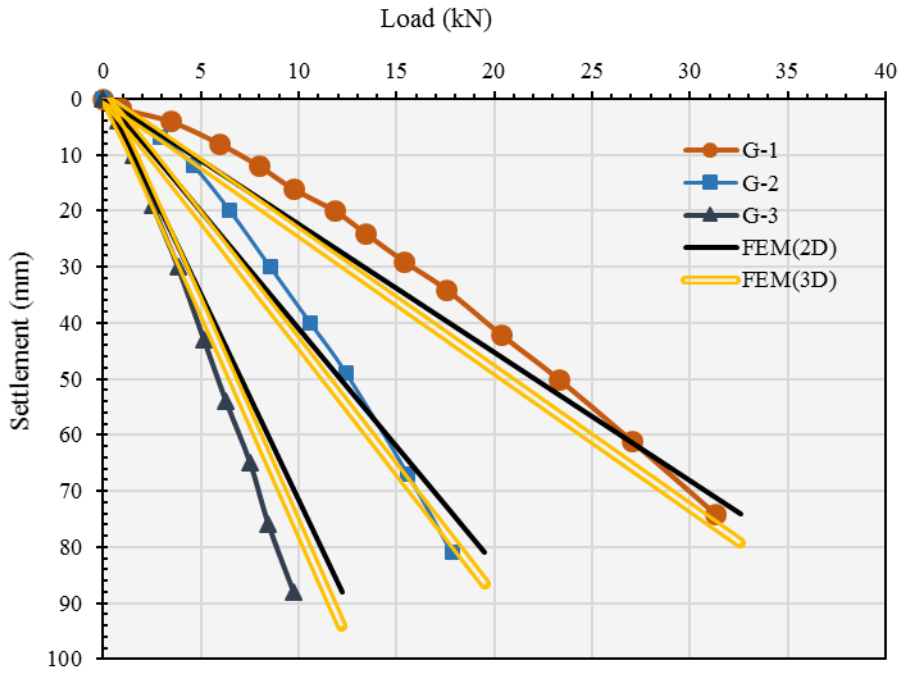

Figure 4.31. Comparison of the loading tests and numerical results for encased CW column.

4.7.5. LATERAL BULGING

Figure 4.32 depicts the values of maximum bulging obtained from the numerical analyses and the laboratory tests. The differences between numerical results and those of the tests varied from almost 50% to 66% and to 61% for 2D and 3D results, respectively. These differences can be due to the column failure that has occurred at the final stage of loading test. In other words, in the laboratory tests, the loading was continued until the failure of the column that led to the ripping of the geotextile at the seam. This could affect the maximum value of lateral bulging.

The depth of the maximum lateral bulging for the laboratory tests was measured to be from 15 to 18 cm from the settled surface of column. This value for the numerical analyses was obtained at 15 cm which represents a good agreement between predictions and measurements.

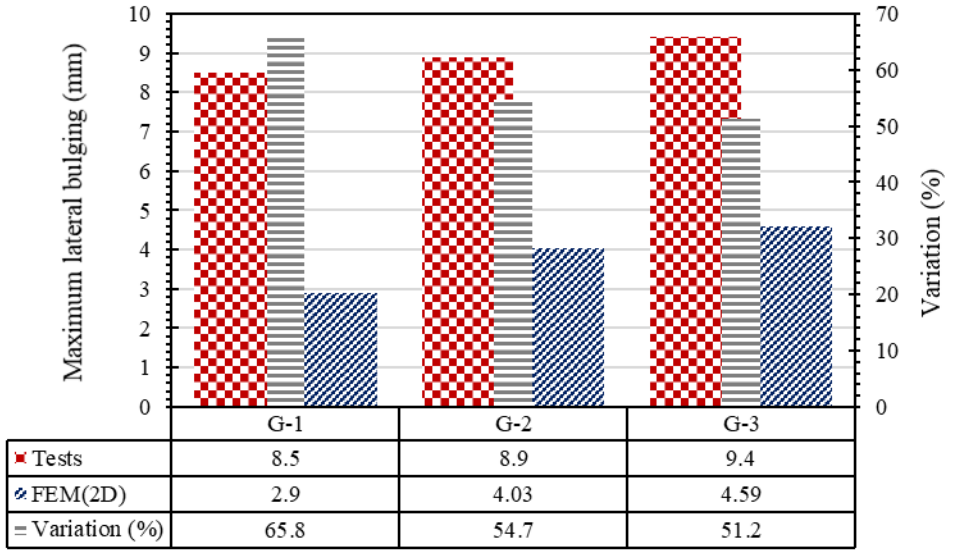

	G-1	G-2	G-3
Tests	8.5	8.9	9.4
FEM(2D)	2.9	4.03	4.59
Variation (%)	65.8	54.7	51.2

(a)

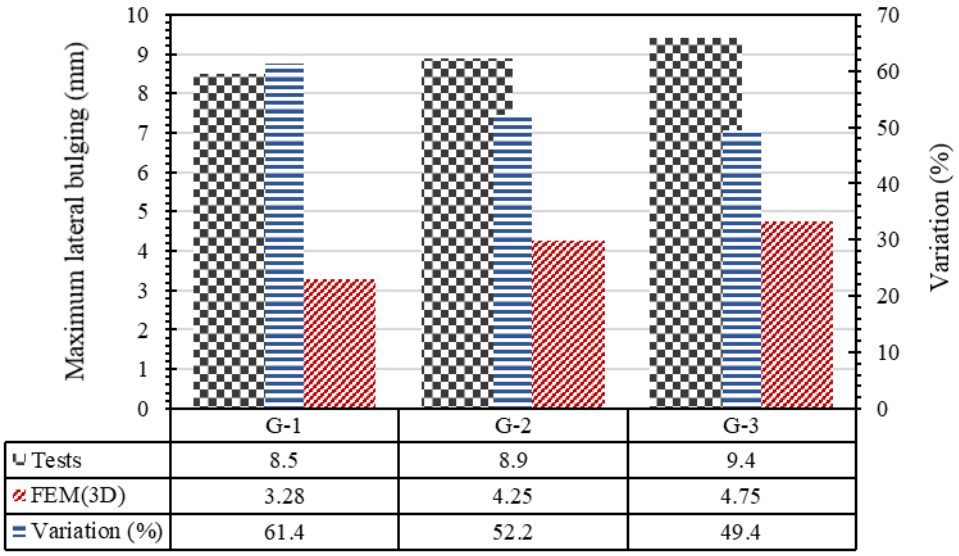

	G-1	G-2	G-3
Tests	8.5	8.9	9.4
FEM(3D)	3.28	4.25	4.75
Variation (%)	61.4	52.2	49.4

(b)

Figure 4.32. Maximum lateral bulging for different types of geotextile: (a) 2D analysis and (b) 3D analysis.

4.7.6. EXCESS PORE WATER PRESSURE

Since the tests were run in an undrained condition, there was employed six piezometers in different depths and distances (from the column) to monitor the changes in the excess pore water pressure. For two of the piezometers that were installed at a depth of 25 cm, there was no

change in records registered by data logger. On the other hand, the data registered for the rest of piezometers in all the tests were quite similar. Figure 4.33 details the changes in excess pore water pressure during the loading of the column for the numerical simulations and the tests. The highest changes were registered for the piezometer 1 that was placed close to the bottom of the column. It seems that the lateral bulging imposed no excess pore water pressure to the piezometers. This can be due to the dissipation of this value that was already in running during the loading test.

The comparison of the values obtained from numerical analyses and the laboratory test, show that, for piezometer 1, at the final stage of loading there is a difference of about 9.6% and 16% for 3D and 2D results, respectively. This difference for piezometers 2, 3, and 4, are measured to be 6.4%, 22%, and 13% for 2D results and 9.4%, 14.8%, and 8.6%, respectively, for 3D results. These differences can be due to the sensitivity of sensors.

In this study, it was of interest to monitor the difference between Soft Soil and Cam-Clay model, since both of them uses compression and swelling indices of the soil. In this study, it was found that Soft Soil model provides quite more appropriate results in case of excess pore water pressure around the column. The difference between Cam-Clay model results and those of the tests for piezometers 1, 2, 3, and 4 were measured to be 144%, 257%, 44.4%, and 13.3%, respectively (Figure 4.33 and 4.34).

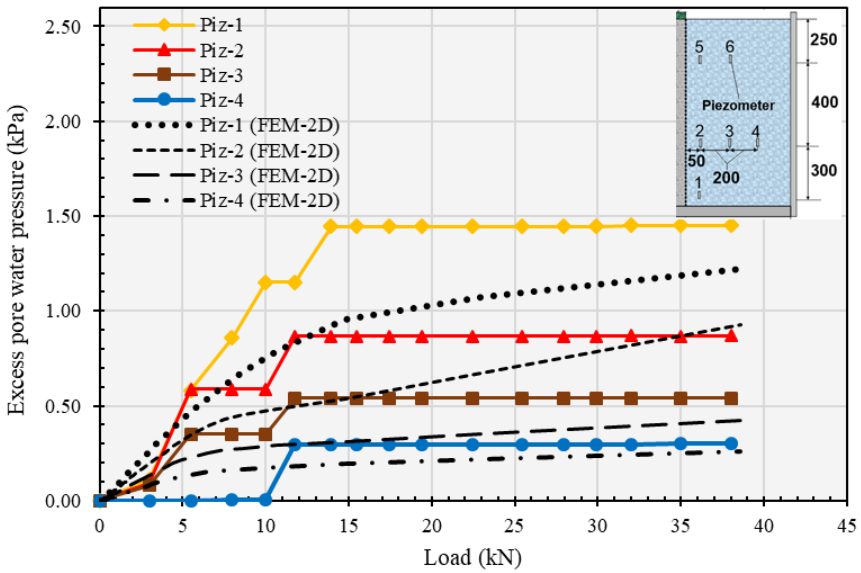

(a)

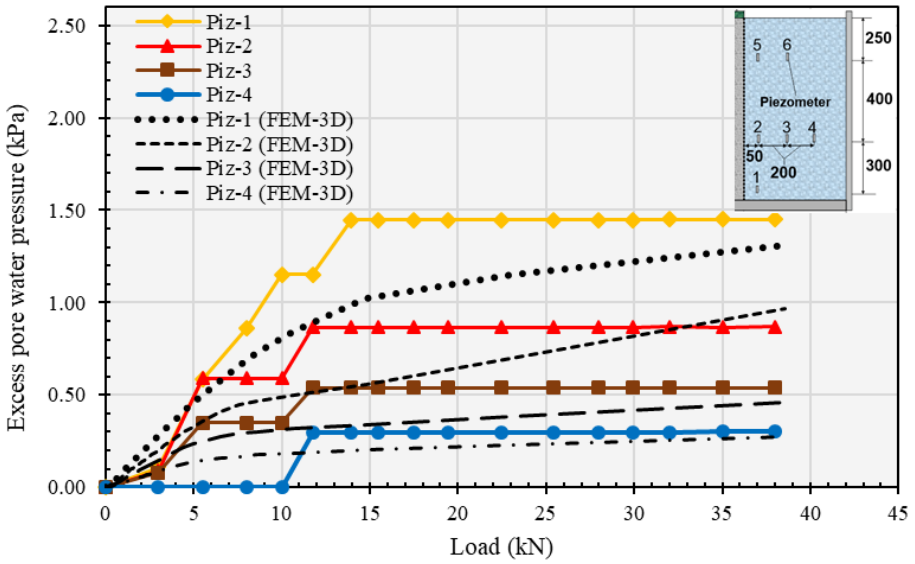

(b)

Figure 4.33. Excess pore water pressure during loading test: (a) 2D analysis and (b) 3D analysis.

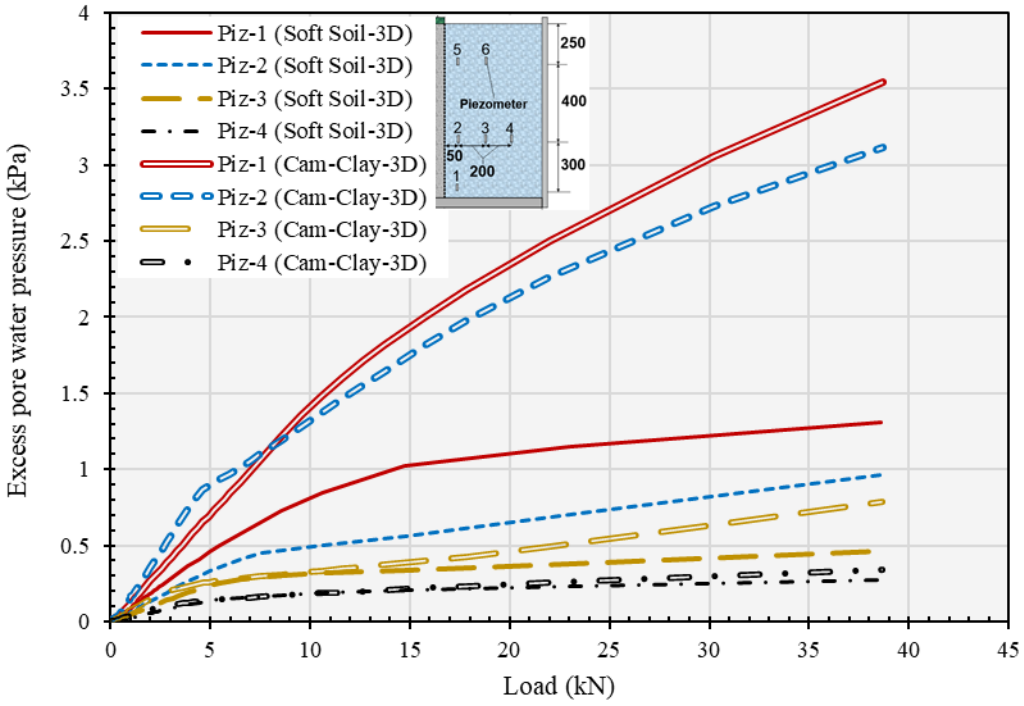

Figure 4.34. Prediction of excess pore water pressure around the column by Soft Soil and Cam-Clay model.

Figure 4.35 indicates the excess pore water pressure (negative values) around the column after loading. It can be seen that at the final stage of loading, there is some water on the surface of

the soil. The very similar phenomenon has been observed for the loading tests as shown in Figure 4.36.

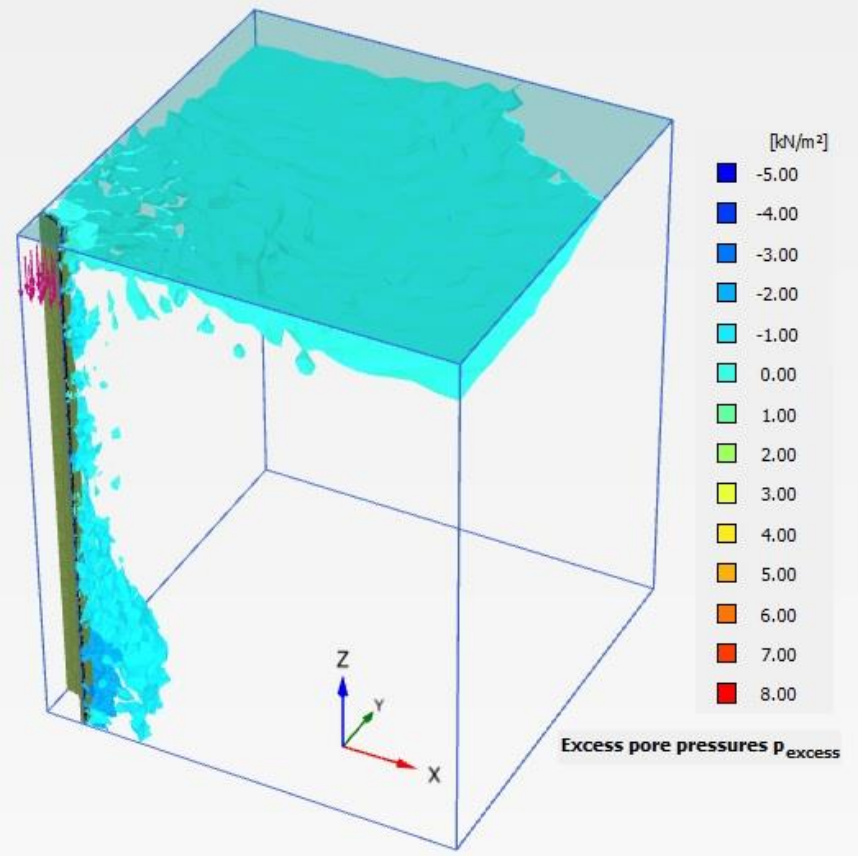

Figure 4.35. Excess pore water pressure around the column and on the soil surface after loading.

(a)

(b)

Figure 4.36. Soil surface after the loading test: (a) column surface with the loading platen and (b) column surface after removing the loading platen.

4.7.7. FAILURE MECHANISM

The results of numerical analyses confirmed the failure mechanism that was described in section 4.6. Figure 4.37-a depicts the horizontal displacement of the column material. By taking into consideration both horizontal displacement of the column materials and failure points along the column (Figure 4.37-b), it can be concluded that the maximum value of shear stress has occurred at the same depth where the maximum value of lateral bulging occurred. In other words, the column failed by continuous shearing of its content at the radial zone. The very intensity of shear stresses and also the shear zones of interest are illustrated in Figure 4.37-c.

The column content at the radial zone experience Direct Simple Shear (DSS) conditions which as it was mentioned before in section 4.6, is based on the Coulomb's soil model.

Almeida et al. (2013) proposed these areas that are located inside the radial zone as the dilating zone which is quite in line with both experimental and numerical analyzes of this study.

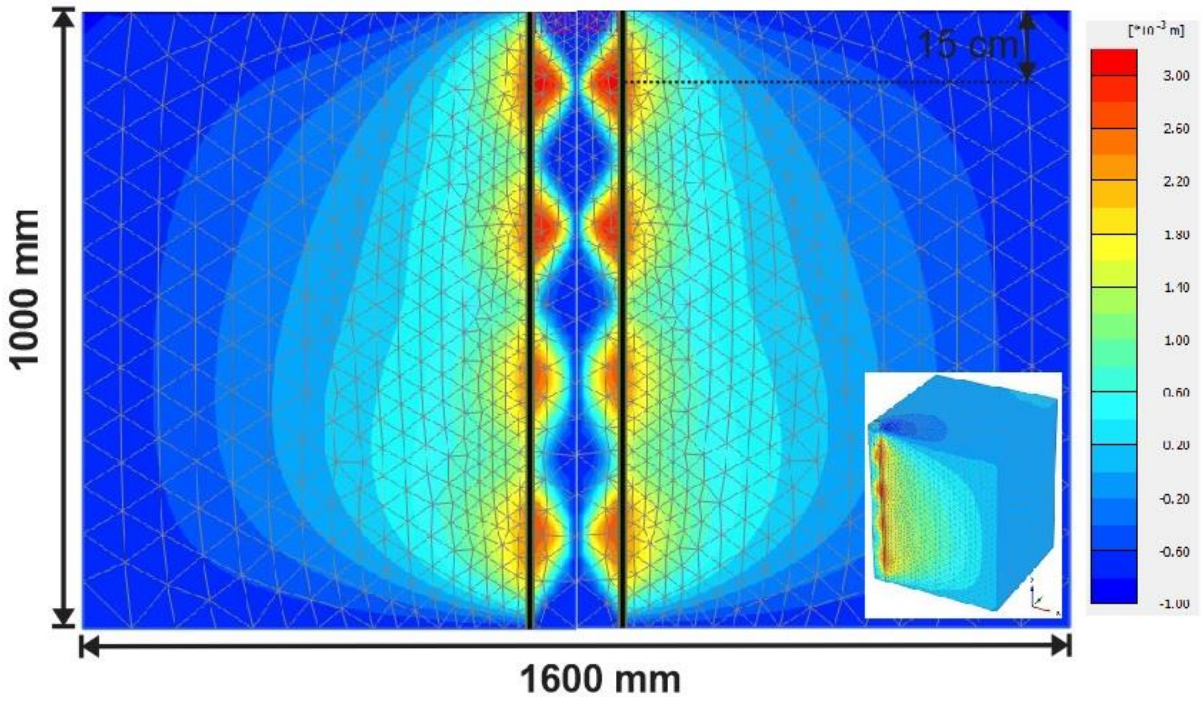
15 cm
1000 mm
1600 mm
[*10^-3 m]
3.00
2.60
2.20
1.80
1.40
1.00
0.60
0.20
-0.20
-0.60
-1.00

(a)

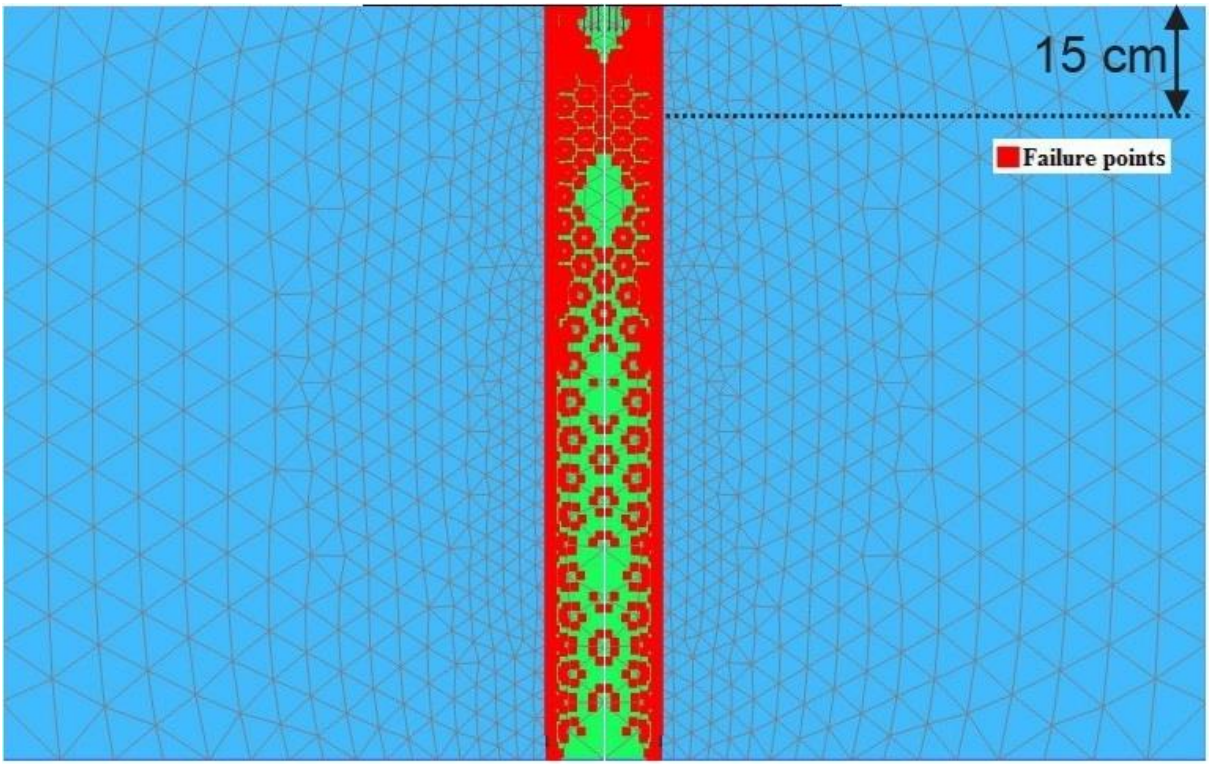
15 cm
Failure points

(b)

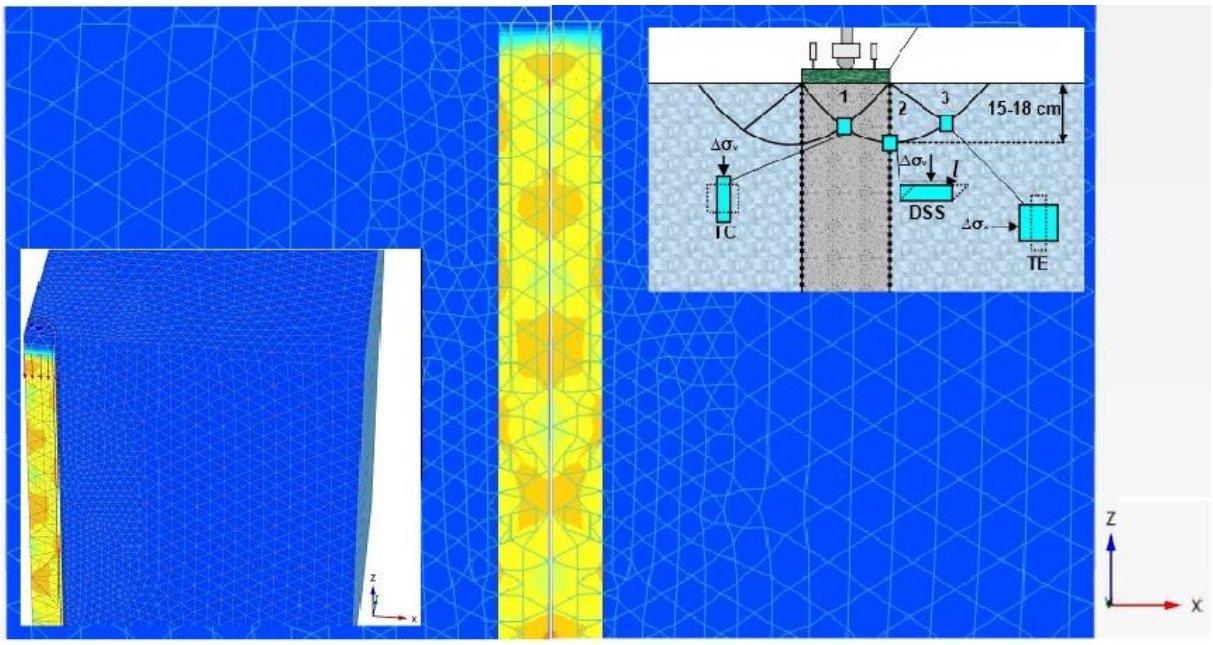

(c)

Figure 4.37. Failure mechanism; (a) horizontal displacement of the column materials, (b) distribution of failure points along the column and (c) shear zones of the column.

Figure 4.38-a depicts the tension cut-off points around the column on the soil surface after completion of imposing settlement. These points are considered as the soil surface tensile cracks around the settled area which were also observed in the loading tests (Figure 4.38-b).

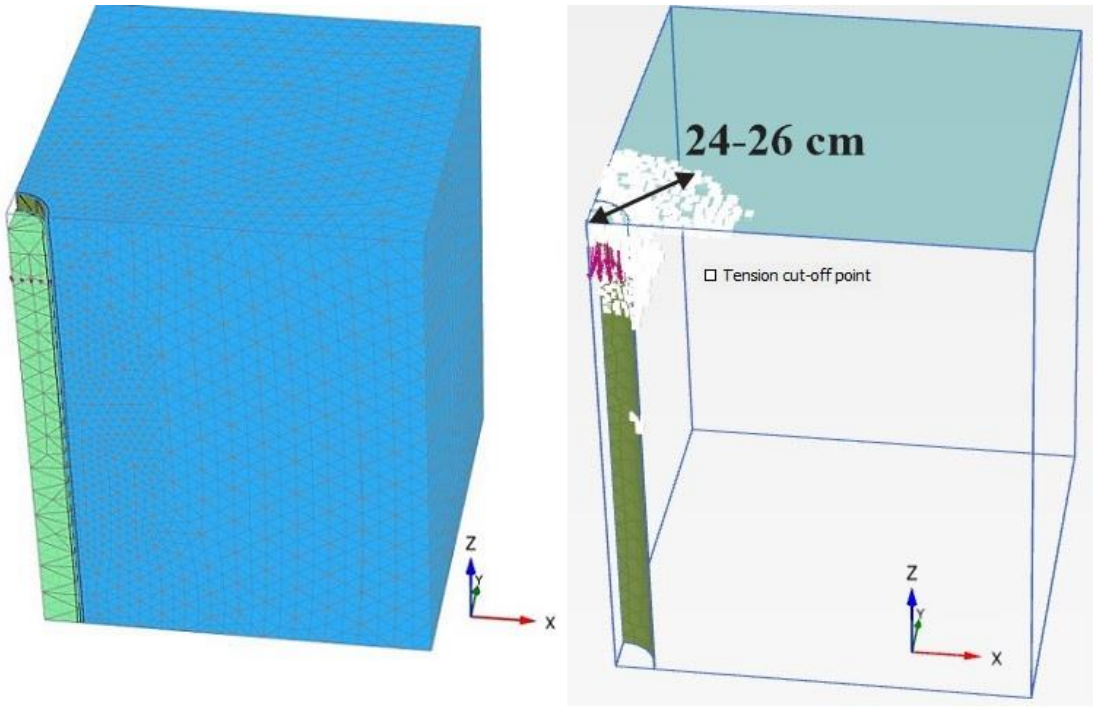

(a)

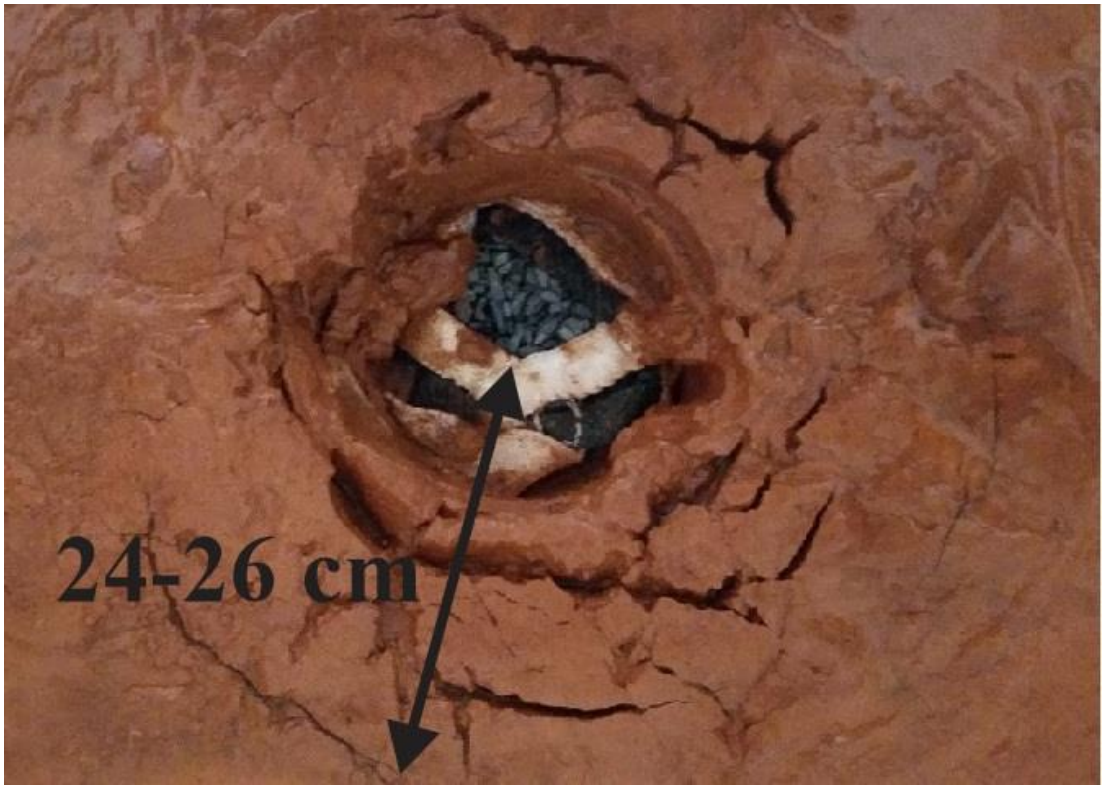

(b)

Figure 4.38. Rupture of the soil surface around the column after the loading: (a) tension cut-off points and (b) cracks around the column.

4.8. NUMERICAL FULL SCALE ANALYSIS

In order to have a better understanding on the laboratory tests, the simulation of an embankment reinforced by conventional and encased granular columns was considered by taking into account a scale factor of about 5.

Baker et al. (1991) widely explained the similarity analysis. The relationship provided by the author, assumes scaling factor (λ) to be calculated as:

$$\lambda = \frac{f_P}{f_m} \qquad (4.1)$$

where f_P and f_m are physical measures that relate to the prototype and the model, respectively.

In case of GEC, the performance of the column is a function of tensile strength (T_g), tensile stiffness (J_g), geosynthetic thickness (t_g), the height of column (H), undrained shear strength of the surrounding soil (S_u), unit weight (γ_c) and friction angle (φ_c) of the column materials. It can be conservative to ignore S_u for the case of very soft soil. In this study the thickness of the geosynthetic material has not taken into account since the laboratory tests were in large scales. Table 4.3 shows the parameters that were considered for scale factor. The diameter of encased columns employed in the projects reported by Raithel et al. (2002, 2004), Alexiew et al. (2003) and Araujo et al. (2009) was 0.4-1 m and the model test diameter was selected to be 0.15 m. Thus, the scaling factor (λ) was calculated to be approximately 2 to 7. For numerical simulations, it was decided to take the λ^2 equal to 5.

Table 4.3. Scale factors for laboratory large scale tests.

Dimensionless factor	Parameters	prototype	model
$D_1 = \frac{T_g}{\rho . g . L . t_g}$	T_g (kN/m)	1	$1/\lambda^2$
$D_2 = \frac{J_g}{\rho . g . L . t_g}$	J_g (kN/m)	1	$1/\lambda^2$

where, T_g = Tensile strength, J_g = Tensile stiffness, ρ = the geosyntheic density, g = the gravity acceleration, L = Encasement length, t_g = Encasement thickness.

Figure 4.39 shows the numerical simulation of the embankment reinforced by conventional and encased granular column. To this end, the columns were arranged by an area replacement ratio equal to 15% since this value was used for real cases of this method (Alexiew et al., 2015). Area replacement ratio (A_r) is a function of cross section of column to the cross section of the influence area ($A_r = \frac{A_c}{A_i} = \frac{r_c^2}{r_i^2}$).

The columns were simulated in a soil layer of 5 m and their diameter was equal to 80 cm. Closed consolidation boundaries were applied to the model at two sides in Y-direction, at the bottom of the soil layer (Z-direction), and also at the side of symmetry (X-direction).

The analysis of the model has been continued until the minimum excess pore water pressure has achieved (|p-stop| = 1 kPa). Figure 4.40 depicts the generated mesh of the embankment.

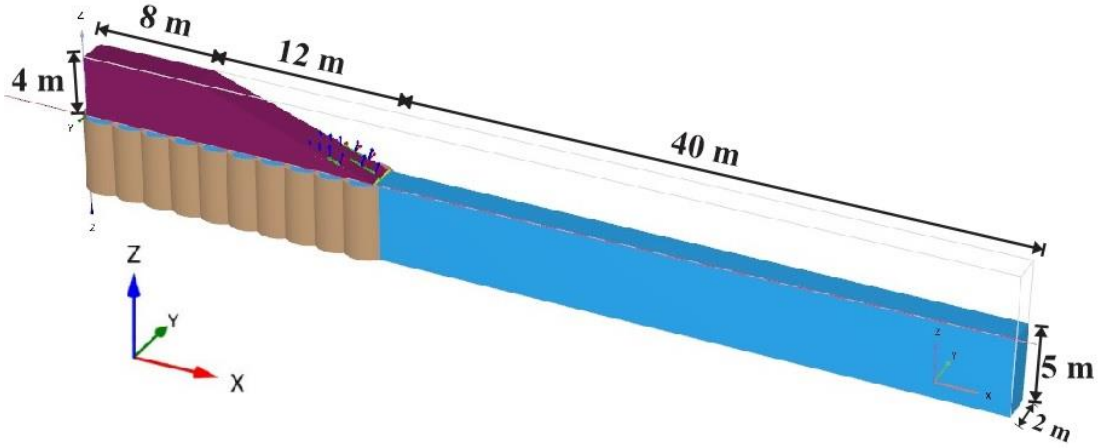

Figure 4.39. Modelling of embankment reinforced by encased columns.

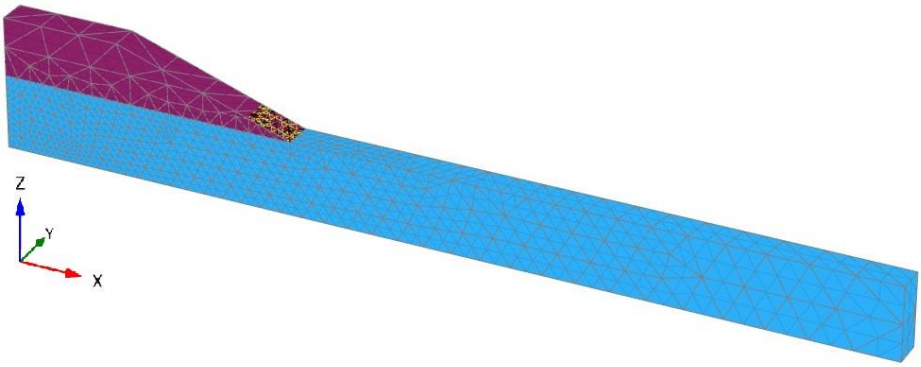

Figure 4.40.Generated mesh in PLAXIS 3D.

Figure 4.41 represents the water table that is one meter below the soil surface, the encased columns and the reinforcement (geogrid) at the bottom of the embankment or at the top of columns. Its tensile stiffness was taken to be equal 3500 kN/m (this value was taken from typical materials that are used in real projects, Huesker, 2012). Since the aim of study was not the influence of this reinforcement on the settlement behavior of embankment, this value has not changed for the cases of conventional and encased columns. The properties of soil, columns and embankment are presented in Table 4.4 and were obtained by back analysis. Young's modulus of granular column was equal to that of numerical simulations for the laboratory tests. Young's modulus used in Sexton & McCabe (2013) and Hosseinpour et al. (2014) was quite similar to value obtained for this study.

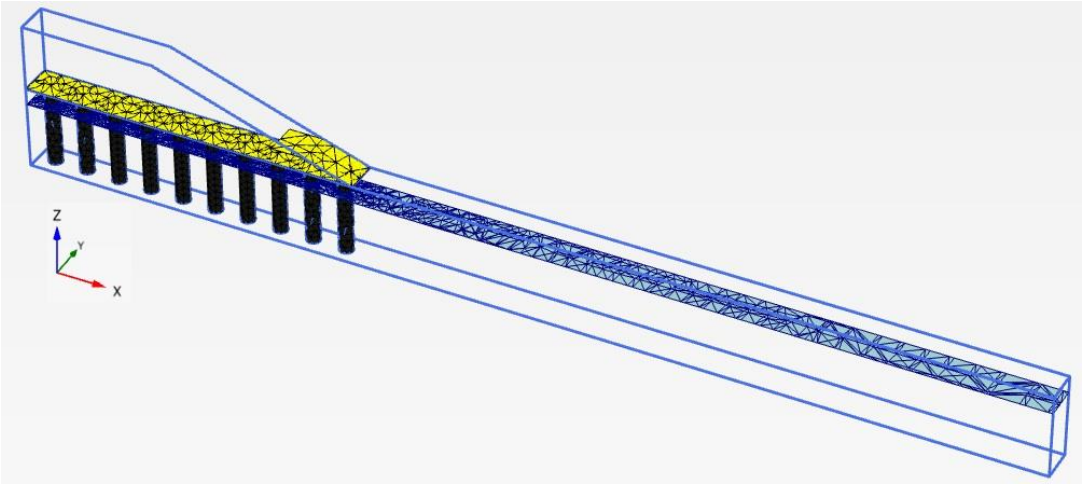

Figure 4.41. Reinforcement at the top of the columns.

Table 4.4. Properties of materials for full scale modelling.

Material Properties	Soft clay	Sand column	Embankment
	Soft soil	Mohr-Coulomb (MC)	Mohr-Coulomb (MC)
γ_{sat} (kN/m^3)	17	20	19
E' (kPa)	-	80,000	27000
ϕ' (^{o})	25	40.5	30
Ψ (^{o})	0	10	0
ν'	-	0.3	0.3
λ^*	0.088	-	-
κ^*	0.011	-	-
K_0	0.57	0.35	0.43
OCR	1	-	-

4.8.1. SETTLEMENT

The numerical results showed that the maximum settlement has occurred for the elements of soil (point B) and column (point A) which are closer to the axis of symmetry and are subjected to higher level of vertical stress (Figure 4.42).

The results have shown that encasement highly influenced the column behavior and considerably improved the embankment settlement behavior. The tensile stiffness of the three types of geotextile (G-1, G-2, and G-3) for the full scale analysis of the embankment was multiplied by the scaling factor which was adopted to be equal to five.

The results of settlement obtained for G-1 (J_1 = 650 kN/m), G-2 (J_2 = 500 kN/m) and G-3 (J_3 =267 kN/m), at point A have offered an improvement of about 1507%, 705%, and 466%, respectively. These results have indicated that the geotextile stiffness has an important role in the performance of the embankment. At point B, the improvement for G-1, G-2, and G-3 was measured to be about 290%, 232%, and 197%, respectively (Figure 4.43). It can be concluded that the encasement stiffness has not improved the settlement at the point B as much as the settlement at point A.

The results indicated that more than 90% of the primary consolidation settlement has occurred during the construction of embankment which is in agreement with Alexiew et al. (2015).

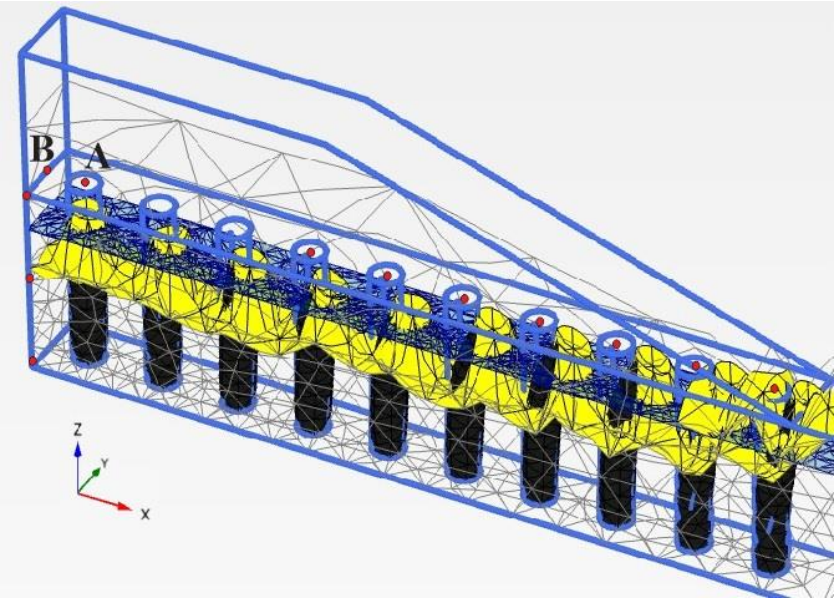

Figure 4.42. Deformation of the column after completion of analysis.

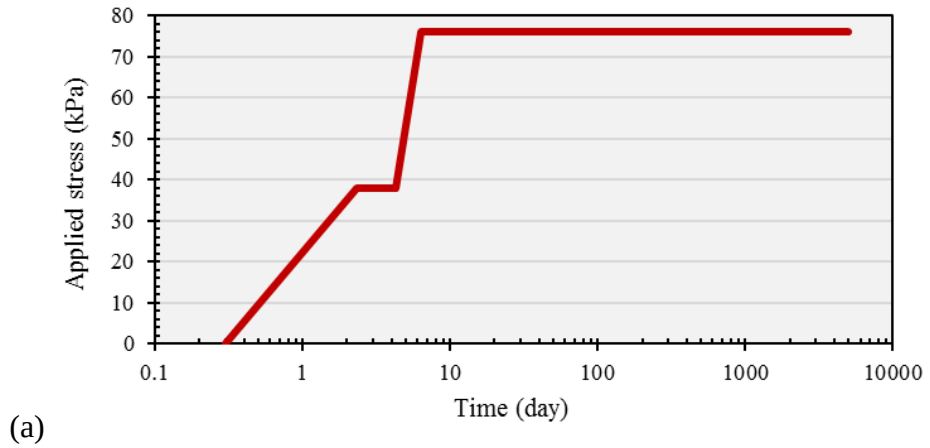

(a)

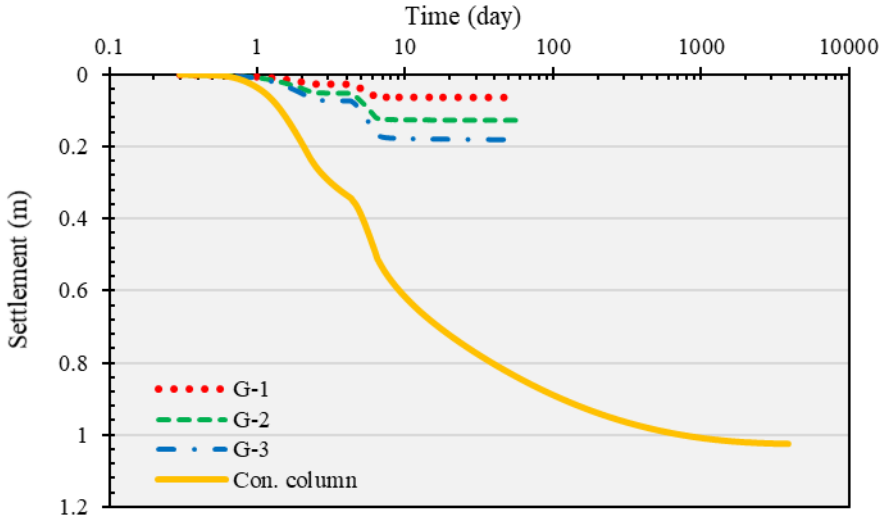

(b)

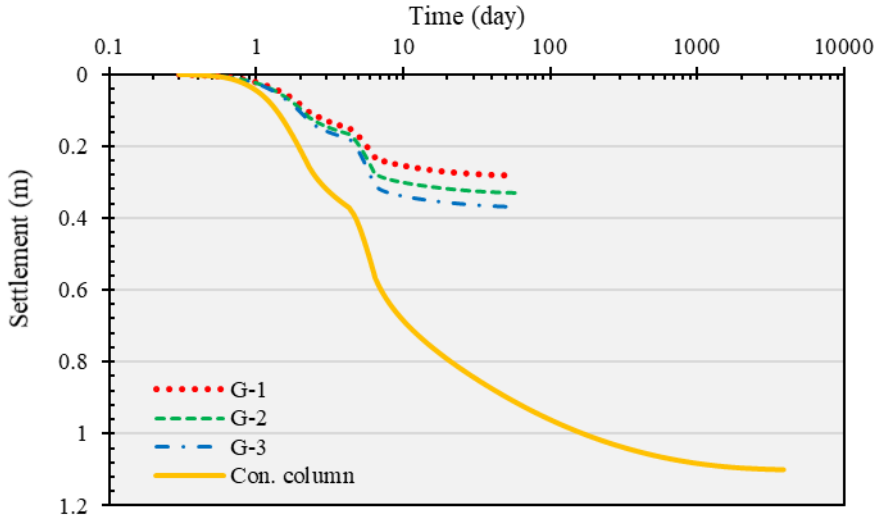

(c)

Figure 4.43. (a) Embankment construction stress, (b) Settlement of point A and (c) Settlement of point B.

For any kind of structure depending on the type of it (flexible or non-flexible) one of the principal factors is the differential settlement. This type of settlement can impair the function of structure and cause considerable maintenance costs. Thus for the design of any structure it must be taken into account. Besides, GEC´s technique is applicable in very soft soils where the foundation soil suffers from high compressibility and low shear strength. Thus, the differential settlement can be controlled by the reinforcement at the bottom of embankment.

Figure 4.44 illustrates that the higher values of the columns geotextile tensile stiffness do not necessarily provide a better design condition since the largest value of difference was obtained for G-1 which is about 442%. This value for G-2 and G-3 was measured to be about 260% and 204%, respectively. The lowest difference was obtained for conventional column which is about 107%.

On the other hand, the differential settlement can be reduced by using geogrid, at the bottom of embankment, with larger values of tensile stiffness which was not the case for the present study.

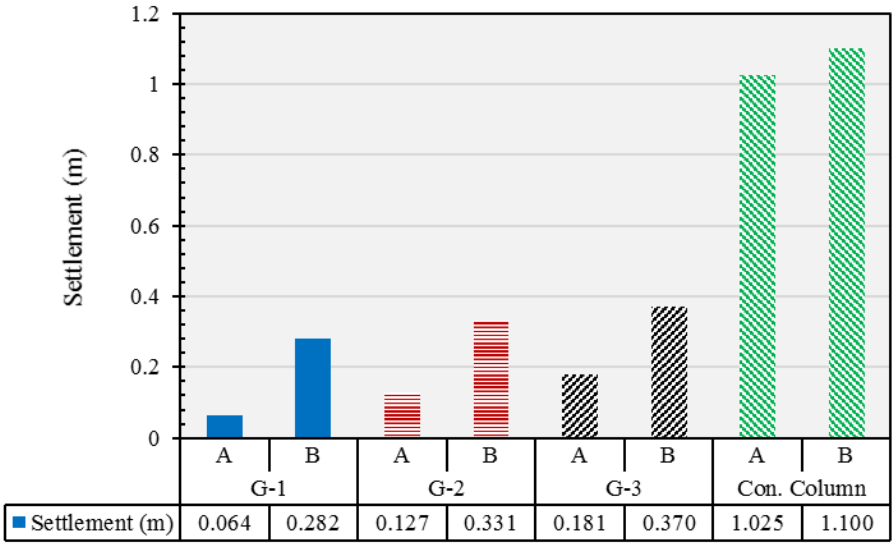

(a)

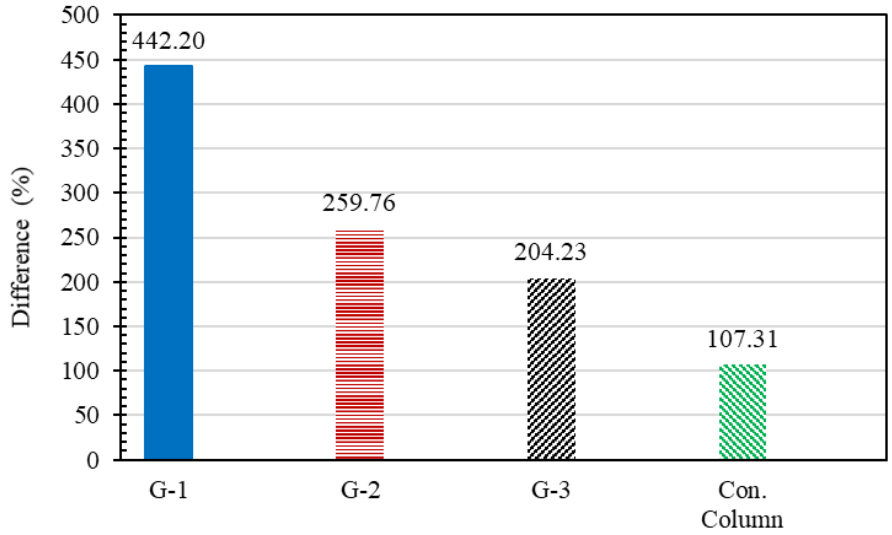

(b)

Figure 4.44. (a) Settlement at point A and B for different geotextiles and (b) Difference between settlement on top of column and adjacent soil.

4.8.2. LATERAL DEFLECTION

By getting away from the axis of symmetry, the settlement of columns reduces due to the decrease in vertical stress. On the other hand, the columns undergo higher values of lateral deflection as much as the columns getting closer to the toe of embankment. Figure 4.45 illustrates the deformation of the columns along the embankment. The columns with greater values of bending were named by letters D to J.

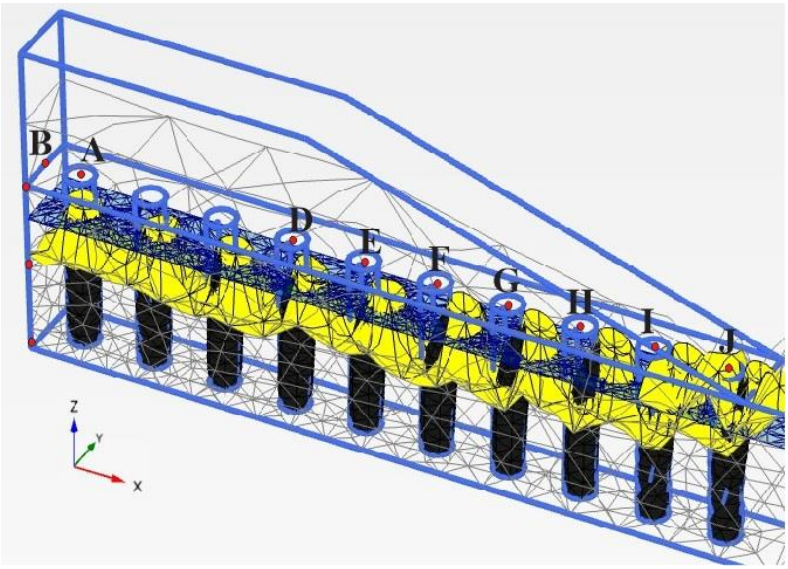

Figure 4.45. Lateral deflection of encased columns.

Figure 4.46 reports that the lateral deflection of the marked columns for G-1. As it can be seen, the maximum value of lateral deflection was obtained for the columns H, I, and J which are closer to the toe. By comparing the column D, which is closer to the center of embankment, and the column J, which closer to the toe, it can be concluded that from the column D to J, the lateral deflection grew by a value of about 75%. The results are in agreement with the results obtained by Chen et al. (2015) which were indicated that the encased column failure under the slope was caused by the bending.

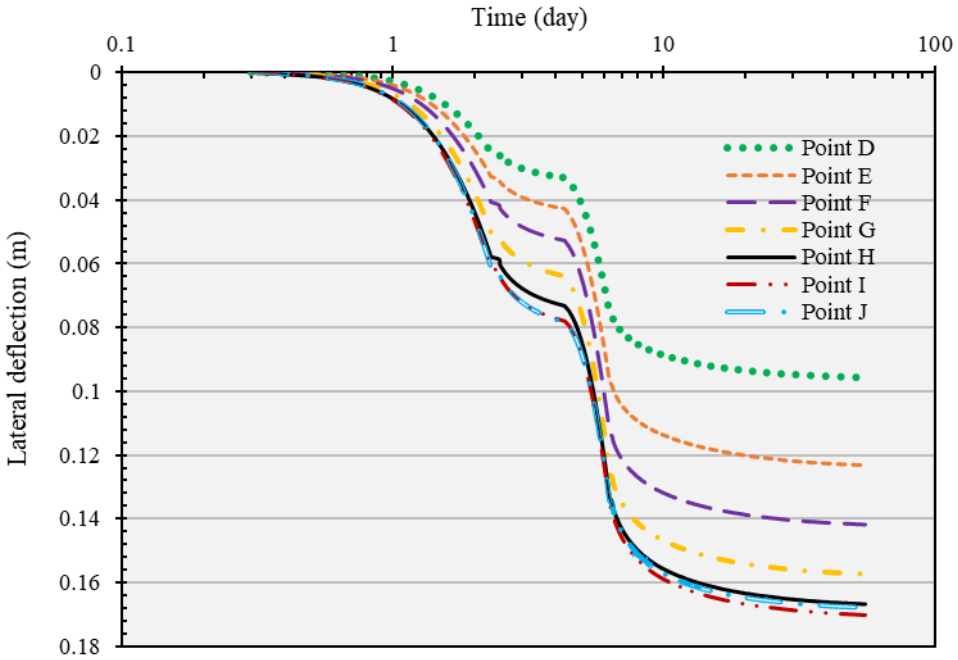

Figure 4.46. Lateral deflection of the columns for G-1.

The influence of geotextile stiffness on the lateral deflection, imposed by the sliding of slope, is presented in Figure 4.47. The maximum and minimum values of lateral deflection were measured for the conventional columns and the columns reinforced by G-1, respectively. By comparing this value for the column J, in the case of conventional and encased column (G-1), it can be concluded that the lateral deflection grows by about 77% for the conventional columns.

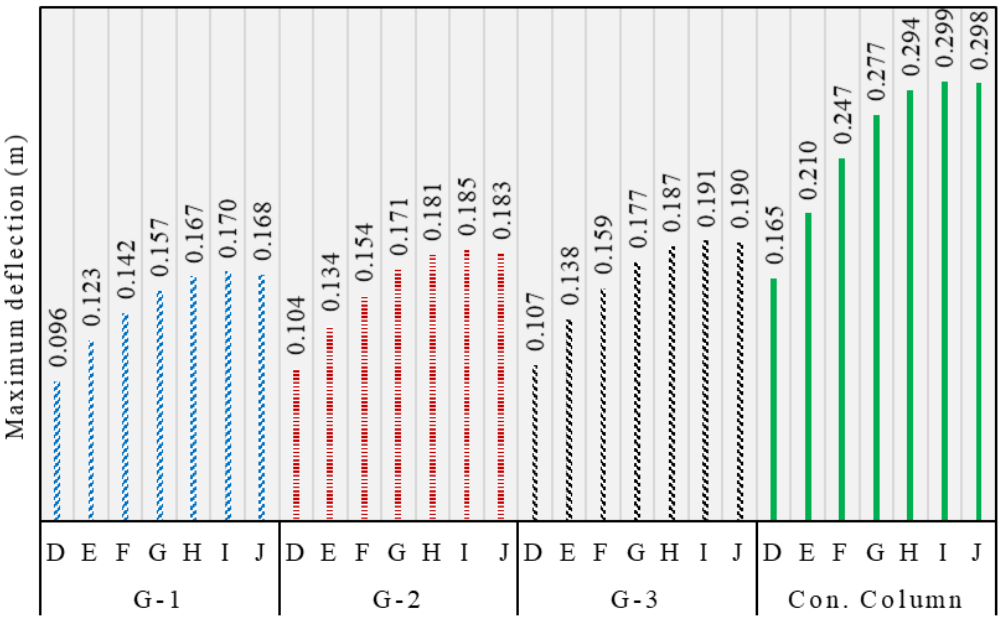

Figure 4.47. Maximum lateral deflection for encased and conventional column.

4.8.3. EXCESS PORE WATER PRESSURE

Figure 4.48 depicts the points of interest for evaluating the excess pore water pressure. To this end, the point K, L, and M were chosen at surface, middle and bottom of the foundation soil, respectively.

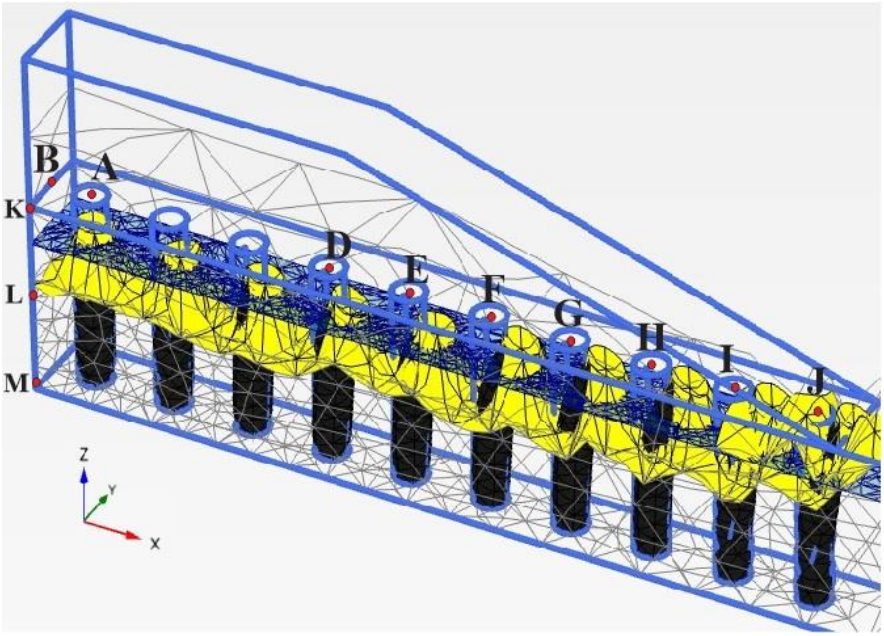

Figure 4.48. Points of interest for measuring excess pore water pressure.

The development and dissipation of excess pore water pressure, during the construction of embankment for encased (G-1) and conventional columns, is represented in Figure 4.49. As it can be seen the presence of the encasement, by providing rigidity to the foundation soil and decrease the settlement, has improved the development of excess pore water pressure. Thus, the dissipation has occurred in a shorter period of time. For instance, the value of excess pore water pressure for G-1 at the middle of foundation soil (point L) decreases by about 91% and consequently, the dissipation time reduces by about 98.5% comparing with that of conventional column.

As shown in Figure 4.49-b, the improvement in development of the maximum excess pore water pressure continues to produce almost similar results for all three types (G-1, G-2, and G-3) of encasement.

By comparing the numerical results, it can be concluded as the geotextile tensile stiffness decreases or settlement increases, the maximum value of the excess pore water pressure moves from the point K to the point L. Thus, the maximum value for G-1 and G-2 was obtained at the point K but on the other hand, this value for G-3 and conventional column comes to the point L. In other words, the increase of settlement can cause the foundation soil to experience the maximum value of excess pore water pressure at its deeper layers.

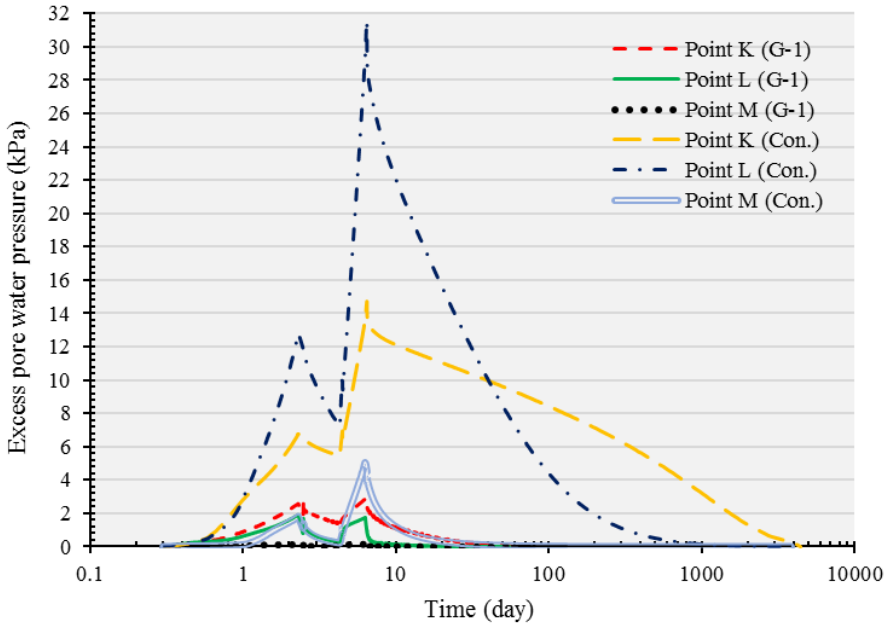

(a)

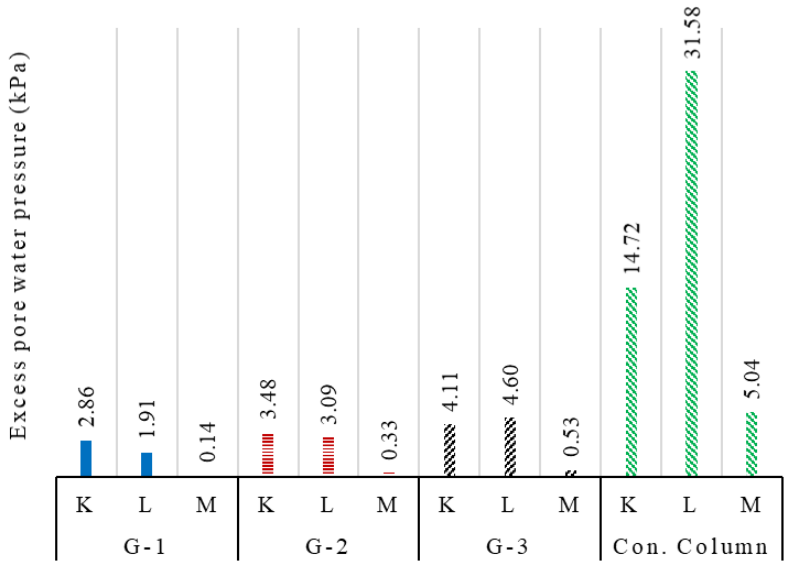

(b)

Figure 4.49. (a) Development and dissipation of the excess pore water pressure for conventional and encased (G-1) column and (b) Maximum value of excess pore water pressure for encased (G-1, G-2 and G-3) and conventional column.

4.8.4. SAFETY FACTOR

One of the important parameters for any geotechnical project is the safety factor of the desired structure. In this study, it was decided to evaluate the influence of column encasement on the safety factor of embankment.

The safety factor of the embankment without the reinforcements (columns and geogrid at the base of embankment) was calculated by Jambu (1954). As it can be seen in Figure 4.50, the reinforcements significantly increased the slope stability of the embankment. By comparing the results, it can be deduced that the difference between the maximum (G-1) and minimum (without reinforcements) value of safety factor is almost 1000%.

Figure 4.51 depicts that the slip surface for G-1 was controlled by the geogrid reinforcement at the bottom of embankment. The same scenario was observed for the other two types (G-2 and G-3) of encasement and conventional columns. Hence, the miniscule percentage of improvement (3%) due to the increase in tensile stiffness of encasement can be realized. In other words, the results indicated that the safety factor was a function of the geogrid

reinforcement at the bottom of embankment since the presence of the encasement has not significantly improved this factor. These small differences in SF were only due to failure taking place in the fill material.

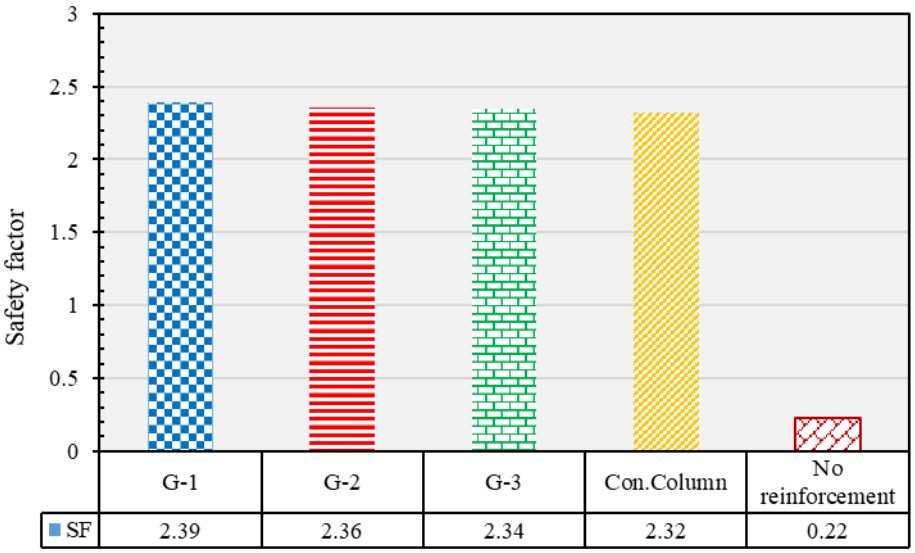

Figure 4.50. Safety factor of the embankment for encased and conventional columns.

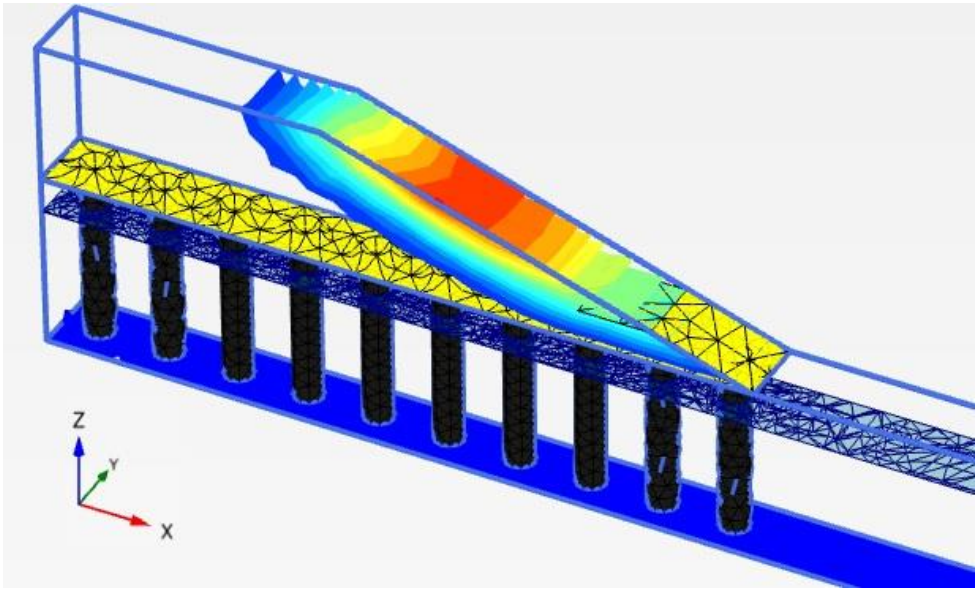

Figure 4.51. Slip surface for the embankment reinforced by G-1.

5. CONCLUSIONS AND RECOMMENDATIONS

5.1. CONCLUSIONS

This study presented the behavior of encased and conventional granular columns by means of laboratory tests and numerical analyzes. Large scale laboratory tests were carried out with three types of materials (sand, gravel and construction waste) where the behavior of the columns and the deformation along them were evaluated. Before large scale tests having been carried out, small compression tests were implemented for three types of geotextile (G-1, G-2, and G-3) in order to achieve some measurement of load bearing capacity of each type. Finally, numerical analyzes were also performed using the finite element method. Based on the obtained results, the main conclusions obtained in this study are presented below.

Encased sand columns had a significant increase in the load bearing capacity compared to the conventional sand column. Based on the results, there was an increase of about 7080%, 3986% and 2093% for geotextiles G-1 (J_1=130 kN/m), G-2 (J_2=100 kN/m), and G-3 (J_3=53 kN/m), respectively. It was also observed that the results obtained by analytical method (Braiud, 2013) for bearing capacity, generally, showed a good agreement with those of the tests. The maximun difference showed was about 19.8%.

The maximum lateral bulging for encased columns was obtained for the weakest encasement (G-3) and the maximum value of lateral bulging for all types of encasements occurred at a depth between 15 to 18 cm.

Horizontal stresses close to the column indicated that during loading there was a limited area around the column which was affected by lateral bulging in a depth of about 15 to 18 cm.

Due to installation method, the tests also showed that, the diameter of smear zone was about 1.8 to 1.9 the column diameter. The results of vane shear tests in this zone did not show any significant increase in soft soil undrained shear strength (S_u). Also they showed that after the dissipation of excess pore water pressure the soil inside the smear zone gained some strength as much as twice its value before installation.

The results showed some increases of excess pore water pressure during loading around the columns. The maximum value was obtained for the piezometer that was installed at the deepest part of the soft soil and closest to the column.

Breakage index (B_g) measured for different sections of column and the lateral bulging proved the proposed mechanism of failure. As the maximum values of B_g and lateral bulging occurred at the sections 1 and 2 (from the column surface to the depth of 30 cm) and this value for section 2 showed greater amount of B_g.

The results of 2D and 3D numerical analysis, generally, showed good agreement with the results of load tests.

The proposed failure mechanism was corroborated by the numerical results, as the results of lateral bulging, failure points, and shear zones were in agreement with that mechanism.

The full scale numerical results indicated that the maximum value of settlement occurred for the column which was at the center of the embankment. On the other hand, the columns that were below the embankment slope suffered lateral displacements and the maximum value was measured for those columns which were close to the slope toe. In addition, the results showed that the differential settlement between the column and the adjacent soil may be of concern, since it increased to a value of about 442% for geotextile G-1. The results also showed the great role of encasement in reducing deformations of the foundation soil and consequently of the embankment. This role can also affect the maximum value of excess pore water pressure so that this value for an encased column is much smaller than that of a conventional column.

Safety factor (SF) of embankment showed that the reinforcements applied to the embankment, significantly increased the stability of it.

5.2. RECOMMENDATIONS

Based on the results obtained in this study, some recommendations can be proposed for further research on the study of granular columns:

- To perform further laboratory tests with higher length of column in order to evaluate the development of excess pore water pressure due to the column installation;

- To install the column simulating the vibration that would be expected when the column is filled and would increase the column material density;

- To perform additional tests with pressure cells, close to the column, since in this study they broke during initial tests. Also to attach strain gauges to the upper half of encasement to have a better understanding on lateral bulging and tensile forces;

- To build (or to simulate) an embankment on encased columns to evaluate the significance of the space between columns, differential settlement, lateral deformation and safety factor;

- To perform additional numerical analyzes considering different materials at the base of the embankment that may affect differential settlement, lateral deflection and safety factor.

REFERENCES

Aboshi, H., Ichimoto, E., Enoki, M., & Harada, K. (1979). The Composer- A method to improve characteristics of soft clay by inclusion of large diameter sand columns. *Proceedings, International Conference on Soil Reinforcements: Reinforced Earth and Other Techniques Vol. 1*, (pp. 211- 216). Paris.

Alexiew, D., & Raithel, M. (2015). Geotextile-Encased Columns. In B. INDRARATNA, C. JIAN, & R. CHOLACHAT, *EMBANKMENTS WITH SPECIAL REFERENCE TO CONSOLIDATION AND OTHER PHYSICAL METHODS* (pp. 451-477). Kidlington, Oxford: Elsevier .

Alexiew, D., Horgan, G. J., & Brokemper, D. (2003). *Geotextile encased column (GEC): Load capacity and geotextile selection. In foundations: innovations, observations, design and practice.* London: Thomas Telford.

Ali, K., Shahu, J. T., & Sharma, K. G. (2012). Model tests on geosynthetic-reinforced stone columns: a comparative study. . *Geosynth. Int. 19 (4)*, 433-451.

Ali, K., Shahu, J. T., & Sharma, K. G. (2014). Model tests on single and groups of stone columns with different geosynthetic reinforcement arrangement. *Geosynthetics International*, *21*(2), 103–118.

Almeida, M. S., Hosseinpour, I., & Riccio, M. (2013). Performance of a geosynthetic-encased column (GEC) in soft ground: numerical and analytical studies. *Geosynthetics International*, 252–262.

Araujo, G. L., Palmeira, E. M., & Cunha, R. P. (2009). Behaviour of geosynthetic-encased granular columns in porous collapsible soil. *Geosynthetics International*, *16*(6), 433–451.

Baker, W. E., Westine, P. S., & Dodge, F. T. (1991). *Similarity Methods in Engineering Dynamics - Theory and Practice of Scale Modeling.* The Netherlands.: Revised Edition. Elsevier Science Publishers B.V., .

Balaam, N. P., & Booker, J. R. (1981). Analysis of rigid rafts supported by granular piles. *Int.Journal for Numerical and Analytical Methods in Geomechanics, 5*, 379–403.

Barksdale, R. D., & Takefumi, T. (1991). Design, Construction and Testing of Sand Compaction Piles", Deep Foundation Improvements: Design Construction and testing,. *ASTM STP 1089, Melvin I. Esrig and Robert C. Bachus, Eds., American Society for Testing and Materials.* Philadelphia.

Barkslade, R. D., & Bachus, R. C. (1983). *Design and construction of stone columns: Final Report SCEGIT-83-104.* Washington D.C. 20590: Federal Highway Administration.

Bergado, D. T., Anderson, L. R., Miura, N., & Balasubramaniam, A. S. (1996). *Soft Ground Improvements In Lowland and other Environments.* New York: ASCE Press.

Bjerrum, L. (1972). Embankments on Soft Ground. *In Proceedings of the ASCE Conference on Performance of Earth-Supported*, 1-54.

Briaud, J. L. (2013). *Geotechnical Engineering: Unsaturated and Saturated Soils.* Hoboken, New Jersey: John Wiley & Sons.

Brinkeve, & Vermeer. (2016). *PLAXIS MANUAL*. Brinkeve &Vermeer: PLAXIS.

Castro, J. (2017). Groups of encased stone columns: Influence of column length and arrangement. *Geotextiles and Geomembranes*, 68–80.

Castro, J., & Sagaseta, C. (2011). Deformation and consolidation around encased stone columns. *Geotext. Geomembr., 29(3), ,* 268–276.

Chen, J., Li, L., Xue, J., & Feng, S. (2015). Failure mechanism of geosynthetic-encased stone columns in soft soils under embankment. *Geotextile and Geomembrane*, 424-431.

EBGEO. (2011). *Recommendations for Design and Analysis of Earth Structures Using Geosynthetic Reinforcements.* Essen-Berlin: German Geotechnical Society (DGGT), Ernst & Sohn.

Elsawy, M. B. (2013). Behaviour of soft ground improved by conventional and geogrid-encased stone columns, based on FEM study. *Geosynthetics International, 20*(4), 276–285.

Gäb, M., & Schweiger, H. F. (2009). Numerical analysis of a floating stone column foundation using different constitutive models. *SECOND INTERNATIONAL WORKSHOP ON GEOTECHNICS OF SOFT SOILS,* (pp. 137-142). GLASGOW, SCOTLAND, 3–5 SEPTEMBER 2008: CRC PRESS.

Gniel, J., & Bouazza, A. (2008). Improvement of soft soils using geogrid encased stone columns. *Geotextiles and Geomembranes, 27*, 167–175.

Goughnour, R. R., & Bayuk, A. A. (1979). Analysis of stone column-soil matrix interaction under vertical load. *Proc. Int. Conf. on Soil Mechanics Reinforcement*, (pp. 271–277). Paris.

Greenwood, D. A. (1970). Mechanical improvement of soils below ground surface. *In: Proceedings of Conference on Ground Engineering, Institution of Civil Engineers*, (pp. 11-22). London .

Han, J. (2015). *Principles and Practices of Ground Improvement.* Hoboken, New Jersey: John Wiley & Sons.

Han, J., & Ye, S. L. (2001). Simplified method for consolidation rate of stone column reinforced foundations . *Journal of Geotechnical and Geoenvironmental Engineering,127(7)*, 597-603.

Hong, Y., Wu, C., Kou, C., & Chang, C. (2017). A numerical analysis of a fully penetrated encased granular column. *Geotextiles and Geomembranes*.

Hong, Y.-S., Wu, C.-S., & Yu, Y.-S. (2016). Model tests on geotextile-encased granular columns under 1-g and undrained conditions. *Geotextiles and Geomembranes 44*, 13-27.

Hosseinpour, I., Riccio, M., & Almeida, S. (2014). Numerical evaluation of a granular column reinforced by geosynthetics using encasement and laminated disks. *Geotextile and Geomembrane*, 363-373.

Hu, W. (1995). *Physical modelling of group behaviour of stone column foundation, PhD Thesis.* Glasgow: University of Glasgow.

Huesker. (2017, June 17). *Huesker*. Retrieved from http://www.huesker.com/

Hughes, J. M., & Withers, N. J. (1974). Reinforcing of soft cohesive soils with stone columns. *Ground Engineering*, (pp. 42–49).

Hughes, J. M., Withers, N. J., & Greenwood, D. A. (1975). A field trial of the reinforcing effect of a stone column in soil. *Geotechnique 25 (1)*, 31-44.

Jambu, N. (1954). Application of composite slip surfaces for stability analysis. *EUROPEAN CONF. ON STABILITY OF EARTH SLOPES.* Stockholm.

Keller, F. E. (2002). Vibro-Stone column. Courtesy of Keller Foundation.

Kitazume, M. (2005). *The Sand Compaction Pile Method.* Taylor and Francis.

Lynx. (2017, June 17). *Lynx*. Retrieved from http://www.lynxtec.com.br/aq_dados.htm

Madhav, M. R., & F, V. I. (1994). Loas transfer through a gravel bed on stone column reinforced soil. *Geotechnical Engineering*, 47-62.

Malarvizhi, S. N., & Ilamparuthi, K. (2007). Comparative Study on the Behavoir of Encased Stone Column and Conventional Stone Column. *Soils and Foundations, 47*(5).

Malarvizhi, S. N., & Ilamparuthi, K. (2010). Mechanism of Geogrid Encased Stone Column. *Indian Geotechnical Conference,* (pp. 949-952). Mumbai.

Marsal, R. (1967). Large Scale Testing of Rockfill Materials. *Journal of the Soil Mechanics and Foundation Division ASCE*, 27-43.

Miranda, M., & Costa, A. (2016). Laboratory analysis of encased stone columns. *Geotextiles and Geomembranes*, 269-277.

Mohapatra, S., Rajagopal, K., & Sharma, J. (2017). 3-Dimensional numerical modeling of geosynthetic-encased granular columns. *Geotextiles and Geomembranes*, 131–141.

Moroto, N. &. (1991). Settlement of Box Caissons Founded on Improved Ground by Sand Compaction Pile Method. *Proceedings of the International Conference on Geotechnical Engineering for Coastal Development: Theory and Practice on Soft Ground. Geo-Coast '91. Sept. 3-6* (pp. 373-376). Yokohama, Japan: Edited by Port and Harbour Research Institute, Vol. 1.

Murugesan, S., & Rajagopal, K. (2008). Performance of Encased Stone Columns and Design Guidelines for Construction on Soft Clay Soils. *Proc of the 4th Asian Regional Conference on Geosynthetics*, (pp. 729-734). Shanghai, china.

Murugesan, S., & Rajagopal, K. (2009). Investigations on the behavior of geosynthetic encased stone columns. *Proc. of the 17th ICSMGE.* Alexandrina, Egypt.

Nakata, S., Kimura, T., Shiota, K., & Shinomiya, H. (1991). Restoration of Pile Foundation Displacement by Sand Compaction Pile Method. *Proceedings of the International Conference on Geotechnical Engineering for Coastal Development Theory and Practice on Soft Ground. Geo-Coast '91. Sept. 3-6*, (pp. 713-718). Yokohama, Japan: Edited by Port and Harbour Research Institute, Vol. 1.

Priebe, H. J. (1995). The design of vibro replacement. *28*(10), 31–37.

Pulko, B., Majes, B., & Logar, J. (2011). Geosynthetic-encased columns: Analytical calculation model. *Geotextiles and geomembranes*, 29-39.

Raithel, M. (1999). Zum Trag- und Verformungsverhalten von Geokunststoffummantelten Sandsäulen. In *Ph.D Thesis.* Kassel, Germany: Kassel University.

Raithel, M., & Kempfert, H. G. (2000). Calculation models for dam foundations with geotextile coated sand columns. *Proceeding of the International Conference on Geotechnical and Geological Engineering.* Melbourne.

Raithel, M., Kempfert, H. G., & A, K. (2002). Geotextile-Encased Columns (GEC) for Foundation of a Dyke on very Soft Soils. Nizza.

Raithel, M., Kirchner, A., Schade, C., & Leusink, E. (2005). Foundation of construction on very soft soils with geotextile encased columns. *state of the art." Proceedings of GeoFrontiers 2005.* Austin, Texas.

Sexton, B., & McCabe, B. (2013). Numerical modelling of the improvements to primary and creep settlements offered by granular columns. *Acta Geotechnica*, 447-464.

Sharma, R. S., Kumar, B. R., & Ngendra, G. (2004). Compressive load response of granular piles reinforced with geogrids. *Canadian Geotechnical Journal, 41, No. 1*, 187–192.

Van Impe, W. F. (1989). Soil improvement techniques and their evolution. Rotterdam, Netherlands: A.A Balkema.

Van Impe, W., & De Beer, E. (1983). Improvement of Settlement Behavior of Soft Layers by Means of Stone Columns. *Proc 8th Conference of Soil Mechanics and Foundation Engineering*, (pp. 309-312). Helsinki.

Walker, R., & Indraratna, B. (2007). Vertical drain consolidation with overlapping smear zones. *Géotechnique*, 463-467.

Wang, G. (2009). Consolidation of Soft Soil Foundations Reinforced by Stone Columns under Time Dependant Loading. *J. Geotech. Geoenviron. Engrg., ASCE*, 1922–1931.

Weber, T., Plotze, M., Laue, J., & et al. (2008). Smear Zone Identification and Soil Properties around Stone Columns Constructed In-Flight in Centrifuge Model Tests. *Geotechnique*, 197–206.

Wei, J., & Khoo, T. K. (1992). Reclamation at Marina Bay and Tanjong Rhu. *ECD 1992 Proceedings, 1992 Seminar on Engineering for Coastal Development, ,* (pp. 179-193). Singapore.

Wood, D. M., Hu, W., & Nash, D. F. (2000). Group effects in stone column foundations: Model tests. *Geotechnique, 50, No. 6*, 689–698.

Yoo, C., & Kim, S.-B. (2009). Numerical modeling of geosynthetic-encased stone column-reinforced ground. *Geosynthetics International, 16*(3), 116–126.

Yoo, C., & Lee, D. (2012). Performance of geogrid-encased stone columns in soft ground: full-scale load tests. *Geosynthetics International, 19*(6), 480–490.

Zhang, L., & Zhao, M. (2014). Deformation analysis of geotextile-encased stone columns. *Int. J. Geomech. 10.1061/(ASCE)GM.1943-5622.0000389, 04014053.*

Zhang, Y., Chan, D., & Wang, Y. (2012). Consolidation of composite foundation improved by geosynthetic-encased stone columns. *Geotextiles and Geomembranes, 32, June*, 10–17.

Zornberg, J. G., Sitar, N., & Mitchell, J. K. (1998). Performance of geosynthetic reinforced slopes at failure. *Journal of Geotechnical and Geoenvironmental Engineering, ASCE, 124, No.8*, 670–683.

APPENDIX

A. LOAD CELL CALIBRATION

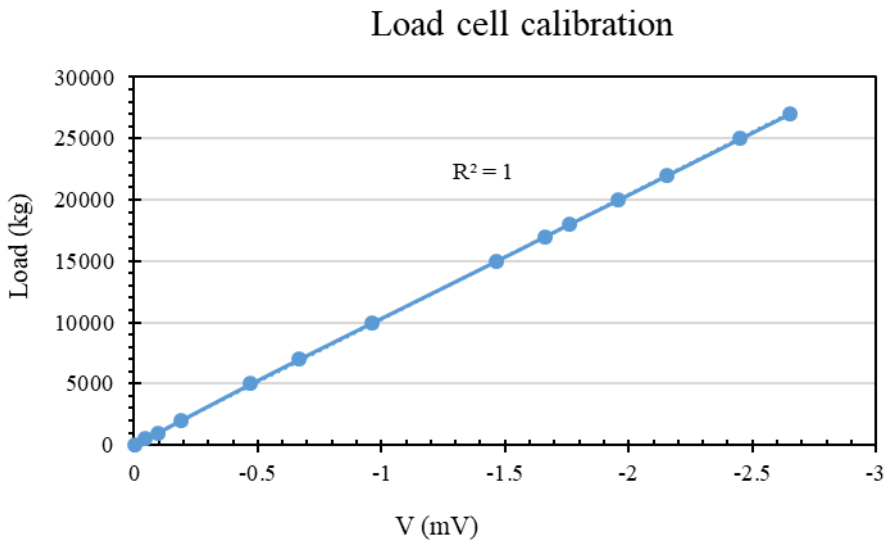

Figure A.1. Calibration of load cell.

B. DISPLACEMENT TRANSDUCER

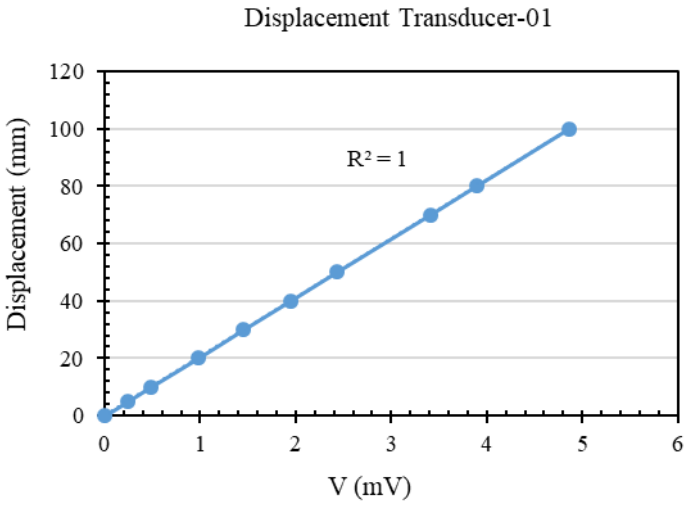

(a)

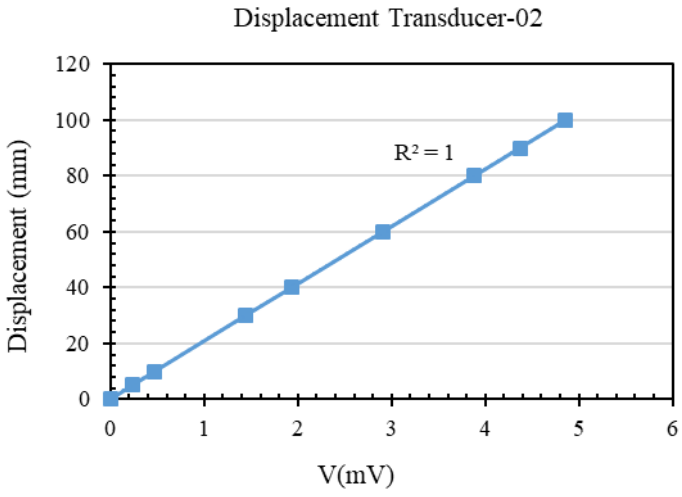

(b)

Figure B.1. Calibration of displacement transducers.

C. PIEZOMETER

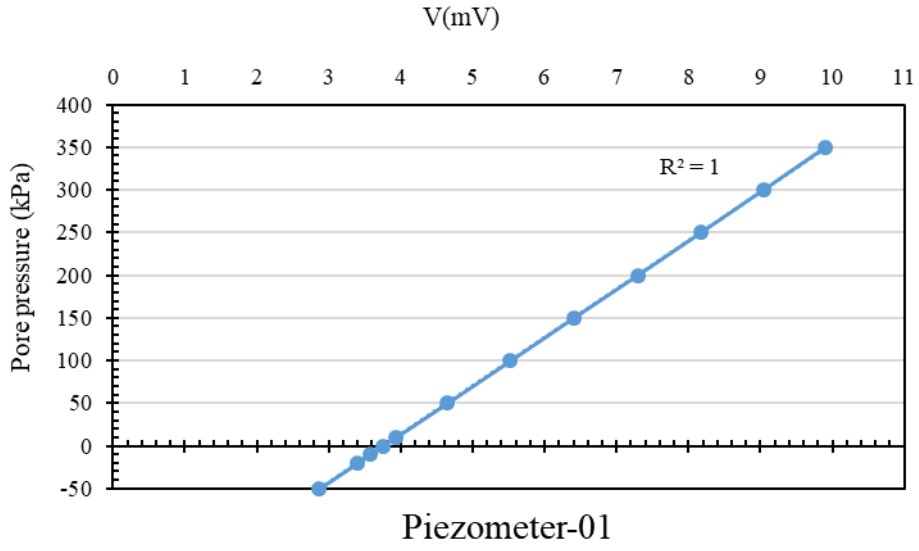

(a)

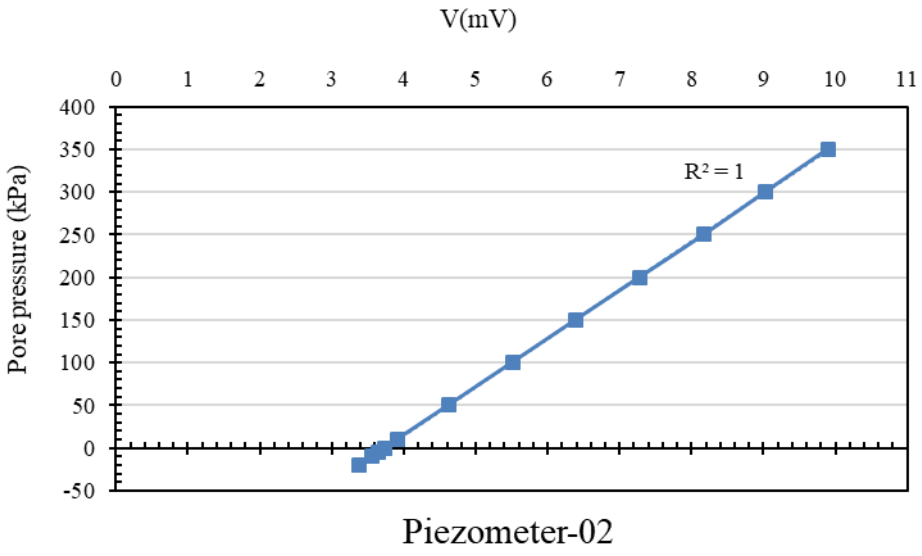

(b)

Figure C.1. Calibration of piezometers.

D. PRESSURE CELL

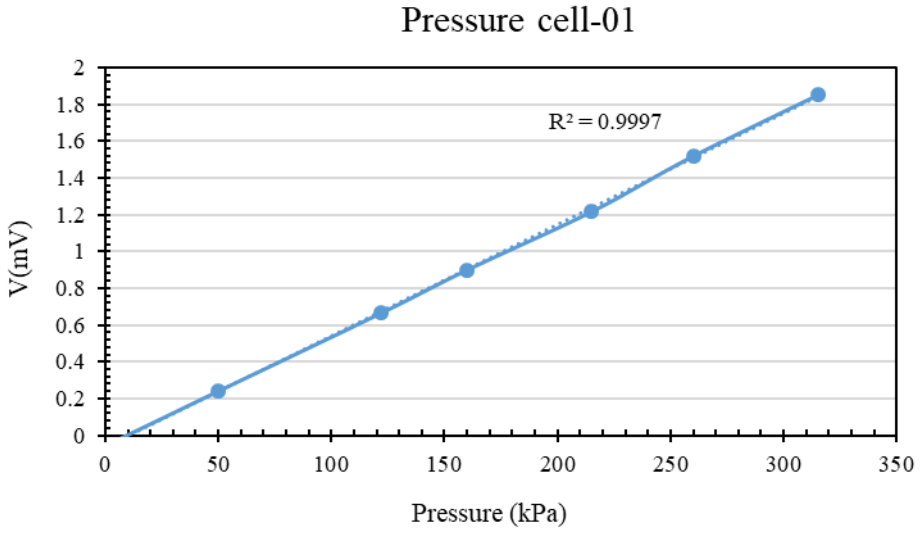

(a)

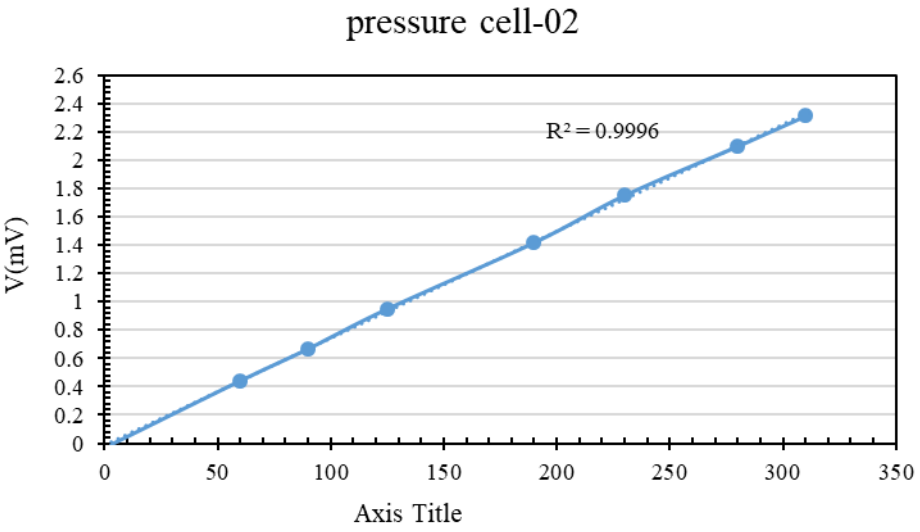

(b)

Figure D.1. Calibration of pressure cells.